

Anna Nora Sandborg Mathisen

Evaluation of hPSCs-derived Hepatocyte-like cells in native and modified alginates

May 2020



Norwegian University of
Science and Technology

Evaluation of hPSCs-derived Hepatocyte-like cells in native and modified alginates

Anna Nora Sandborg Mathisen

Biotechnology, MBIOT5

Submission date: May 2020

Supervisor: Berit Løkensgard Strand (IBT) and Ludovic Vallier (CSCI)

Co-supervisor: Rute Tomaz (CSCI)

Norwegian University of Science and Technology
Department of Biotechnology and Food Science

Preface

This master's thesis has been a collaboration between the Norwegian University of Science and Technology (NTNU) and the University of Cambridge. Preparation and analyses of alginates were conducted at NTNU, while cell culturing and all other experiments were conducted at Jeffrey Cheah Biomedical Center at the University of Cambridge. *In vivo* work was performed by Dr Kourosh Saeb-Parsy with help from Dr Olivia Tysoe.

Towards the end of the experimental procedures, the Covid-19 pandemic influenced this work in several ways. Despite assistance from my supervisors, the rapid shutdown of laboratory facilities and borders forced the discontinuance of several ongoing experiments, including *in vivo* work. Several samples from *in vitro* experiments that were stored for future analyses were also abandoned.

I would like to thank my supervisors, Professor Berit L. Strand and Professor Ludovic Vallier, for giving me the opportunity to work with this exciting collaborative project. I am grateful to Berit for all her experienced advice and for her prompt actions to get me back to Norway before the borders closed as a result of the pandemic. I wish to thank Ludovic for giving me the opportunity to work and learn in his laboratory and for encouragements and regular discussions regarding the direction of the project. I would also like to express my deep appreciation to Dr Rute Tomaz for her infinite patience in teaching me all the cell culture techniques and answering my many questions. Her assistance in finishing or storing my final experiments when I had to leave abruptly made the decision to leave possible, for which I am very grateful.

I also want to thank Dr Daria Zaytseva-Zotova and Ph.D. students Abba Coron and Joachim Kjesbu for invaluable guidance in the preparation and functionalization of alginate solutions, and Wenche Iren Strand for performing the structural analyses of the alginates for this work.

Lastly I would like to thank my family for all the encouraging words and for providing a supportive work environment while this thesis was written from home.

Abstract

This work studies the therapeutic potential of human pluripotent stem cells-derived hepatocyte-like cells (HLCs) generated by a novel forward programming (FoP) method. While the deficit between the need for whole-organ liver transplantation and available liver donors grows, using HLCs for cell therapy is a promising approach. HLCs have traditionally been generated through a direct differentiation pathway which follows the natural lineage of hepatocytes during embryonic development. However, a criticism of the approach, which is supported by the findings of this work, has been that it only succeeds in generating cells with more immature characteristics rather than those of the mature hepatocytes of the adult liver. The forward programming strategy was formulated in an attempt to increase the therapeutic effect of the cells, which would also improve potential uses in disease modeling. Both strategies of differentiation generated cells with some fetal characteristics, yet the protocol for differentiation through forward programming was found to be more reproducible and less time-consuming. For use in cell therapy, function and maturity of the HLCs were also investigated after encapsulation in alginate microcapsules.

Alginate encapsulation of therapeutic cells for immunoprotective purposes have been widely studied elsewhere and is a promising method for cell therapy medicine without need for immunosuppressants. Alginates studied in this work have been functionalized with the aim of increasing cell function of encapsulated cells through galactosylation of the polymer to provide adhesion sites, or suppressing the foreign body response of the host which bionert alginates have been known to elicit. Chemical sulfation of alginate has previously given alginate hydrogels that succeed in suppressing some of these immune responses, while still providing a physical barrier between encapsulated therapeutic cells and their surroundings. Genetic, functional and viability assays conducted in this work demonstrates that sulfated alginate mixed with unmodified alginate in a 20:80 ratio could also have a positive effect on the function and mature gene expression of encapsulated FoP-derived HLCs compared with other alginates tested. Additionally, gene expression analysis of the encapsulated HLCs indicates that immobilization in the sulfated alginate might even improve the maturity of some hepatocyte markers compared with the 2D cultures.

The findings of this work can be used to inspire further research into the encapsulation of HLCs generated by forward programming in functionalized alginates for future use in cell therapy, as well as the possibility of future use in 3D culturing.

Sammendrag

Dette arbeidet studerer det terapeutiske potensialet til hepatocyt-liknende celler (HLC-er) generert fra humane pluripotente stamceller ved en ny metode kalt "forward programming" (FoP). Knappheten av tilgjengelige leverer for donasjon i forhold til det økende behovet for levertransplantasjon, gjør bruk av HLC-er i celleterapi til en lovende metode. HLC-er har tradisjonelt blitt generert gjennom en direkte differensieringsvei som følger den naturlige avstamningen til hepatocytter under embryoutviklingen. Kritikken av denne metoden, som støttes av funnene i dette arbeidet, har likevel vært at den kun lykkes med å generere celler med egenskaper og karakteristikk som likner mer på umodne hepatocytter enn de modne cellene som finnes i den voksne leveren. FoP-metoden ble utviklet i et forsøk på å øke den terapeutiske effekten til cellene, hvilket også kan forbedre andre potensielle bruksområder, som i sykdomsmodellering. Begge strategiene for differensiering genererte celler med flere umodne egenskaper, men protokollen for FoP-differensiering ble demonstrert å være mer reproducerbar og mindre tidkrevende. For bruk i celleterapi ble funksjonen og modenheten til HLC-ene også undersøkt etter innkapsling i alginat mikrokapsler.

Alginatinnkapsling av terapeutiske celler for immunbeskyttende formål har blitt undersøkt i flere studier og er en lovende metode for celleterapi uten behov for medfølgende immunsuppressiv behandling. Alginatene som studeres i dette arbeidet har blitt funksjonalisert med det formål å øke cellefunksjonen til innkapslede celler gjennom galaktosylering av polymeren for å skape adhesjonssteder, eller å undertrykke immunreaksjonen på det implanterte fremmedlegemet som bioinert alginat tidligere har vist seg å fremkalle. Kjemisk sulfatering av alginat har gitt hydrogeler som lykkes i å undertrykke flere av disse immunreaksjonene, og samtidig utgjøre en fysisk barriere mellom innkapslede terapeutiske celler og deres omgivelser. Genetiske, funksjonelle og viabilitetstester utført i dette arbeidet demonstrerer at sulfatert alginat blandet med umodifisert alginat i et 20:80-forhold også kan ha en positiv effekt på funksjonen og det modne genuttrykket til innkapslede FoP-genererte HLC-er sammenliknet med andre testede alginater. Analyser av genuttrykket til de innkapslede cellene indikerer i tillegg at immobilisering i sulfatert alginat muligens også bidrar til å øke modningen av noen hepatocytmarkører sammenliknet med cellekulturene dyrket i 2D.

Funnene i dette arbeidet kan brukes til å inspirere til videre forskning på innkapsling av FoP-genererte HLC-er i funksjonalisert alginat for fremtidig bruk i celleterapi, i tillegg til muligheten for fremtidig bruk i dyrking av celler i 3D.

Symbols and Abbreviations

A1AT	α -1-antitrypsin
AFP	α -fetoprotein
ASGPR	Asialoglycoprotein receptor
ECM	Extracellular matrix
EDTA	Ethylene diamine-tetraacetic acid
FBR	Foreign-body response
FGF	Fibroblast growth factor
G	α -L-guluronate
$^1\text{H-NMR}$	Proton nuclear magnetic resonance
hESCs	Human embryonic stem cells
HGF	Hepatocyte growth factor
hiPSCs	human induced Pluripotent Stem Cells
HLCs	Hepatocyte-like cells
HNF4 α	Hepatocyte nuclear factor 4 alpha
M	β -D-mannuronate
NPCs	Non-parenchymal cells
PBS	Phosphate-buffered saline
PHHs	Primary human hepatocytes
POAred	Reduced periodate oxidized alginate
qRT-PCR	Quantitative real-time polymerase chain reaction
SEC-MALLS	Size exclusion chromatography - Multi-angle laser light scattering
TGF- β	Transforming growth factor β
TF	Transcription factor
UP-LVG	Ultra-pure, low viscosity, high-G alginate
UP-MVG	Ultra-pure, moderate viscosity, high-G alginate

Contents

Preface	I
Abstract	II
Sammendrag	III
Symbols and Abbreviations	IV
1 Background	1
1.1 Aims of the study	1
2 Introduction	2
2.1 Liver morphology	2
2.1.1 Hepatocytes	3
2.1.2 Hepatocyte-like cells	4
2.2 Alginate hydrogels	4
2.3 Cell encapsulation in alginate beads	6
2.3.1 Functionalization of alginates	7
3 Materials and methods	10
3.1 Alginates	10
3.1.1 Functionalization of alginates	10
3.2 Cell Culturing	12
3.3 Cell differentiation	13
3.3.1 Direct differentiation of A1ATD ^{R/R}	14
3.3.2 Forward programming of H9	15
3.4 Immobilization of cells in alginate capsules	15
3.4.1 The capsule generator	16
3.4.2 Capsule characterisation	17
3.5 Functional analyses of encapsulated cells	17
3.5.1 Live/dead staining	18
3.5.2 Cell viability	19
3.5.3 CYP3A4 activity	19
3.6 Gene expression analysis	20
3.6.1 Dissolution of 3D capsules	20
3.6.2 cDNA synthesis	20
3.6.3 qRT-PCR	21
3.7 Immunohistochemical staining	22
3.8 Statistical analyses	23
3.9 <i>In vivo</i> work	23
4 Results	25

4.1	Characterisation of HLCs generated by direct differentiation	25
4.2	Alginate encapsulation of HLCs generated by direct differentiation	27
4.2.1	Gene expression analysis of encapsulated hiPSCs-derived HLCs	29
4.2.2	Functional analyses of encapsulated hiPSCs-derived HLCs	31
4.3	Characterisation of FoP-derived HLCs	33
4.4	Encapsulation of HLCs generated by forward programming	35
4.4.1	Gene expression analysis of FoP-derived HLCs	37
4.4.2	Functional analyses of encapsulated FoP-derived HLCs	39
4.5	Performance of encapsulated HLCs generated by forward programming and direct differentiation	41
5	Discussion and Future work	43
5.1	Generation of Hepatocyte-like cells	43
5.2	Alginate encapsulation of HLCs	45
5.2.1	Encapsulation in functionalized alginates	45
5.3	Functional analysis of encapsulated HLCs	46
5.3.1	Embedding of HLCs generated by direct differentiation and forward programming in native alginate	46
5.3.2	Embedding of FoP-derived HLCs in functionalized alginates	48
5.4	<i>In vivo</i> studies	51
6	Conclusion	52
	References	53
A	¹H-NMR spectra	61
B	Primer sequences for qPCR	63
C	Functional assays of HLCs encapsulated in POAred and Gal-Alg	64

1 Background

Liver diseases represent a major health care challenge. This group of diseases accounted for approximately 2 million deaths worldwide in 2010, with 1 million deaths from complications with cirrhosis alone [1]. In cases of end-stage liver disease, orthotopic liver transplantation (OLT) remains the treatment of choice. There is, however, a shortage of donor livers available for transplantation [2]. This has prompted the need for cell therapy methods to alleviate the imbalance of healthy donor livers and patients requiring transplantation. Cell therapy using human pluripotent stem cells (hPSCs) has thus been widely researched [3–5], and cell therapy methods that can act as a short-term treatment for acute liver failure while the recipient awaits a transplant could be especially useful.

Some previous experiments with cell therapy have utilized alginate as a vessel for cell entry to the host [6–8]. Alginate is a biocompatible biopolymer that can form a hydrogel for cell encapsulation [9]. The meshwork of the hydrogel allows the diffusion of nutrients and biologically active substances produced by the cells in and out of the alginate capsule, while providing a physical barrier between the encapsulated cells and the immune responses of the host [7]. However, transplantation of alginate capsules has been shown to elicit the foreign body response (FBR) in non-human primates and some mice [7, 10]. To circumvent this problem, it is of interest to investigate the effects of functionally modified alginates, and their effect on the therapeutic cells.

1.1 Aims of the study

The overall aim of this work was to develop alginate based microcapsules for transplantation of hepatocyte-like cells (HLCs) derived from stem cells. Firstly, experimental protocols for the encapsulation in alginate capsules of HLCs generated by direct differentiation of hPSCs was set up. Subsequent performance of suitable *in vitro* assays for encapsulated HLCs were conducted to compare their functionality to the cells left to grow in 2D. Secondly, as HLCs generated by direct differentiation are known to acquire features of fetal hepatocytes [11], to transfer the knowledge to the embedding of HLCs generated by forward programming (FoP). FoP methods have been developed in an attempt to generate more mature and functional cells. Hence, these experiments would provide a proof-of-concept for the ability to use FoP-derived HLCs in cell therapy. FoP-derived HLCs were encapsulated in different alginates as some alginate modifications have been shown to be beneficial in reducing the foreign-body response (FBR) to transplanted alginate beads *in vivo* [12], or increase cell function [13]. To assess how the alginates affects the FoP-derived HLCs and assess if some provide a more beneficial environment than others, *in vitro* functional assays were performed. Lastly, *in vivo* testing using the overall best-performing alginates for the encapsulation of FoP-derived HLCs was conducted to investigate cell survival and function after transplantation.

2 Introduction

2.1 Liver morphology

The liver is one of the largest organs in the human body, constituting 2-5% of total body mass [14]. Its large size reveals the many varied and important functions of the organ. These range from endocrine and exocrine functions, to detoxifying the blood from harmful substances like toxins and drugs. The histology of the liver is highly complex and arranged at the very beginning of embryonic development, with a broad spectrum of cell types organized in a precise architecture [14, 15].

These cells work together to perform all the functions of the organ. They are commonly divided into parenchymal and non-parenchymal cells (NPCs), which comprise 60% and 40% of all hepatic cells, respectively [16]. The NPCs include Kupffer cells, which are liver-resident macrophages that make up 15% of the organ. They respond quickly to any damage by releasing pro-inflammatory cytokines [17]. The NPCs also include hepatic stellate cells and liver sinusoidal endothelial cells. The former is a major storage site of vitamin A and is responsible for fibrosis upon injury [18], while the latter is both a barrier for the blood and participates in the immune response by detecting pathogen-associated molecular patterns and releasing cytokines [19]. The hepatic stellate cells reside in the space of Disse, created between the sinusoidal endothelial cells and the parenchymal cells discussed next [14], see Figure 2.1. Lastly, in addition to several immune cells, the non-parenchymal cells also include the cholangiocytes. Cholangiocytes line the biliary tracts which receive and transport bile produced in the liver [20]. The cells that take up the bile substances and excrete them in the bile canaliculi leading to the bile tracts are the parenchymal cells, i.e. the hepatocytes [21].

The last vital part of the liver is the hepatic extracellular matrix (ECM). The ECM is a vast and complicated structural network of macromolecules that provides a physical scaffold for cells to adhere to and grow [23]. The ECM is also active in communication with the surrounding cells through adhesion proteins such as the integrin family [24], while the mechanical characteristics of the matrix itself has also been shown to influence cell behaviour and fate [25]. The ECM, and the molecules that comprise it, is thus important in a diverse range of mechanisms, including cell migration, polarity, survival and differentiation [26]. This is also true for the hepatic ECM, even though it constitutes a relatively small part of the organ. The components and stiffness of the ECM vary with location in the liver. The ECM of the hepatocytes is found in the space of Disse, which is especially rich in fibronectins [27]. Fibronectins are large glycoproteins that bind and interact with several other components of the ECM such as collagens, fibrin and heparin which is discussed later [28]. Type I collagen is found through most of the liver ECM, and the fibronectins are in contact with the hepatocyte microvilli and type I collagen bundles, thus connecting the hepatocytes to the other elements in its surroundings [27].

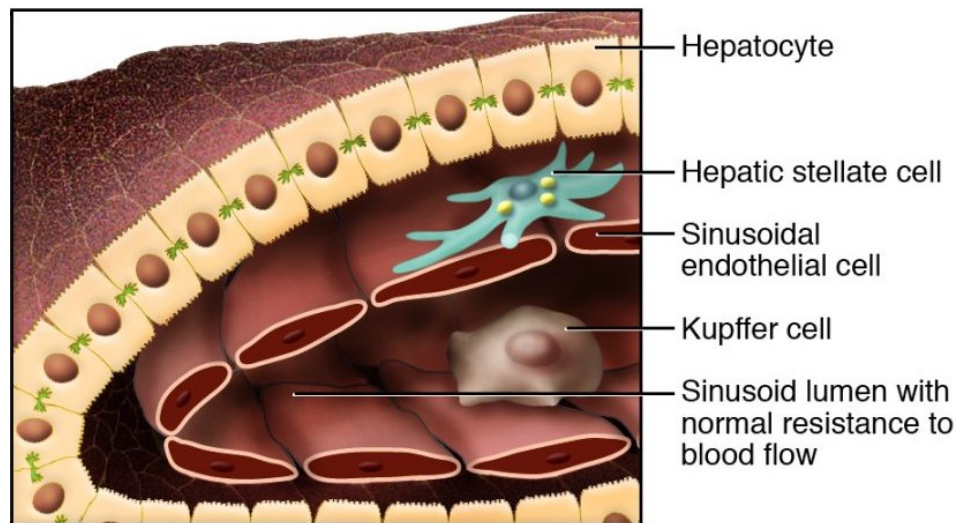


Figure 2.1: Cellular organization in the liver. The hepatocytes create a cord that surrounds the space of Disse in which the hepatic stellate cells reside. The sinusoidal endothelium provides a barrier to the blood, and the liver-resident macrophages (Kupffer cells) reside in its lumen [22].

2.1.1 Hepatocytes

In addition to absorbing bile substances and excreting them in the bile canaliculi, the hepatocytes are the cells that perform the many metabolic functions of the liver. The dominant share of all circulating plasma proteins such as albumin, protease inhibitors like α -1-antitrypsin, and blood coagulation factors are produced by the hepatocytes. They also control the homeostasis of many essential molecules, by taking part in the metabolism and/or storage of glucose, triglycerides, vitamins A and D, amino acids and many more [29]. An additional important function of the hepatocytes of the liver is the detoxification and metabolism of xenobiotic drugs and toxins. Major contributors to this function are the Cytochrome P450 (CYP) family of enzymes [30].

Hepatocytes are highly polarized epithelial cells, with the basal side facing the sinusoidal endothelium and the apical side facing an adjacent hepatocyte. The basal side is specialized for exchange of substances with the blood [14]. Transporters embedded in the basal membrane import toxins and ingested substances, which are either stored or metabolized before secretion back into the blood stream. The apical side contains tight junctions binding the cell firmly to adjacent hepatocytes, in addition to specialized transporters for movement of bile substances into bile canaliculi formed between two neighboring hepatocytes [31]. As the cells develop into hepatocytes, they take on a polygonal shape, increase in size, and at least 20% become binucleated [32]. Their control of triglyceride homeostasis also increases their intracellular storage of lipids in the form of cytosolic lipid droplets [33].

While the prevalence of liver diseases and the need for orthotopic liver transplantation increases worldwide, there is no comparable increase in available donor livers. While it is true that primary human hepatocytes (PHHs) are also used in cell therapy medicine to overcome this worsening deficit,

the harvesting of liver primary hepatocytes is an invasive and perilous procedure [34]. In addition, PHHs are fully differentiated cells that are impossible to expand *in vitro*, and harvested cells quickly lose their metabolic functions [35]. Consequently, human pluripotent stem cells (hiPSCs)-derived liver cells represent an opportunity to overcome these limitations.

2.1.2 Hepatocyte-like cells

Unlike primary human hepatocytes which seldom divide and are impossible to maintain *in vitro* for an extended period of time, pluripotent stem cells are characterized by their potential for endless self-renewal and ability to differentiate into virtually any cell type [34, 36]. There are two types of human pluripotent stem cells (hPSCs), the embryonic stem cells (ESCs) and the induced pluripotent stem cells (iPSCs). hiPSCs are cells derived from human somatic cells, and subsequently reprogrammed into pluripotent stem cells through transcription factor overexpression. They are relatively easy to maintain *in vitro*, and protocols have been developed to induce the differentiation of hPSCs into several different cell types [37, 38].

Hepatocyte-like cells (HLCs) are the results of *in vitro* differentiation of hPSCs to hepatocytes through manipulation of signaling pathways which mimic different stages of embryonic liver development, a method known as direct differentiation. Several protocols have been established to obtain the most mature HLCs possible [38–40], utilizing a variety of transcription factors, polymers serving as ECMs, and growth media. However, a prevailing problem of HLCs generated by direct differentiation that has limited their use in cell therapies is their resemblance to immature, or fetal, hepatocytes rather than adult PHHs [11]. The differentiation is also time-consuming and with high cytokine requirements [38]. In an attempt to overcome these limitations, a method called forward programming (FoP) has been developed with promising results for several cell lineages [41, 42]. Forward programming refers to the direct reprogramming of hPS cells through forced expression of a few lineage-specific master regulators [43]. This is most commonly achieved through lentiviral transduction of the host hPSCs to introduce genes with modified promoters that are inducible through exogenous TF manipulation [43]. However, a novel technology using inducible transgene overexpression has recently been developed. This method is currently being tested for generation of functional and mature hepatocyte-like cells, with less variability between differentiations (Tomaz et al, unpublished).

2.2 Alginate hydrogels

Alginates are unbranched biopolymers produced as a structural component by marine brown algae (*Phaeophyceae*), and as protective exocellular polysaccharides by some soil bacteria [44, 45]. It is an anionic polymer that has been investigated and widely used for biomedical purposes due to its biocompatibility, ease of gelation with a relatively mild gelling agent at neutral pH, and low cost [9,

46]. Alginate consists of the monomers β -D-mannuronate (M) and α -L-guluronate (G) linked through 1 \rightarrow 4-linkages, see Figure 2.2. During naturally-occurring alginate biosynthesis, all polymers are produced through polymerization of M monomers. The G monomers are introduced to the polymer afterwards through C-5 epimerase conversion of M residues [44]. The monomers are thus organised in the polymer in varying lengths of undisturbed G-units (G-blocks), blocks of M-units, or alternating MG-units (MG-blocks) [44, 47], depending on the source of the alginate [46].

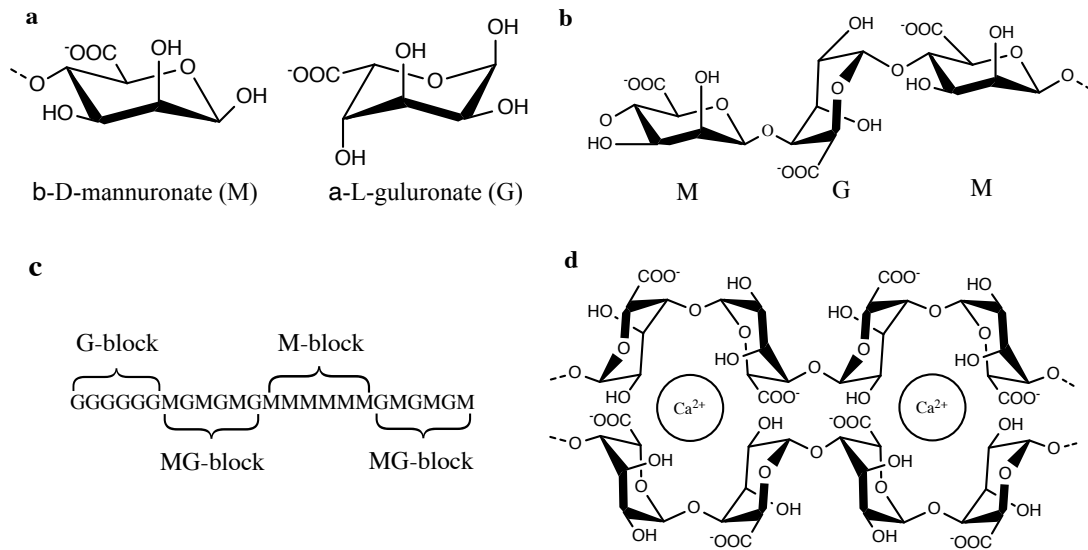


Figure 2.2: Molecular structure of alginate. Structure of the M and G monomers of alginate (a), M and G units linked in a polymer (b), Alginate polymer as M-, MG- and G-blocks (c) (adapted from Draget and Taylor, 2011)[48], Cross linked G-blocks illustrated in an egg-box configuration (d) (modified from Braccini and Péres, 2001)[49].

The ratio and distribution of the blocks affects the gelling properties of the alginate as the two epimers interact differently with the divalent cation that constitutes the gelling agent of ionic cross-linking, and the interactions occur through a mechanism termed the egg-box model (See Figure 2.2, c) [50]. The structure of the G-units allows them to interact with divalent cations (e.g. Ca^{2+} -ions) at multiple sites, with a G-unit in a G-block on a separate alginate polymer creating the same connections with the same cation [51], see Figure 2.3. For increased stability of the resultant gel, the traditionally used Ca^{2+} -ions can be exchanged for Ba^{2+} -ions which are less sensitive to chelating agents. These cations have a higher affinity to the G-blocks of the alginate than Ca^{2+} -ions, and will thus form stronger gels. Unlike Ca^{2+} -ions, they will also bind M-blocks, but not MG-blocks [52]. As the ionic cross-linking is most dependent on the G-units, the fraction of G-units (F_G) is an important measure of the gelling capacity of any alginate, together with the average G-block length ($N_{G>1}$) [53]. Previous work has found that the number of consecutive G-units needed to form stable cross-links with Ca^{2+} -ions is eight, though this number is lower for Ba^{2+} -ions [54]. F_G and F_M is possible to measure using Nuclear Magnetic Resonance (NMR) spectroscopy. The method has also allowed for determination of the frequency of

the four possible sequences of neighboring monomers (diads), and the frequency of the eight possible sequences of three neighboring monomers (triads). Diads are denoted F_{GG} , F_{GM} , F_{MM} , F_{MG} , and likewise for the eight triads. These frequencies are subsequently used to determine $N_{G>1}$ [44]. In addition to the frequency and distribution of G-units, the molecular weight is of importance for both the gel strength and viscosity of the alginate. As alginates are polydisperse with respect to molecular weight, this also varies greatly between alginates and between polymers within an alginate solution. The molecular weight of alginate is therefore an average of the distribution of molecular weights [44, 55].

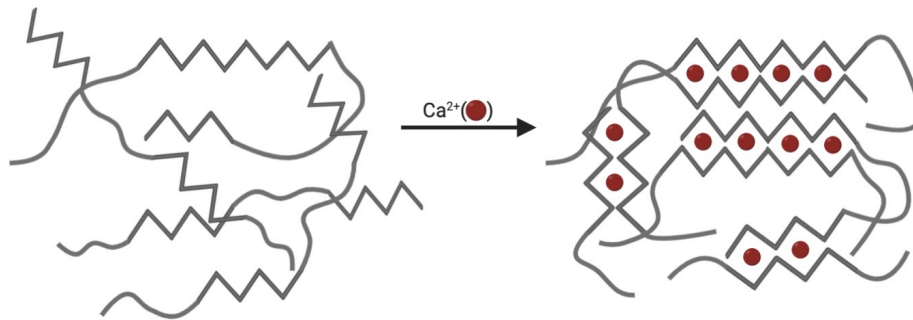


Figure 2.3: Ionic cross-linking of alginate polymers. Addition of a divalent cation (Ca^{2+}) to a disordered alginate solution causes the G-units of the alginate polymers to interact with the cations and with G-blocks on a different polymer through the egg-box model. This leads to gelling of the alginate solution through ionic cross-linking (adapted from Smidsrød and Skjåk-Bræk, 1990)[56]

2.3 Cell encapsulation in alginate beads

Ionically cross-linked alginates are some of the most common systems for cell immobilization. The mild gelling conditions, together with its non-toxicity, makes the polymer ideal for cell survival during and post gelation [46]. Immobilization of cells in alginate microcapsules have therefore been extensively researched as a method for transplantation of cells for cell therapy [4, 7, 57]. There are several strategies for alginate encapsulation [9]. One method involves the controlled release of droplets of an alginate solution mixed with the therapeutic cells into a bath containing the gelling agents. The gelling of individual droplets produces alginate microbeads containing immobilized cells. Figure 2.4 displays a simplified scheme of the process. The hydrogel provides a semipermeable barrier as the pores of the gel are too small to allow direct contact with the immune system cells of the host, while still allowing the free diffusion of nutrients, oxygen and therapeutic compounds produced by the encapsulated cells [6, 58]. This method could potentially avoid therapeutic cell rejection without host immune system suppression [57]. However, unmodified alginate capsules have previously been shown to elicit the foreign body response (FBR) in humans and non-human primates (NHPs), which can lead to a fibrotic build-up isolating the capsules from the host [7]. This will, in turn, create an hypoxic environment

within the capsules, as well as stop the diffusion of nutrients and therapeutic molecules in and out of the capsules [59].

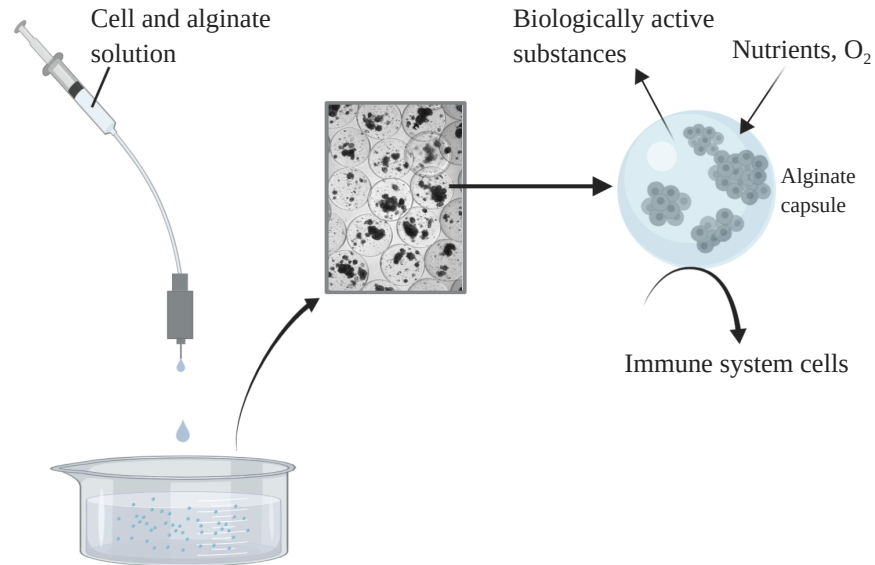


Figure 2.4: Schematic figure of alginate encapsulation of HLC clusters. Clusters are mixed with alginate in solution, and dripped into a bath containing the gelling agent through controlled release by a syringe. The cations induces alginate gelling and bead formation through cross-linking. Alginate capsules allow diffusion of nutrients, oxygen and substances produced by the cells, while protecting the clusters from host immune responses (adapted from Aljohani et al., 2017)[60].

2.3.1 Functionalization of alginates

To circumvent the issue of pericapsular fibrosis, research has been focused on functionalizing alginate to lower the adverse responses in the host [58, 61]. The foreign body response is an immune-mediated reaction that follows chronic inflammation after biomaterial implantation. The fibrous capsule subsequently forms outside the cellular components of the host FBR, which surrounds the transplanted material [62]. Strategies to avoid or suppress host immune responses or inflammation is therefore of great interest. As alginate is a relatively bioinert substance without sites for cell attachment or communication, functionalization through covalent modification has been explored as a method to increase bioactivity [58].

Heparin is a glycosaminoclycan (GAG) widely used as an anticoagulant, but it has also been recognized as having anti-inflammatory properties [63]. Heparin is made up of units of trisulfated disaccharides, and sulfated GAGs like heparin and heparan sulfate (HS) are the main sources of negative charge and hydration in the ECM, where they protrude from the proteoglycans, the major components

of the matrix [64, 65]. A promising alginate modification for increased bioactivity is chemical sulfation of the free hydroxyl groups of alginate. The increased negative charge from the sulfate groups promotes electrostatic interactions with a range of proteins similar to the protein interactions of the sulfated GAGs [66]. These biomimetic sulfated alginates have been shown to lower, or suppress, inflammatory responses when encapsulating human chondrocytes [12, 67]. This makes the alginate modification a promising option for the prevention of the foreign body response and fibrous capsule formation following transplantation. However, the chemical sulfation of alginate is indiscriminate between the M- and G-units of the alginate polymers. This negatively impacts the gel-forming ability of alginate G-blocks, mainly due to steric hindrance by the bulky sulfate groups [45]. Additionally, chemical sulfation strategies, such as the use of chlorosulfonic acid (HCLSO_3) in formamide, illustrated in Figure 2.5, is highly acidic which results in some depolymerization of the alginate and thus lowering of the average molecular weight. It is therefore necessary to incorporate unmodified alginate in the sulfated alginate to preserve gelling capacity and gel stability when the degree of substitution (DS) of sulfate groups exceeds 40% [12]. Previous research have demonstrated that alginate capsules made from sulfated alginate (DS = 75%) mixed with native alginate in a 20:80 (w/w) ratio, successfully reduced the immune responses in blood samples exposed to the beads compared with native alginate alone [67].

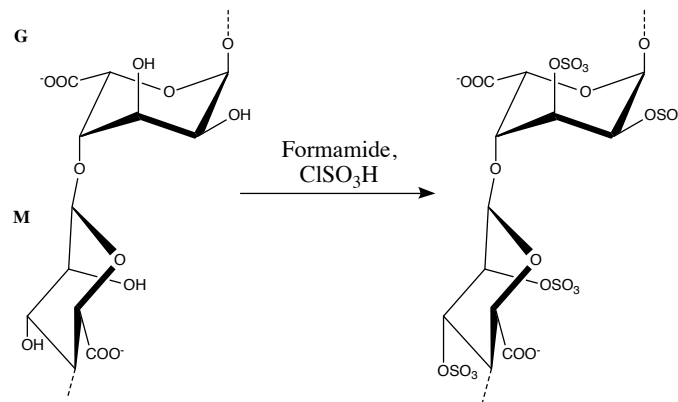


Figure 2.5: Chemical sulfation of alginate. Unmodified alginate (left) can be chemically modified through addition of chlorosulfonic acid (HCLSO_3) in formamide, creating sulfated alginate by the addition of sulfate groups on both the M- and G-units of the polymer (adapted from Smidsrød and Skjåk-Bræk, 2017)[45].

In addition to functionalizing alginates as a means to lower the fibrotic response, it could also improve cell attachment, maturation, and survival of the encapsulated cells. Anchorage-sensitive cells such as the parenchymal cells of the liver is dependent on ECM-interactions for their development and maintenance of mature functions [68]. Hepatocytes contain asialoglycoprotein receptors (ASGPRs) to remove desialylated glycoproteins from the circulation, and the proteins are recognized by exposed galactose residues, among other ASGP-specific moieties [69]. While the ASGPs are normally internalized by the cells, it has been reported that primary hepatocytes exhibit an ASGPR-mediated adhesion to galactose-modified hydrogels [70]. Alginates functionalized with galactose residues exhibit a

higher degree of hepatocyte attachment, and improved cell function compared with the unmodified hydrogel [13]. An efficient method for creating galactosylated alginates utilizes periodate (NaIO_4) oxidation which opens the ring structure of the alginate monomers, leaving periodate oxidized alginate (POA) with dialdehydes on the reacting carbons [71]. Without an ensuing reduction, the aldehyde groups makes POA susceptible to degradation through alkaline β -elimination even at physiological pH [72]. A subsequent two-step reductive amination first introduces 1-amino-1-deoxy- β -galactose (NH_2Gal) to the solution resulting in the formation of a Schiff base, before reduction with a reducing agent such as picoline borane (pic-BH_3) to a stable secondary amine and reduction of the remaining aldehyde to a hydroxyl group. This creates reduced alginate with a galactose residue connected through an amine group on one of the previously oxidized carbons [58, 73], see Figure 2.6.

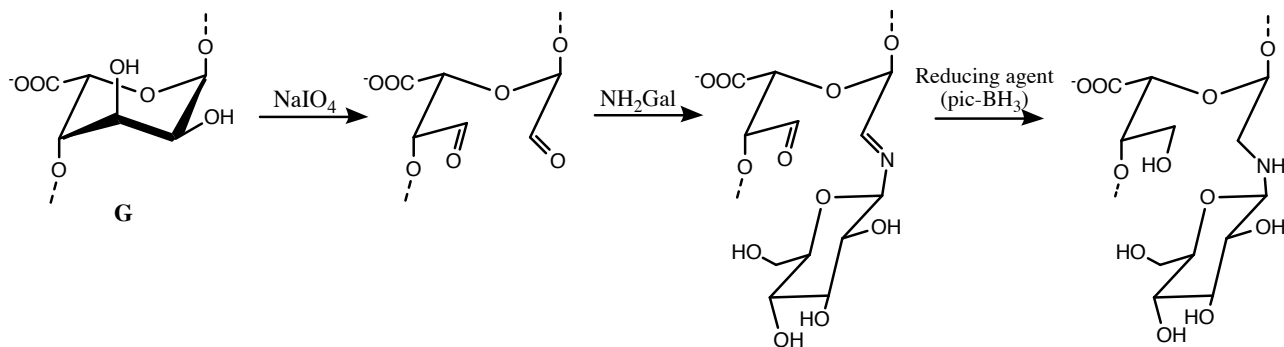


Figure 2.6: Periodate oxidation and reductive amination of alginate. Periodate (NaIO_4) oxidation of alginate opens the ring structure of the polymer subunits and leaves two aldehyde groups. Subsequent introduction of a galactose substituent connected through an amine linkage and reduction of the remaining aldehyde group with the reducing agent (pic-BH_3) to a hydroxyl group creates galactosylated alginate (adapted from Dalheim et al., 2016)[58].

Periodate oxidation is faster on G- than on M-units [74], and breaking the ring structure and subsequent coupling of the galactose residues will therefore happen to a relatively greater number of G-units [58]. Together with a decrease in the molecular weight which is common during periodate oxidation, this leads to a poorer gelling alginate. The opening of the ring structure also causes the otherwise rigid alginate polymer to become more flexible [71]. Mechanical properties of a scaffold material is important for cell growth and differentiation, and different tissues might require different mechanical properties from its scaffold [75]. The changes to the mechanical properties of alginate induced by periodate oxidation might affect various cell types differently, but both mouse myoblasts grown on top of POA [58], and human dermal fibroblasts grown inside POA (Zaitseva-Zotova, unpublished) have demonstrated good cell viability.

3 Materials and methods

3.1 Alginates

Four alginates were prepared for this project, aimed at minimizing fibrosis upon transplantation and providing a beneficial environment in which the cells can mature and perform their function. The base alginates used were unmodified ultra-pure low-viscosity high-G alginate (UPLVG) from *Laminaria hyperborea*, batch number BP-0907-02 (Promega[®]), and ultra-pure moderate-viscosity high-G alginate (UP-MVG), batch number BP-505-01 (Promega[®]). Freeze-dried samples of the alginates were collected for analyses with proton nuclear magnetic resonance (¹H-NMR) spectra and Size exclusion chromatography - Multi-angle laser light scattering (SEC-MALLS) analysis which were performed as previously described [76]. The results are summarized in Table 3.1. A share of the alginates were subsequently functionalized to three types of modified alginates; sulfated alginate, galactosylated alginate and reduced periodate oxidized alginate. All functionalized alginates were mixed with unmodified UPLVG in a 20:80 and a 40:60 ratio prior to the cell encapsulation to create modified alginates of different concentrations that would still be capable of gelling.

Table 3.1 Characterisation of base alginates. The two base alginates used in this work were UPLVG and UPMVG. Fractions of monomers, diads and triads of M- and G-units in the two alginates were determined by ¹H-NMR spectra. Molecular weight (M_w) was obtained by SEC-MALLS analysis.

Name	M_w (kDa)	F_G	F_M	F_{GG}	$F_{GM},$ F_{MG}	F_{MM}	$F_{MGG},$ F_{GGM}	F_{MGM}	F_{GGG}	$N_{G>1}$
UP-LVG	237	0.68	0.32	0.57	0.11	0.21	0.04	0.07	0.53	16
UP-MVG	235	0.66	0.34	0.55	0.12	0.22	0.05	0.09	0.50	13

3.1.1 Functionalization of alginates

Galactosylation of alginate was achieved through a previously described protocol for oxidation and reductive amination [58]. From the same batch of UPLVG, periodate oxidized alginate (POA) was produced. Sodium (meta) periodate ($NaIO_4$) was used as the oxidizing agent to create partially oxidized alginate with an 8% degree of oxidation. All work with periodate took place in the dark as the substance is unstable and can form free radicals, especially in the presence of light [71]. The unmodified starting material was dried out in a desiccator to achieve a higher accuracy of alginate concentration, before the alginate was dissolved in MilliQ (mQ) water. 10% (v/v) 1-propanol was then added to the solution as a free radical scavenger, before it was degassed using N_2 to remove

oxygen. A 0.25 M stock solution of periodate was also degassed as an additional precaution against the formation of free radicals. The alginate solution was cooled to 4°C before the periodate was added in a 0.08:1 molar ratio of periodate per 1 alginate monomer to achieve an 8% degree of oxidation. The periodate ions (IO_4^-) reacts with the alginate, which results in cleavage of the C2-C3 bond. This leaves an aldehyde group at both the C3 and C2 carbon. Lastly, the alginate solution was dialyzed to 0.05 M NaCl in mQ water in Labs Spectra/Por™ 5 12-14 kD MWCO Standard RC (Spectrum™) dialysis tubes until conductivity was measured using a conductometer to less than 2 μS . The resulting structure was POA, and $^1\text{H-NMR}$ analysis confirmed that oxidization had taken place. $^1\text{H-NMR}$ spectra from analyses of functionalized alginates are displayed in Appendix A.

The POA was subsequently used as the starting material for the production of three modified alginates. A 6 mg/mL stock solution of POA was made by dissolving the alginate in mQ water, before adding 12% (v/v) of methanol (MeOH) to act as a solvent. Two parallel reactions then took place, as two stock solutions of two amine-coupled substituents were made. 1-amino-1-deoxy- β -D-galactose (GalNH_2) and 4-aminophenyl β -D-galactopyranoside ($\beta\text{NH}_2\text{PheGal}$) were each dissolved in mQ water to stock solutions of 0.05 M. The substituent solutions were subsequently added to two parallel POA-MeOH stock solutions, for a final concentration of 2.42 mM. One reaction then resulted in oxidized alginate with a galactose substituent connected to carbon C3 through the amine group. The parallel reaction resulted in a galactose substituent connected through a phenyl ring and amine group to carbon C3, thus mimicking the first reaction. The phenyl group is detectable through $^1\text{H-NMR}$ analysis and can therefore give an approximate of the degree of substitution (DS) of galactose alginate in the first reaction. GalNH_2 - and $\beta\text{NH}_2\text{PheGal}$ -coupled oxidized POA was then reduced along with a third POA-MeOH stock solution through the addition of a 250 mM stock solution of picoline borane (pic-BH_3), for a final concentration of 24.24 mM. All three alginate solutions were subsequently pH-adjusted to pH 5.8, before the addition of mQ water to a final POA concentration of 3 mg/mL. The reactions were left to incubate on a shaker for 72h. This resulted in reduced POA (POAred), POAred-Gal (Gal-Alg), and a phenyl-containing control for Gal-Alg. All alginates were then dialyzed for two shifts against 0.05 M NaCl before dialysis against mQ water until conductivity was measured to below 2 μS . Lastly, the alginates were freeze dried and stored for use. A sample of each alginate type was harvested for SEC-MALLS analysis, while the phenyl-containing control for Gal-alg was also taken for $^1\text{H-NMR}$ analysis. Results are summarized in Table 3.2.

Sulfation of the alginate was performed as previously described [66]. The starting material was UP-MVG, and it was transferred to formamide (HCONH_2), before chlorosulfonic acid (ClSO_3H) was added to the suspension in a 3% (v/v) ratio for a DS of approximately 75%. The acid was added slowly to reduce adverse events like smoke formation, before the suspension was placed in a water bath (60°C) to dissolve and react. Acetone was added for alginate precipitation, before centrifugation (4700 rpm, 7 minutes, 10°C) and removal of supernatant. The alginate was subsequently transferred

to mQ water, and pH was adjusted to pH 7. Lastly, the alginate solution was dialyzed to mQ water until conductivity was measured to less than 2 μ S. The alginate was subsequently freeze dried, before the actual degree of substitution was determined by inductively coupled plasma mass spectrometry (ICP-MS) analysis, and the M_w after chlorosulfonic acid exposure was determined by SEC-MALLS analysis. Results are summarized in Table 3.2. The lower M_w and high DS resulted in a less viscous alginate than the starting material.

Table 3.2 Characterisation of functionalized alginates. The three functionalized alginates used for cell encapsulation in this project are listed below. Degree of substitution (DS) of the covalent modification was determined by 1 H-NMR spectra and ICP-MS analysis. Molecular weight (M_w) was obtained by SEC-MALLS analysis. *determined by DS analysis of phenyl-Gal-Alg.

Name	M_w (kDa)	DS (%)
POAred	93	-
Gal-Alg	127	8.1*
S-Alg	163	80

The modified alginates were coal filtered to remove any impurities, and freeze-dried for storage. Before the experiments, all alginates were dissolved in sterile water and 0.3 M mannitol to a final concentration of 2.0% (w/v) alginate. The solutions were then pH-adjusted to physiological pH, and subsequently sterile filtered using a 0.22 μ m filter (Corning) to eliminate microbial contamination. Mannitol was used in all solutions to create a favorable osmolarity for cell growth.

3.2 Cell Culturing

Human induced pluripotent cell (hiPSC) line A1ATD^{R/R} and human embryonic stem cell (hESC) line H9rtTa-AAVS1-136R were cultured and induced to differentiate into hepatocyte-like cells (HLCs). Cell line A1ATD^{R/R} is derived from biopsied somatic cells from patients with α_1 -antitrypsin deficiency (A1ATD) and induced to hiPSCs [77]. The point-mutation responsible for A1ATD was subsequently corrected, resulting in A1ATD^{R/R} [78]. hES cell line H9rtTa-AAVS1-136R has been genetically engineered for forward programming (FoP)(Tomaz et al, unpublished). The cell line was constructed for the constitutive expression of a reverse tetracycline-controlled transactivator (rtTA) on the ROSA26 locus and a TRE-dependent expression of the transcription factors (TFs) HNF1 α , FOXA3, HNF6 and RORc on the AAVS1 locus, which is induced by the presence of doxyxycine (Dox). This combination of factors has been shown to generate cells with an hepatocyte-like identity after 15-20 days.

Both pluripotent cell lines were seeded on 6-well plates (Falcon[®]) coated for at least 1 hour with 10 μ g/mL Vitronectin XFTM in phosphate-buffered saline (PBS, Gibco[®]), with a growth area of 9.5 cm²

per well. The cells were fed daily with Essential 8 media (E8), which is a growth media supplemented with eight essential components for the growth of PSCs [79]. Dulbecco's Modified Eagle Medium/Nutrient Mixture F-12 (DMEM/F-12, 500mL, Gibco®) is supplemented with Insulin-Transferrin-Selenium solution (10 mL, Gibco®), Penicilin/Streptomycin (5 mL), L-Ascorbic acid 2-Phosphate (5mL, Sigma-Aldrich), and sodium bicarbonate (3.6mL, Gibco®). This basal media of 6 components (E6) was filtered using a 0.22 µm filter system (Corning), and dispensed into polycarbonate storage bottles (Corning). Prior to cell feeding, the media was also supplemented with Transforming growth factor β (TGF-β, 2 ng/mL) and Fibroblast growth factor 2 (FGF2, 25 ng/mL) (E8), for a total of eight essential components. The cell cultures were incubated at 37°C and 5% CO₂.

When the wells achieved an approximate confluence of 70-80%, they were routinely passaged to ensure the continued health of the cells. The cells were incubated for 2-5 minutes in 0.5 mM Ethylenediaminetetraacetic acid (EDTA, Gibco®) in PBS. EDTA chelates divalent cations such as Ca²⁺ which acts in cell-cell and cell-matrix interactions [80], thus weakening the attachments of the adherent cells to the plate. This allowed the cells to be collected with E8, before cell clusters large enough to sediment was diluted and replated in vitronectin coated 6-well plates. The dilution varied with confluency of the passaged well and time of next splitting.

3.3 Cell differentiation

As the cells were passaged for maintenance, 90% confluent wells were also chosen for hepatocyte differentiation (HD). Dead cells were removed through washing with PBS, and Accutase treatment caused the cells to loose their detachment to neighbouring cells and the wells through proteolytic and collagenolytic enzymes [81], creating single cells or small clumps. The cells were subsequently collected with E6 and spun down at 1200 rpm for 3 minutes. Following resuspension in E8, an aliquot of 10µL was collected from the cell solution, and mixed with 10 µL TrypanBlue. 10 µL of the mix was transferred to a chamber slide, and cell number estimated using Countess™ II Automated cell counter (Life Technologies™). Based on the desired seeding confluence (cells/cm²) for each HD (generally 30 000-60 000 cells/cm² well area), the measured cell number was used to calculate the amount of cell suspension to be plated for each differentiation. Seeding confluence was determined by the observed speed of proliferation of the hPSCs, as this was observed to decrease with higher passage numbers.

The calculated number of cells were subsequently seeded on 12-well plates (3.8 cm², Falcon®) coated with gelatine (0.1%) and murine embryonic fibroblast (MEF) solution. MEF media consists of Advanced DMEM F12 (450 mL, Gibco®) supplemented with fetal bovine serum (50 mL, Gibco®), L-glutamine (5 mL), Pen/Strep solution (5 mL) and β-Mercaptoethanol (3.5µL) with subsequent filtration with 0.22 µm filter (Corning). The cells were cultured in E8 supplemented with Rho kinase (ROCK, Y27632) inhibitor for one day (day -1), and in pure E8 the day after (day 0). The following

day marked day 1 one of the differentiation, and the point at which the treatment of the two cell lines diverged.

3.3.1 Direct differentiation of A1ATD^{R/R}

Cell line A1ATD^{R/R} was differentiated to HLCs as previously described [38], see Figure 3.1, and moved to 37°C in hypoxic conditions (5% oxygen, 5% CO₂). The media was changed at the same time point every day until the cells entered the foregut stage at day 4 of differentiation. At day 1 and 2 the cells were cultured in chemically defined media supplemented with polyvinyl alcohol (CDM-PVA) consisting of F12 Nutrient Mix (250mL, Gibco[®]) and Iscove's Modified Dulbecco's Medium (IMDM, 250 mL, Gibco[®]). This basal media mix was supplemented with Chemically defined lipid concentrate (5 mL, Gibco[®]), Pen/strep solution (5 mL), Insulin (350µL), Transferrin (250 µL), 1-Thioglycerol (20 µL), and PVA (0.5 g). The media was subsequently filtered through a 0.22 µm filter (Corning). Prior to feeding, the media was also supplemented with Activin (100ng/mL), FGF2 (80ng/mL), BMP4 (10ng/mL), LY294002 (10µM) and CHIR99021 (3µM, day 1 only). From day 3-8, daily media change continued with Roswell Park Memorial Institute (RPMI, 480mL, Gibco[®]) media supplemented with Non-essential amino acids (NEAA, 5 mL, Gibco[®]), Penicillin-streptomycin (5 mL) and B-27 supplemented with insulin (10 mL, Gibco[®]). TFs were added prior to feeding, with Activin (100ng/mL) and FGF2 (80ng/mL) added on day 3, and Activin (50ng/mL) alone on day 4-8. At day 9 the cells have stopped proliferating and were therefore fed every other day till end of experiment with HepatoZYME-SFM (470mL, Gibco[®]) supplemented with Chemically defined lipid concentrate (10 mL), NEAA (10mL), Penicillin-Streptomycin (5mL), L-Glutamine (5mL), Insulin (700µl) and Transferrin (500µl), making HepatoZYME-SFM complete without transcription factors (HPZ-OH). Prior to feeding, Hepatocyte growth factor (HGF, 50ng/mL) and Oncostatin M (OSM, 20ng/mL) was added to the media (HPZ+OH).

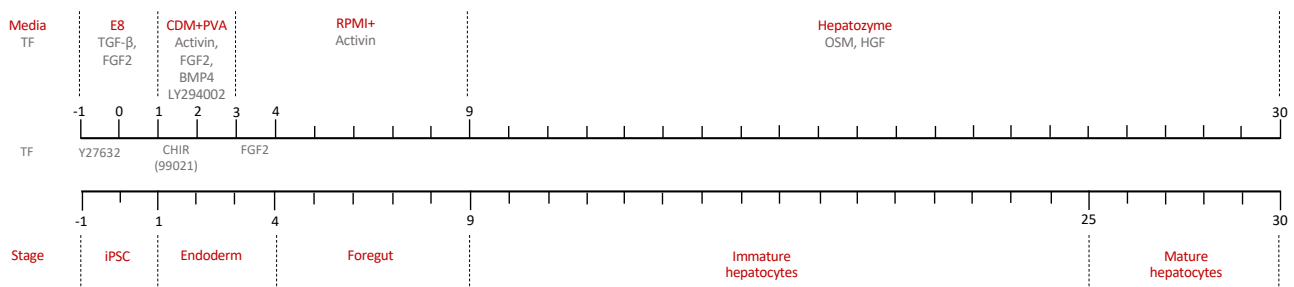


Figure 3.1: Set-up and stages of direct differentiation of human induced pluripotent stem cell line A1ATD^{R/R} to HLCs. The protocol describes a differentiation over 30 days. TF = Transcription factor. (adapted from Hannan et al., 2013)[38].

3.3.2 Forward programming of H9

Cell line H9rtTa-AAVS1-136R is genetically modified for differentiation by forward programming to HLCs (Tomaz et al. unpublished). The cells are engineered to bypass all the normal stages of differentiation. The initial transgene induction occurs over a 24h period in E6 supplemented with Dox 1:2000. Induced cells are then fed with HPZ+OH supplemented with Dox 1:2000 every day up to day 5, and every other day from day 5 onward, see Figure 3.1. The differentiation is conducted without direct lighting and all media is wrapped in foil, as Dox is light-sensitive.

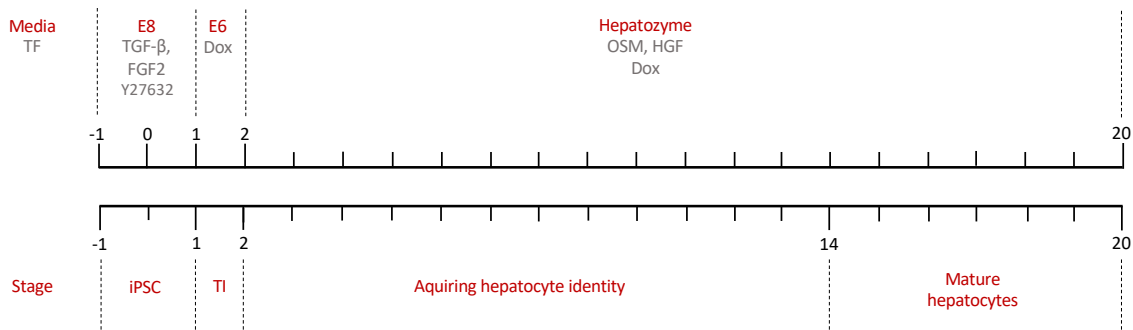


Figure 3.2: Set-up and stages of forward programming differentiation of genetically engineered H9 hP-SCs to HLCs. The protocol takes 20 days. TF = Transcription factor, TI = Transgene induction (adapted from Tomaz et al., unpublished).

3.4 Immobilization of cells in alginate capsules

As the HLCs generated by the two methods approached maturity, they were encapsulated using identical techniques. At full maturity, the cells adhere too strongly to the culture plates to be removed from the wells easily. The HLCs generated by direct differentiation and by forward programming were therefore harvested for encapsulation on day 24 and 15, respectively. A few wells of HLCs from both cell lines were kept in 2D and allowed to continue growth. The dissociation of the 2D cell layer from the wells was achieved by washing the wells with PBS, before Hanks'-based enzyme-free cell dissociation buffer (Gibco[®], Life Technologies[™]) was added to the cells. Optimization trying several exposure times (15, 8 and 5 minutes) revealed that incubation at 37°C for 8 minutes in the buffer gave cells readily removed from the plates, without creating too small cell clumps. Using the tip of a 5mL stripette, the cells were scraped off the wells and cells and buffer were collected in HPZ-OH to dilute the buffer. The cells were spun at 1200 rpm for 3 minutes, and the supernatant was removed. After resuspension in 1 mL of HPZ-OH, the cells were allowed to sediment before the supernatant was aspirated to remove any single cells and small cell clumps. The clumps were resuspended again, broken up by pipetting with P1000 three times, before the largest clumps were allowed to sediment. While the supernatant still contained medium-sized clumps, it was collected into another tube for use in the

encapsulation. These steps were repeated until all clumps reached a size suitable for encapsulation. Generation of appropriate clump size was optimized by varying amount of pipetting and by aspirating the first two supernatants.

All the supernatants were pooled and spun at 1200 rpm for three minutes, before resuspension in HPZ+OH. The clumps were loaded onto a chamber slide and cells counted as described in section 3.3. As approximately 4.5×10^6 cells were generated by direct differentiation when using 9 wells of a 12-well plate to leave 3 wells for 2D growth, it was decided to encapsulate that cell number across all conditions. The calculated amount of cell clump suspension was then spun again at 1200 rpm for 3 minutes before resuspension in approximately 120 μ l HPZ+OH for a total cell suspension volume of 150 μ l. This was inserted into a syringe (5 mL, Plastipak™) containing 1.35mL 2.0% alginate solution, for a final alginate concentration of 1.8%. This gave 3 million cells/mL.

3.4.1 The capsule generator

The capsules generator was built by the mechanical workshop at the Department of Physics at NTNU. It consists of a protective cage surrounding the podium for the beaker collecting the alginate capsules and an autoclavable needle holder. It also has a 10kV power supply with an automatic safety switch and an adjustable voltage meter for selecting the applied voltage [82].

The strategy for encapsulation of HLCs was adapted from previously described protocols for the encapsulation of pancreatic islets [83, 84]. All reusable equipment was autoclaved before use. The syringe was placed vertically with 0.8 mL air above the alginate solution in a single-syringe infusion pump (74900 series, Cole Parmer), in which the calculated inner diameter of the syringe (12.07 mm) and the speed of infusion (mL/h) was plotted. The syringe was also connected through a tube to a needle (Staedler) with a 0.35 mm tip inserted in the needle holder of the bead machine. The high voltage source provided by the machine creates an electric field between the needle through which the alginate solution escapes and the gelling solution approximately 2 cm below, see Figure 3.3. The gelling solution used was pH adjusted to pH 7.3-7.4, consisted of CaCl₂ (50mM), BaCl₂ (1mM), Hepes (10mM) and mannitol (0.15M) in sterile water, and it was placed on the podium of the machine, over a magnetic stirrer. After adjusting the voltage of the bead machine, the syringe pump and electric field provided a steady release of droplets into the gelling bath where the alginate was allowed to gel all the way through for 10 minutes after the last droplet fell. The resulting alginate capsules sedimented, and the gelling solution was discarded. The capsules were subsequently washed twice with washing solution consisting of CaCl₂ (2mM), NaCl (0.9%) and Hepes (10mM) in sterile water, and pH adjusted to pH 7.3-7.4. Lastly, the beads were washed with HPZ-OH. The beads containing HLCs generated by direct differentiation were resuspended in HPZ+OH, while beads containing HLCs generated by forward programming were resuspended in HPZ+OH supplemented with Dox. The suspensions were plated in 12-well plates and stored at 37°C in hypoxic conditions. Fresh media

was added to the beads on the second day, before a media change on the third day.

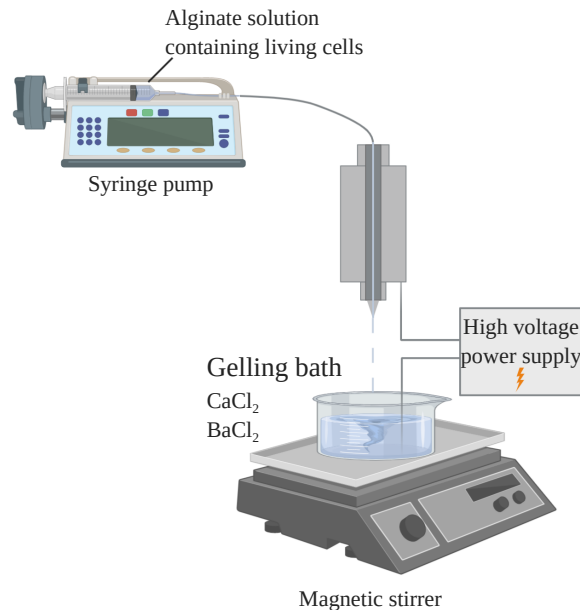


Figure 3.3: Formation of ionic cross-linked alginate beads using a capsule generator. The power supply is connected to both the needled tip and the gelling bath containing the divalent gelling agents, thus pulling the droplets of alginate and cell solution through the nozzle. A syringe pump ensures a steady release of alginate solution, while the magnetic stirrer provides movement of the gelling solution to ensure that the beads do not sediment until they have gelled all the way through (modified from Strand et al., 2002)[82].

3.4.2 Capsule characterisation

Every batch of alginate capsules produced were imaged on the day of encapsulation, and day 6 post encapsulation, with a light microscope (AxioCam MR3, Zeiss). Using ImageJ, the average size was determined by measuring the diameter of 30 beads. This allowed for monitoring of any swelling or shrinking resulting from suspension in the culture media. Outliers in capsules diameter was removed from the average and counted as irregularities, along with the percentage in 30 beads of ellipse-formed capsules and tailed capsules.

3.5 Functional analyses of encapsulated cells

To study how the alginate affects the encapsulated HLCs, functional analyses were performed on the 3D cultures and the corresponding 2D wells on several timepoints. HLCs generated by direct differentiation were assayed for viability and enzymatic activity on day 27, 30 and 33 of differentiation, see Figure 3.4 (A). RNA was extracted for gene expression analysis on day 0, 24, 30 and 33 of differentiation, while a live/dead assay was performed on day 30 of differentiation. HLCs generated by forward

programming were assayed for viability and enzymatic activity on day 20 and 27 of differentiation. RNA was extracted on day 0, 15, and 20 of differentiation, while live/dead staining was performed 24 hours after encapsulation and on day 20 of differentiation (B). Viability and enzymatic activity measurements were performed on the same well at each time point, as the cell number can vary after plating of the cell suspension.

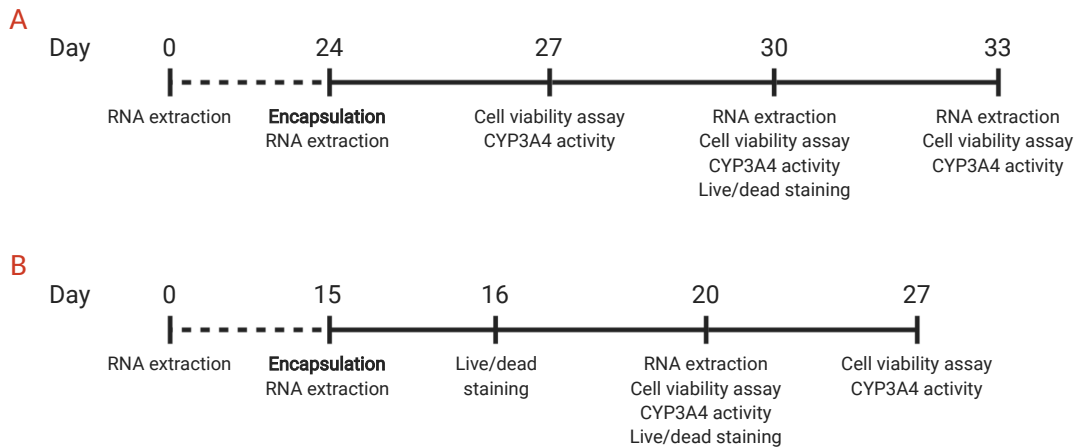


Figure 3.4: Experimental timeline of functional and genetic assays. The experimental timelines of assays performed for HLCs generated by direct differentiation (A) and forward programming (B) indicates the assays performed and samples harvested on different days of the differentiation.

3.5.1 Live/dead staining

To determine the survival of cells in the capsules, a single-step live and dead kit that differentially labels live and dead cells was used. Live and Dead Cell Assay (abcam[®]) exploits two of the indications for live and viable cells, which are enzymatic activity and an intact plasma membrane. Calcein-AM is membrane-permeant and turns fluorescent with emission-max at 515 nm (green) due to esterase activity in the intact and live cells. Ethidium Homodimer-1 (EthD-1) is not membrane-permeant, and increases its fluorescence at 617 nm (red) more than 30-fold when bound to DNA, and will thus only fluoresce when the cell membrane is compromised [85].

The stock concentration of the one-step dye mix is 1000x, and should be used at 5x for staining of immobilized cells [85]. 2.5µl stock solution was therefore mixed with 500µl of growth medium, and applied to a small sample of the encapsulated cells for 10 minutes. The cells were immediately visualized and the fluorescence was detected with the FITC filter (green) and the TRITC filter (red) using an inverted fluorescent/brightfield microscope (AxioCam MR3, Zeiss).

3.5.2 Cell viability

To measure any changes in cell viability over time due to encapsulation, a cell viability kit that utilizes the reducing environment of viable cells was used on both 3D and corresponding 2D cultures. Presto-Blue™ HS Cell Viability Reagent (Invitrogen™) is a one-step viability kit containing a resazurin-based reagent. Resazurin is cell-permeant, and the reducing environment of living cells reduces resazurin to the highly fluorescent red resorufin [86]. The color change can be detected measuring absorbance or fluorescence.

The stock solution was diluted 1:10 in HPZ+OH media, and left on the cells in the 2D and 3D cultures for 1 hour at 37°C incubation along with a negative control. The media and negative control was subsequently pipetted in triplicate using an electronic multi-step pipette onto a black Falcon™ 96-Well Imaging Microplate with Lid (Corning™). The plate was inserted into a 2104 EnVision® Multilabel Plate Reader (Perkin Elmer), and the fluorescence was detected through excitation at 531nm and emission at 590nm. The average fluorescence of the negative control was subtracted from the measured fluorescence (relative fluorescence unit, RFU) of the samples to remove any background fluorescence. Lastly, the RFU of each sample was normalized to the RFU value of the 2D culture on the first day of measurement.

3.5.3 CYP3A4 activity

In addition to continued cell viability, changes in cell function as a result of encapsulation was studied. As one of the major functions of hepatocytes in the liver is to metabolize toxins and drugs, the activity of such drug-metabolizing enzymes is of interest. One of the most important drug-metabolizing enzymes is the Cytochrome P-450 enzyme CYP3A4 [87]. P450-Glo™ CYP3A4 Assay and Screening System (Promega®) is a kit that provides a system for measuring the activity of the enzyme. It contains a substrate for CYP3A4 that is a pro-luciferin, which is converted to a luciferin product by the enzyme. Luminescent D-luciferin is subsequently formed after reactions with a second kit component, the Luciferin Detection Reagent. Measuring the luminescence gives a measure for the activity of CYP3A4 [88].

All work with the kit took place without direct lighting as all the elements are light sensitive. The Luciferin was diluted 1:1000 in HPZ-OH media, and the solution was added to both 2D and 3D cultures and allowed to incubate at 37°C for 1 hour along with a negative control. The Luciferin Detection Reagent was reconstituted with the Reconstitution buffer, which is the last component of the kit. 50 µL reconstituted Detection Reagent was then pipetted in triplicate using an electronic multi-step pipette into a 96-Well White Polystyrene Microplate (Corning™). After the 1-hour incubation, 50 µL of luciferin-media was pipetted into each of the wells containing Detection Reagent before the plate

was wrapped in foil and set to incubate in room temperature for 20 minutes. The plate was subsequently read using GloMax[®] 96 Microplate Luminometer (Promega[®]). The measured luminescence (relative luminescence unit, RLU) from the negative control was subtracted from the measured RLU of the samples. The values were subsequently normalized to RLU per mL media used per measured viability (RLU/mL/RFU) for any particular well and condition. It was normalized to measured RFU because it is difficult to assess cell number in a bead suspension. Lastly, the values were normalized to the 2D value of the first day of measurement.

3.6 Gene expression analysis

Quantitative real-time reverse-transcription PCR (qRT PCR) is a powerful method to measure the gene expression in a sample. The amount of mRNA for any particular gene is a measure of the degree of expression of that gene. The process requires RNA extraction from a cell sample, and a subsequent reverse transcription of the mRNA to complementary DNA (cDNA) allows for PCR amplification of the constructs [89].

3.6.1 Dissolution of 3D capsules

To harvest RNA from alginate capsules, it was necessary to first dissolve them to release the immobilized cells. A protocol for dissolution of alginate capsules was set up testing calcium-chelating EDTA at three concentrations (50mM, 75mM and 100mM) on unmodified alginate capsules. All three EDTA solutions were pH-adjusted to 7.5, as this is the pH at which EDTA is available for bond formation with the divalent cations [90], and subsequently applied to empty capsules after washing twice with PBS. The EDTA-bead suspensions were transferred to 15mL Falcon tubes and placed in a water bath at 37°C. Intermittent pipetting using P1000 to apply mechanical disruption gave dissolved beads after 5 minutes of exposure to 75mM EDTA. After treating alginate capsules containing HLCs with 75mM EDTA and mechanical disruption at 37°C, the dissolved alginate/EDTA solution was spun down at 1200rpm for three minutes. The supernatant was discarded, while the cells in the pellet were resuspended in PBS before being spun down again at 1200 rpm for three minutes. This left a clean HLCs pellet.

3.6.2 cDNA synthesis

To extract RNA from cells from the 3D cultures and the corresponding 2D cultures, GenElute[™] Mammalian Total RNA Miniprep Kit (Sigma-Aldrich) was used. 250 µL of the provided lysis solution was used to lyse the cells before 250 µL clean 70% ethanol was added to the lysates and mixed thoroughly

by pipetting. The mix was transferred to a nucleic acid-binding column in a collection tube. The tube was spun at max speed for 30 seconds, and the flow-through in the collection tube was discarded. 250 μL of Wash Solution 1 was added to the columns to wash away impurities and centrifuged again (max speed, 30 seconds). A mix of DNase Digest Buffer (70 μL) and Deoxiribonuclease I (10 μL) was added to each column and set to incubate at room temperature for 15 minutes. An additional 250 μL Wash Solution 1 was added to the columns before centrifuging at max speed for 30 seconds. The flow-through was discarded before 500 μL of ethanol-containing Wash Solution 2 was added to the columns to remove salts and spun down (max speed, 30 seconds). This step was repeated once, before an additional round of centrifuging at max speed for 2 minutes to remove all traces of alcohol. The nucleic acid binding columns were subsequently moved to a clean collection tube before 50 μL Elution solution was added to each column. The tubes were centrifuged (max speed, 1 min), leaving the RNA in the flow-through in the collection tubes [91].

RNA and all reactants were kept on ice at all times to avoid RNA and enzyme degradation. Quantification of RNA was performed using NanoDrop 1000 Spectrophotometer (Thermo Scientific), calibrated with Elution solution. The results (ng/ μL) were used to calculate the volume of each RNA sample needed to give 500 ng RNA per reverse transcription reaction. The calculated volume of each sample was added to 200 μL tubes along with Nuclease Free Water (Invitrogen™) to a final concentration of 11.8 μL . 0.5 μL Random Primers (Promega®) was added to the tubes, as the random primers will prime from different parts of the RNA constructs. Lastly, 1 μL dNTP Mix (Promega®) was added to the mix to provide free nucleotides for cDNA synthesis. The tubes were spun down and incubated for 5 minutes at 65°C using a DNA Engine Tetrad® 2 (Bio-Rad) thermal cycler to denature the RNA and random primers, before the tubes were placed back on ice and spun down.

For the reverse transcription of RNA to cDNA, a master mix was made with all the necessary components. For each RNA sample these included 4 μL 5X First Strand Buffer (Invitrogen™), 2 μL 0.1M Dithithreitol (DTT, Invitrogen™), 0.5 μL RNaseOUT™ Recombinant Ribonuclease Inhibitor and 0.2 μL SuperScript™ II Reverse Transcriptase (Invitrogen™), for a total of 6.7 μL master mix per RNA sample. After addition of the master mix, the tubes were spun down, vortexed, and spun down again. The tubes were placed back in the thermal cycler with a program of 25°C for 10 minutes, 42°C for 50 minutes and 70°C for 15 minutes. Samples with 500ng RNA starting material, was subsequently diluted to 600 μL with Nuclease Free Water.

3.6.3 qRT-PCR

Master mixes were also made for quantitative PCR with all the components necessary for each gene to be tested. Per sample these included 0.8 μL primer mix (forward+reverse primer) for a specific gene (Appendix B), 1.2 μL Nuclease Free Water, and 5 μL KAPA SYBR® FAST Rox™ Low (Roche)

dye. The primers chosen were specific for genes expected to change as a result of differentiation, as well as for housekeeping genes that was set as a reference for expression increase or decrease. 7 μL of the mastermixes was pipetted into rows of an Applied Biosystems™ MicroAmp™ Optical 384-Well Reaction Plate (Thermo Fisher) using an electronic multiple dispenser pipette. The number of wells of each row corresponded to a duplicate reaction for every sample and a duplicate for a negative control. 3 μL cDNA from each sample was subsequently pipetted in duplicate on each row of primer master mixes on the plate using an electronic multiple dispenser. The negative control wells only contained master mix to check for contaminants. An Optical Adhesive Cover (Thermo Fisher) was applied to the top of the plate to avoid liquid evaporation during the PCR reaction, before the plate was centrifuged using an Axygen plate centrifuge. The quantitative PCR was subsequently performed using Applied Biosystems™ QuantStudio™ 5 Real-Time PCR system (Thermo Fisher) on a program with 40 cycles of 95°C (5 seconds) and 60°C (30 seconds).

The fluorescent dye SYBR green added in the master mix binds to the PCR products, and the numbers of amplification cycles needed to achieve a threshold fluorescence reflects the start amount of cDNA for a particular transcript. In addition, a reference dye (ROX) is included in the SYBR reagent to allow for normalisation of pipetting errors [92]. The threshold set in this project was 0.2, and the cycle number at which each well of the reaction plate reached the fluorescent threshold was termed the cycle threshold (Ct) value. The average Ct value of the duplicates of the two housekeeping genes were subtracted from the average Ct value of the duplicates of the target genes, which gave the change in expression (ΔCt). To find fold expression change over the expression of the housekeeping genes, $2^{-\Delta\text{Ct}}$ was calculated.

3.7 Immunohistochemical staining

The strategy for immunohistochemical (IHC) staining of encapsulated HLCs was adapted from a protocol for IHC for organoids. The encapsulated HLCs generated by direct differentiation and forward programming were fixed for IHC on day 30 and day 20 of differentiation, respectively. The beads were washed with PBS before the encapsulated cells were fixed in 4% paraformaldehyde (Alfa Aesar™) for 20 minutes at room temperature. The samples were washed twice with PBS and stored at 4°C.

The staining was conducted in eppendorf tubes. The fixed cells were incubated for three hours in 10% donkey serum (Bio-Rad) in PBS and 0.1% Triton to permeabilize the cells. Donkey serum was used to block unspecific binding, as that is the species the secondary antibody was raised in. The primary antibody, polyclonal rabbit anti-human A1AT (Dako), was added 1:100 in 1% donkey serum in PBS and 0.01% Triton. The cells were then incubated in the diluted primary antibody overnight at 4°C on a rotating mixer. The primary antibody was subsequently removed, and the cells were washed three times at room temperature for one hour per wash in 1% donkey serum in PBS and

0.01% Triton. The tubes were routinely shaken throughout the washes. After the third wash, the cells were incubated in the secondary antibody, which was Alexa Fluor™ 488 donkey IgG (Invitrogen™) anti-rabbit. The antibody was diluted 1:1000 in 1% donkey serum in PBS and 0.01% Triton. The tubes were wrapped in foil and left to incubate overnight at 4°C on a rotating mixer. The secondary antibody was removed, and the beads were washed three times at room temperature for one hour per wash in 1% donkey serum in PBS and 0.01% Triton while the tubes were wrapped in foil.

To stain the nuclei of the immobilized cells, the beads were incubated with Hoechst diluted 1:1000 in PBS for 30 minutes while wrapped in foil. The samples were then washed twice in 1% donkey serum in PBS and 0.01% Triton, and imaged using a confocal laser scanning microscope (700, Zeiss) with a 20x air objective. The secondary antibody was imaged at 488 nm, and emitted green fluorescence at 525 nm. Hoechst was imaged at 361 nm, and emitted blue fluorescence at 497 nm. The images were inspected and merged using ImageJ.

3.8 Statistical analyses

The diameters of all alginate capsules were measured using ImageJ. Average bead width and the standard deviation of the diameters were calculated in Excel. A standard deviation larger than 10% of the average diameter was deemed too large. The significance of the changes in capsule diameters over time was tested using a two-tailed paired Student's t.test, and considered significant when the p-value was <0.05.

For PCR amplification, a Ct value higher than 35 was considered too high. Any sample with a Ct value higher than 35 was thus considered to be without expression of the target gene. There were two technical replicates analyzed per sample. To ensure proper pipetting had been performed so that the results could be deemed reliable, a difference in Ct between technical replicates of less than 0.5 was attempted. For measurements of CYP3A4 activity and cell viability, two or three biological replicates were performed, with three technical replicates each. All error bars in the plots for cell function and viability and qPCR results are standard deviations of the sample selection. Due to having less than three biological replicates in most of these assays, statistical analysis was only performed on the CYP3A4 activity assay on day 20 of differentiation of HLCs generated by forward programming. Differences was considered significant when the p-value was <0.05.

3.9 *In vivo* work

To study whether encapsulated FoP-derived HLCs can provide a short-term solution to severe liver disease, cell function was studied after encapsulation with the best-performing functionalized alginate and unmodified UPLVG with subsequent transplantation into immunodeficient mice. Protocols

for insertion and extraction of alginate beads from the peritoneal cavity of mice were adapted from previously described protocols [59], and the procedures were performed by Dr Saeb-Parsy (Department of Surgery, University of Cambridge). Each mouse (2 x n=4) was injected with approximately 1 million encapsulated HLCs into the peritoneal cavity. Mice were bled at 24h and eight days after injection, and approximately 30 μ L was collected from each mouse. The mice were culled by cervical dislocation eight days after injection of beads. The peritoneal cavity was opened and beads were flushed and aspirated with a pipette. Blood samples were spun at 1400g for 7 minutes, before the clear serum was collected and frozen for future ELISA analysis of human albumin and A1AT (hAlb and hA1AT) contents. Explanted beads were dissolved and RNA was extracted before samples were frozen at -80°C.

4 Results

4.1 Characterisation of HLCs generated by direct differentiation

The direct differentiation of hiPSCs to HLCs is an established protocol, with well characterized stages of differentiation. The protocol follows the natural lineage of hepatocytes, by differentiating through definitive endoderm and foregut stages before reaching an hepatocyte-like identity. This was observed when differentiating A1ATD^{R/R} cells to HLCs, see Figure 4.1. The cells proliferate rapidly during the endoderm stage, before they take on a triangular shape during the foregut stage. As they become immature hepatocytes, the cells begin to acquire a polygonal shape, which becomes more pronounced at the mature hepatocyte stage.

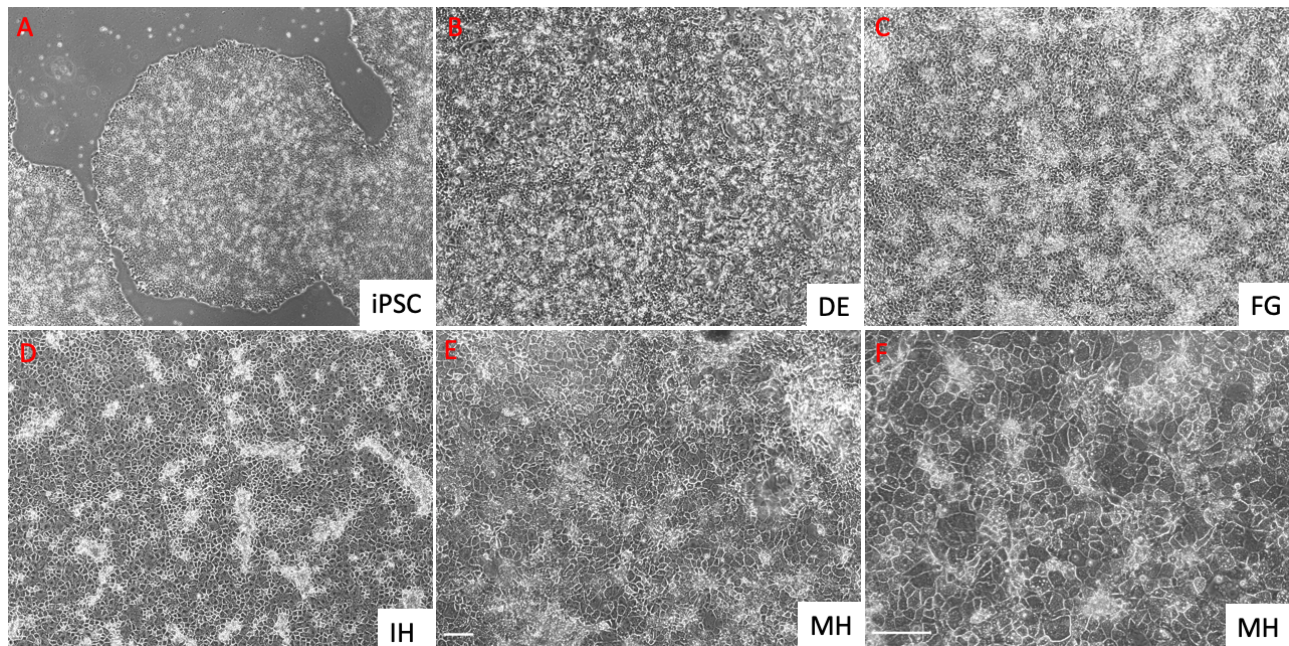


Figure 4.1: Stages of direct differentiation from hiPSCs to HLCs. DE = definitive endoderm, FG = foregut, IH = immature hepatocytes, MH = mature hepatocytes. Scale: 200 μ m.

At the mature hepatocyte stage of direct differentiation the cells also exhibit several hepatocyte characteristics, in addition to the polygonal shape and an increased size. These characteristics include more than one nuclei per cell, see Figure 4.2, as indicated by red arrows. The cells also start accumulating fat in the form of large cytosolic lipid droplets. These were readily visible in the differentiated HLCs, as indicated by blue arrows.

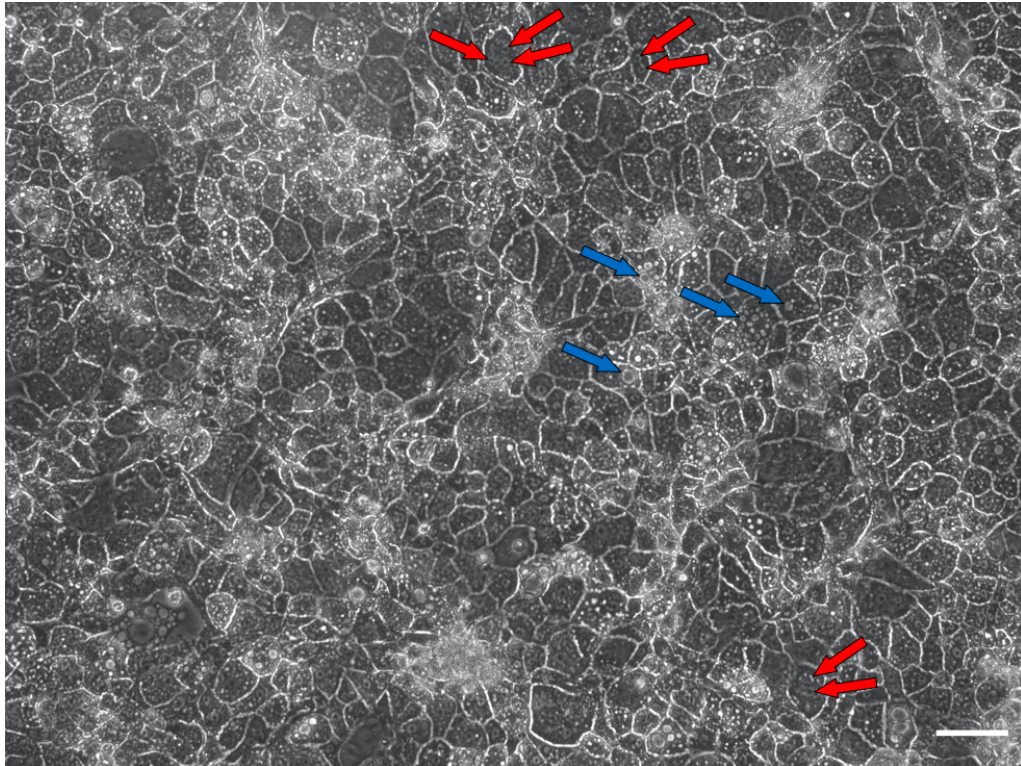


Figure 4.2: Morphology at day 30 of direct differentiation of hiPSCs to HLCs. Several hepatocyte characteristics are visible. More than one nuclei per cell (red arrows) is a common feature, as well as the accumulation of cytosolic lipid droplets (blue arrows). Scale: 100 μ m.

To study the changes in gene expression as a result of the differentiation, quantitative real-time PCR was performed on RNA extracted from the cells at different time points. RNA was also extracted from the pluripotent A1ATD^{R/R} cells to compare the gene expression of differentiated HLCs to their pluripotent progenitors. The gene expression data, see Figure 4.3, revealed that the expression of four essential hepatocyte-specific genes, those for Albumin, α -fetoprotein (AFP), α_1 -antitrypsin (A1AT) and Hepatocyte nuclear factor 4 α (HNF4 α), did change markedly through the differentiation compared with the hiPSCs. This indicates that the direct differentiation of pluripotent stem cells to HLCs was successful. However, it also proved that the quality of the direct differentiation during this project varied considerably between differentiating cell cultures. The expression of albumin, for instance, was approximately 5 times higher in differentiation I compared with differentiation II. The expression of A1AT, meanwhile, was 30 times higher in differentiation I than in differentiation II. The explanation for this discrepancy is unknown, but the starting material of the two differentiations were of different passages (p) of the A1ATD^{R/R} cell line. Differentiation I was split from hiPSCs p14, while differentiation II was split from hiPSCs p29.

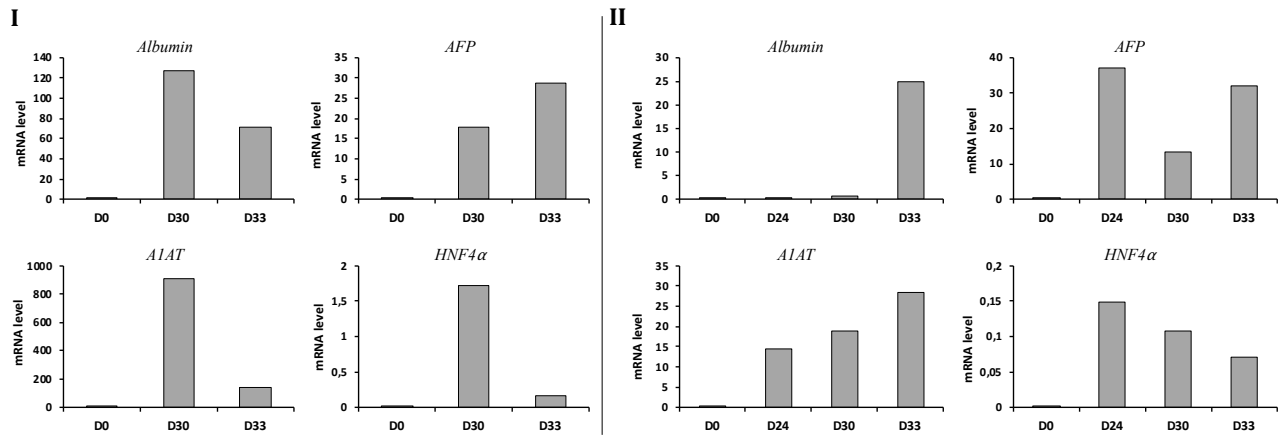


Figure 4.3: Changes in gene expression in HLCs generated by direct differentiation. The expression of each gene increases as a result of the differentiation in HLCs originating from both hiPSCs p14 (I) and p29 (II). mRNA levels were normalised to the average of two housekeeping genes (PBGD, RPLP0). n = 1.

4.2 Alginate encapsulation of HLCs generated by direct differentiation

One part of this project was to optimize the protocol for the creation of HLCs clusters. Optimization was performed using HLCs generated by direct differentiation and they were encapsulated in unmodified UPLVG. By varying time of 2D layer exposure to the cell dissociation buffer and amount of pipetting the cell suspension, HLCs clusters of different sizes were created (Figure 4.4). The cluster sizes in test C in the figure were judged through visual inspection to be appropriate for the cell type. An additional assay measuring the activity of an important liver enzyme to assess the function of the HLCs in clusters revealed a higher function in test C, see Figure 4.4 (II). Some of the HLCs from test B were observed to float around in the cell culture media and was therefore discarded.

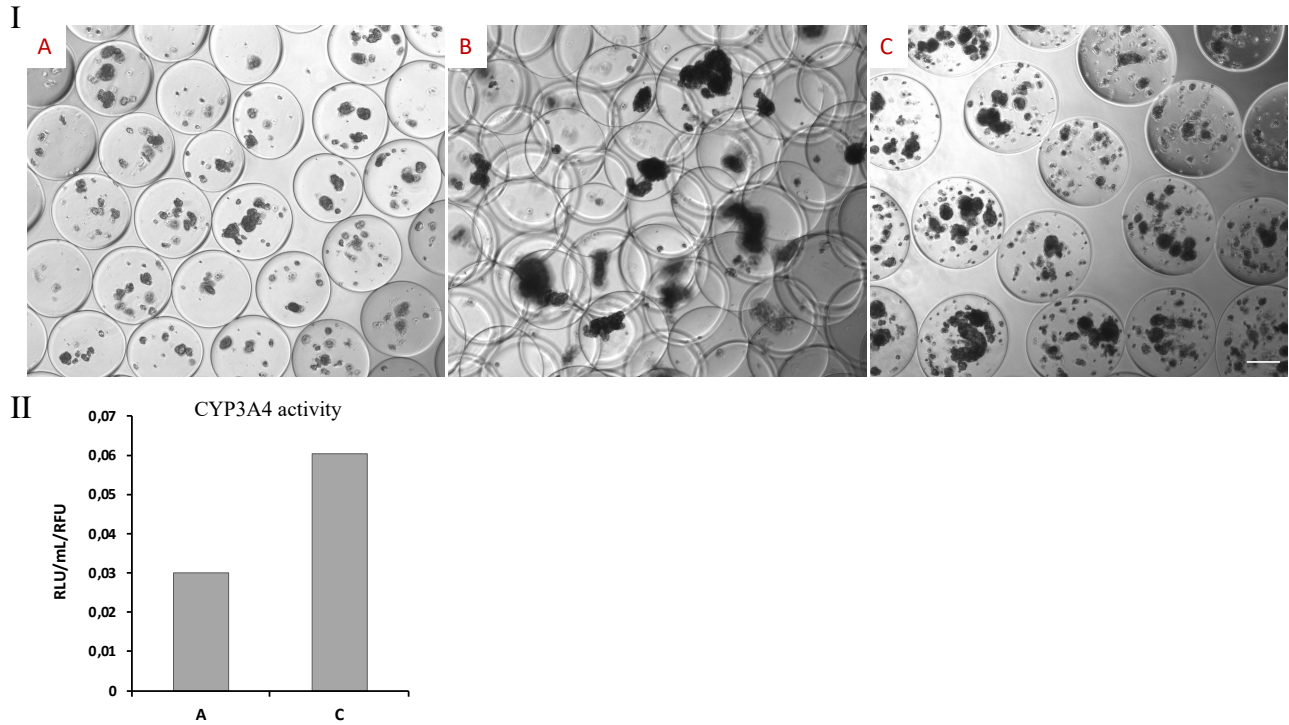
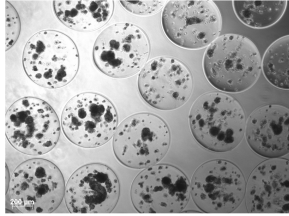
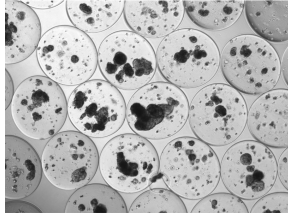


Figure 4.4: Optimization of HLCs cluster size for alginate encapsulation. The three first alginate encapsulations of HLCs generated by direct differentiations were used to optimize the protocol for dissociation of the 2D layer, HLC clump size and encapsulation. The first encapsulation (A) had clumps that were judged to be too small for survival and to retain function. The second batch of capsules (B) contained too large clumps that clogged the needle tip and were thus washed away, while the third try (C) succeeded in creating clumps with appropriate sizes. Scale: 200 μ m (I). Measured CYP3A4 activity normalized to the viability of the encapsulated cells (RFU) shows a higher cell function in test C than A. HLCs from test B were discarded (II).

After optimization, the encapsulation of the two different direct differentiations of HLCs generated capsules of uniform sizes (see Table 4.1), with applied voltage 7.0kV and a syringe pump flow rate of 10 mL/h and 9 mL/h. The lowering of the flow rate lead to an increased number of slightly ellipse formed capsules that were somewhat larger. Encapsulation procedure, number of encapsulated cells, and alginate pH was otherwise identical between the two encapsulations. Six days after encapsulation (day 30 of differentiation) the measured diameter of the beads had changed from $573 \pm 23 \mu\text{m}$ and $600 \pm 26 \mu\text{m}$ to $569 \pm 18 \mu\text{m}$ and $590 \pm 27 \mu\text{m}$, respectively. Using a two-tailed paired t.test, these differences were deemed insignificant ($p > 0.05$), and can thus be explained by a difference in sample selection. The unmodified alginate beads were therefore stable in the cell media. Any differences in encapsulated HLCs performance was thus judged to not be caused by the encapsulation procedure or storage conditions.

Table 4.1 Characterisation of unmodified UPLVG capsules. The two batches of alginate encapsulations contained HLCs generated by two direct differentiations. 30 beads were assessed in each batch on the day of embedding. Size is diameter mean \pm SD.

Unmodified Alginate		
Alginate capsule		
Size (μm)	573 \pm 23	600 \pm 26
Irregularities		
Total	6.7%	36.7%
Ellipse formed	3.3%	33.3%
Tails	-	-
Flow rate (ml/h)	10.0	9.0
Applied voltage (kV)	7.0	7.0
Alginate pH	7.20	7.20
Number of cells (million)	4.5	4.5

4.2.1 Gene expression analysis of encapsulated hiPSCs-derived HLCs

To see the effect of alginate encapsulation on HLCs generated by direct differentiation, it is interesting to study the change in gene expression of encapsulated cells compared with the cells left to grow in 2D. Samples from day 30 and 33 of differentiation, in addition to a sample from the day of encapsulation (differentiation II), gave conflicting answers after qPCR analysis. As shown in Section 4.1, the two rounds of direct differentiations yielded HLCs of very different quality, and the two differentiations gave rise to encapsulated HLCs of similarly diverging levels of expression, see Figure 4.5. Encapsulated cells from differentiation I displayed an even greater expression of albumin than the 2D culture on day 33, while expression decreased for A1AT and HNF1 α in encapsulated cells. However, the lower level of expression still exceeded that of encapsulated HLCs from differentiation II many fold. These cells, meanwhile, displayed an increased expression of the same two genes compared with the 2D culture, but at a low level. Encapsulated cells from differentiation II hardly displayed any increase in expression of albumin compared with the housekeeping genes.

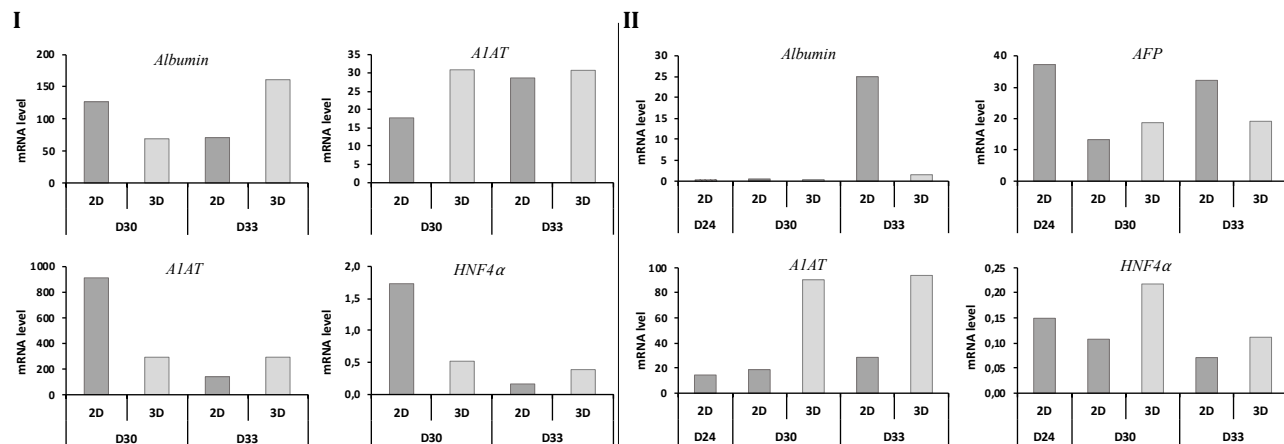


Figure 4.5: Changes in gene expression in encapsulated HLCs generated by direct differentiation. mRNA level of four hepatic markers, normalized to the average of two housekeeping genes (PBGD, RPLP0), in two separate HLC direct differentiations (I and II). Both differentiations were encapsulated at day 24. The expression of each gene changes with the differentiation and encapsulation.

Immunohistochemistry of encapsulated HLCs

To confirm the expression of one of the hepatocyte markers at the protein level, immunohistochemistry (IHC) of encapsulated HLCs clusters was performed. For staining of encapsulated HLCs from direct differentiation II, it was decided to stain for A1AT due to the high level of expression. Confocal laser scanning microscope (CLSM) imaging indicated that the clusters did contain the protein A1AT, bound with the green fluorescing antigen of the protein, see Figure 4.6. However, while the staining of the nuclei was convincing, the distribution of the green fluorescence suggests the antigens were not able to penetrate the center of the clusters.

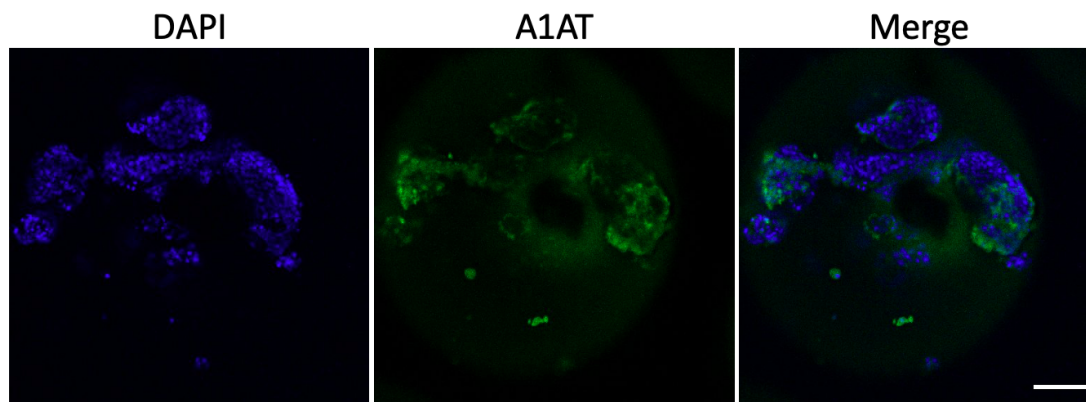


Figure 4.6: IHC of encapsulated HLCs generated by direct differentiation. Nuclei of the HLCs were stained with DAPI, while the cytoplasmic protein A1AT was detected with a green fluorescing secondary antibody with emission max at 525 nm. CLSM images was obtained with a 20x objective. Scale: 100 μ m.

4.2.2 Functional analyses of encapsulated hiPSCs-derived HLCs

Live/Dead staining of encapsulated HLCs

The functional analyses of live encapsulated cells have to utilize compounds and strategies capable of entering or escaping the alginate capsules without destroying the cells. For this, several methods were chosen, among which a Live/Dead kit which allows for determination of live and dead cells without cell lysis. Encapsulated HLCs generated by direct differentiation were stained on day 6 post encapsulation to study the relative survival inside the capsules. Dead cells were stained red (TRITC) while live cells were stained green (FITC), as seen in the brightfield and two fluorescent images of the same segment in Figure 4.7. The red fluorescing dead cells were expectedly located in the small clumps of less than 10 cells visible in the brightfield image, but also in the larger clumps. Nonetheless, the majority of the larger clumps were stained green, indicating a high number of live cells.

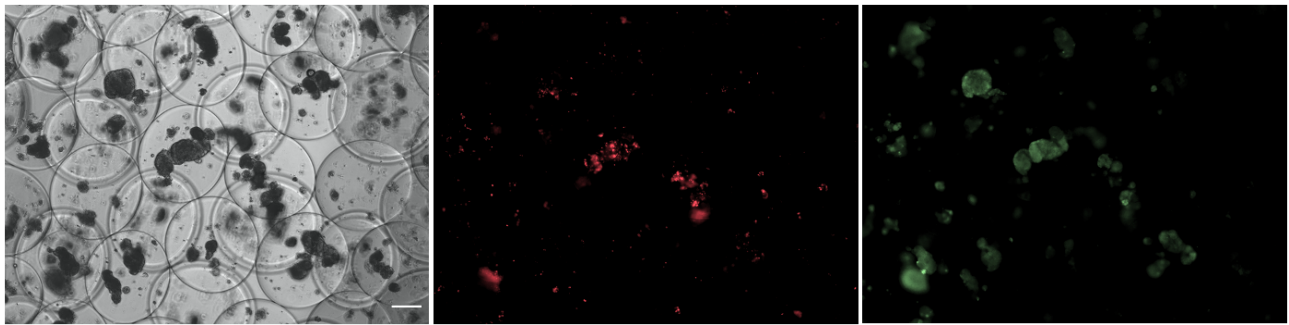


Figure 4.7: Live/dead staining of HLCs generated by direct differentiation encapsulated in unmodified UPLVG. Both dead (red) and live (green) cells were observed at day 30 of differentiation, or day 6 post encapsulation. Scale: 200 μ m.

Cell function and viability of encapsulated HLCs

To study the effect of immobilization in alginate capsules on the viability of HLCs, viability measurements were performed at several time points after encapsulation. These values were subsequently compared to the viability measurements of the corresponding 2D cultures at the same time points, see Figure 4.8 (A). Note that the difference in viability in the 2D and 3D cultures on day 27 of differentiation is not necessarily due to cell death after encapsulation on day 24, but rather due to the difference in cell number in the 2D and 3D wells after plating of the bead suspension. The measurements are therefore used to see the trend of the data for each condition rather than as a comparison of the difference in measured RFU. Cell viability went down between each time point in both conditions. In 2D, the measured RFU decreased by 22% between day 27 and day 30, and 15% between day 30 and 33, for a total reduction in viability between day 27 and 33 of 34% (data not shown). The measured RFU

of encapsulated cells went down 26% from day 27 to day 30, and 22% from day 30 to day 33, for a total reduction of 42% between day 27 and day 33. Immobilization in an alginate hydrogel therefore seems to affect the viability of HLCs generated by direct differentiation negatively compared with the 2D cultures.

Cell function of HLCs generated by direct differentiation did, however, appear to increase after encapsulation compared with the corresponding 2D cultures, see Figure 4.8 (B). The enzymatic activity of the drug metabolizing enzyme CYP3A4 was used as a proxy for cell function, which expectedly showed an increase across both conditions as the cells matured. As the measurements are normalized to the viability of the cells at each time point, it is clear that the cells retain their function even as viability decreases. This was especially true for the measurements of the 3D cultures at day 30. The measured enzymatic activity (RLU/mL/RFU) increased 5.76 fold from day 27 to day 30 in the 3D cultures (data not shown). However, while the enzymatic activity in 2D cultures increased 1.59 fold from day 27 to day 30, and 1.47 fold between day 30 and 33, the activity decreased in 3D cultures by 39% already at day 33.

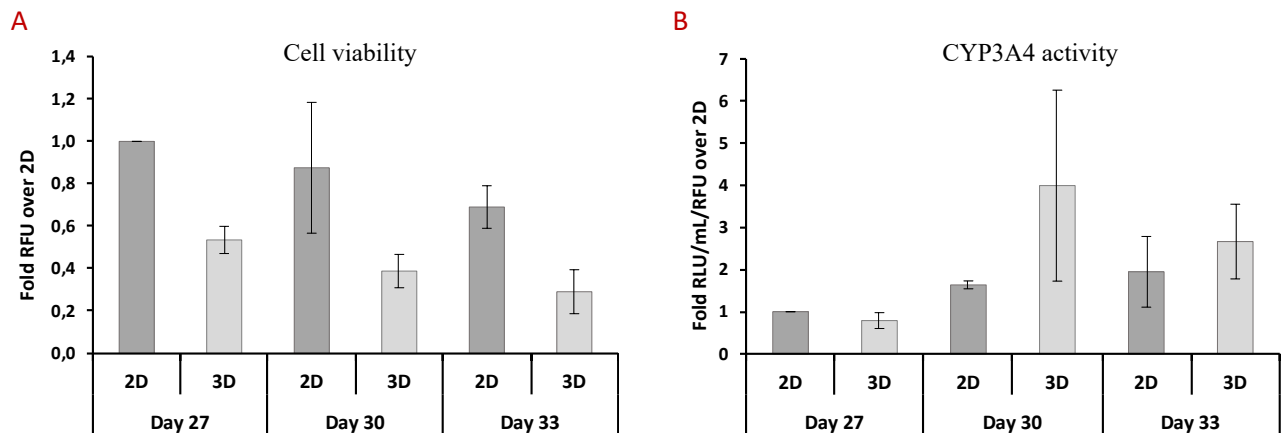


Figure 4.8: Cell viability and enzymatic activity in encapsulated FoP-derived HLCs. Cell viability was assessed using PrestoBlue Cell Viability Reagent (Invitrogen™) at three timepoints, and normalized to the 2D value at day 27 of differentiation. The assay showed a steady decrease of viability in both 2D and encapsulated (3D) cultures (mean \pm SD, n = 2). RFU = relative fluorescence unit (A). The activity of enzyme CYP3A4 at three time points was measured using P450-Glo™ CYP3A4 assay (Promega®), and first normalized to the viability at each time point, and subsequently normalized to the 2D value of day 27. The measurements indicate that both 2D and 3D cultures retain CYP3A4 activity even as viability decreases (mean \pm SD, n = 2). RLU = relative luminescence unit (B)

Collectively the expression data and functional analyses indicates that the expression and performance of encapsulated cells is correlated with the quality of cells to be encapsulated. To increase the function of the encapsulated cells, the next sections describe the differentiation and encapsulation of cells engineered for increased HLCs performance and maturity.

4.3 Characterisation of FoP-derived HLCs

As forward programming relies on the overexpression of a few master regulators rather than the sequential differentiation into hepatocyte progenitors, the strategy bypasses all the normal stages of hepatocyte differentiation. Figure 4.9 illustrates some key time points, with the rapid proliferation of cells until day 5, before the cells begin to acquire the polygonal hepatocyte morphology around day 12. FoP-derived HLCs have a smaller size which allows for a greater cell number per culture well.

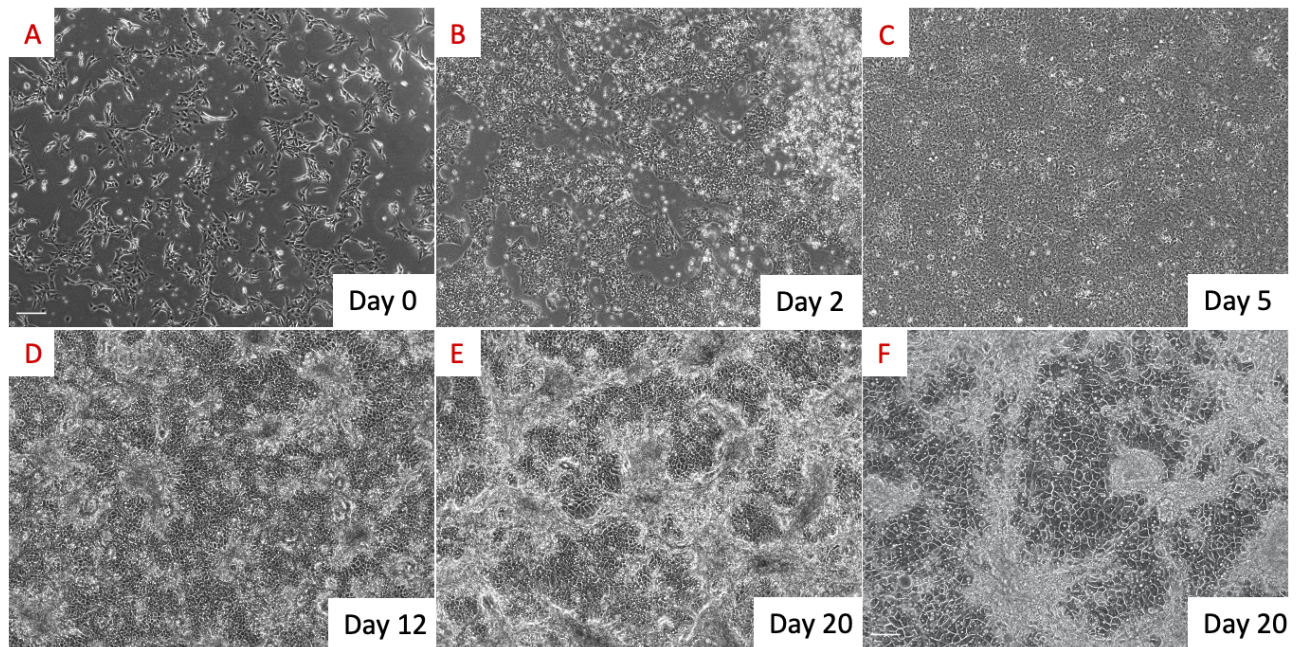


Figure 4.9: Forward programming of hESCs to HLCs. A hepatocyte-like morphology is observed from day 12 of differentiation. Scale: 200 μ m (A-E), 100 μ m (F).

Additionally, the FoP-derived HLCs were observed to be more confluent and comfortable with overgrowth and creating 3D structures on top of the 2D layer, almost independently of the number of cells seeded. This was observed as white structures growing around areas of HLCs with a clear hepatocyte morphology, see Figure 4.10 (black arrows). In addition to the structures resulting from overgrowth that visibly distinguished the FoP-derived HLCs from those derived from direct differentiation, the cells also exhibited several of the normal markers of hepatocytes. Some cells had more than one nucleus per cell (red arrows), and also contained an even greater amount of cytosolic lipid droplets than the cells generated by direct differentiation (blue arrows).

To study the efficiency of the overexpression of four master regulators on altering the gene expression of a few hepatocyte-specific markers, quantitative PCR was performed on samples extracted on several time points during the differentiation. Samples were also harvested from the genetically modified H9 hESCs to see the degree of change in expression as a result of the forward programming differen-

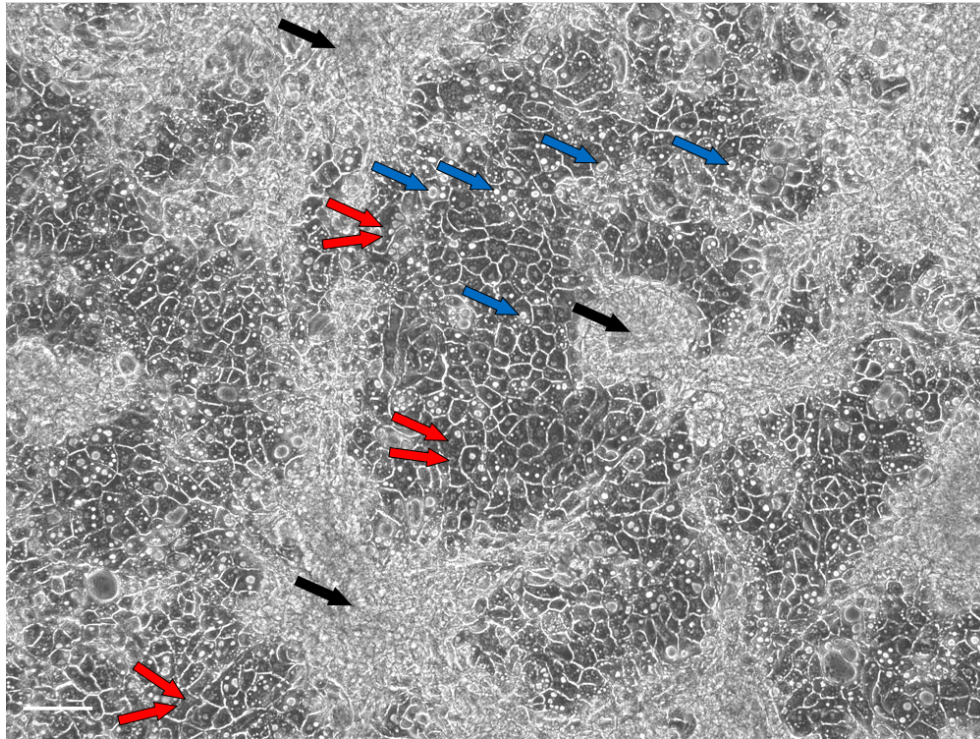


Figure 4.10: Morphology at day 20 of forward programming of hESCs to HLCs. Several hepatocyte characteristics are readily observed. A polygonal cell shape, several nuclei per cell (red arrows) and cytosolic lipid deposits (blue arrows) are visible in the microscope. In addition, cell overgrowth is visible as white 3D structures (black arrows). Scale: 100 μm .

tiation. The data illustrated in Figure 4.11 shows that the expression changed considerably from day 0 and through the course of the differentiation. The analysis also indicates that the expression of all mature hepatocyte markers, except that of albumin, was highest already on day 15 of differentiation. This was also true for the fetal hepatocyte marker AFP. Additionally, the data also shows that the important mature hepatocyte product albumin was expressed in a lower level in FoP-derived HLCs than in HLCs generated by direct differentiation.

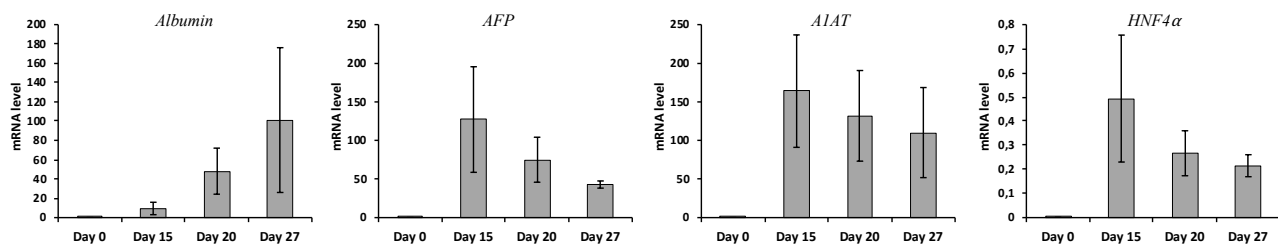


Figure 4.11: Changes in gene expression of HLCs generated by forward programming. The expression of four hepatocyte markers increases from day 0 and changes through the course of the differentiation. The mRNA levels are normalized to the average of two housekeeping genes (PBGD, RPLP0) (mean \pm SD, n = 4 (HLCs), n = 2 (hESCs)).

4.4 Encapsulation of HLCs generated by forward programming

The differentiation of cells to HLCs is a time-consuming procedure. Due to time limitations, as well as limitations in bead machine equipment that needed to be autoclaved between uses, galactosylated alginate and its control, POAred, were only tested once for the encapsulation of HLCs (n=1). As this is not enough to make any conclusions, results are summarized in Appendix C.

The cells were encapsulated in three different mixes of alginate. These included unmodified UPLVG, sulfated alginate mixed with unmodified UPLVG in a 20:80 ratio (SA 20/80) and sulfated alginate mixed with unmodified UPLVG in a 40:60 ratio (SA 40/60). Table 4.2 summarizes the characteristics of the alginate capsules and the parameters of the encapsulation procedure. The number of cells encapsulated between rounds of alginate encapsulations diverged from a 4.5×10^6 cells benchmark because of cell limitations as two alginate conditions were tested on the same day.

The chemical sulfation of alginate severely decreased the viscosity of the alginate solution, which caused the need to lower the flow rate of alginate and cell solution through the nozzle of the needle when encapsulating cells in the functionalized alginates. This was because the observed occurrence of different irregularities correlated with viscosity of the alginate solution and the flow rate setting. The observation was especially true for SA 40/60 which gave alginate capsules with a high percentage of irregular bead structures, see Figure 4.12 (C). The observed irregularities included capsules with tails, ellipse-formed capsules, and capsules with outlier diameters. Less viscous alginate mixes gave a higher percentage of tailed capsules, while the viscous UPLVG solution gave a higher percentage of ellipse-formed capsules. However, the majority of capsules made during this project were observed to have a high degree of sphericity, see Figure 4.12 (A and B).

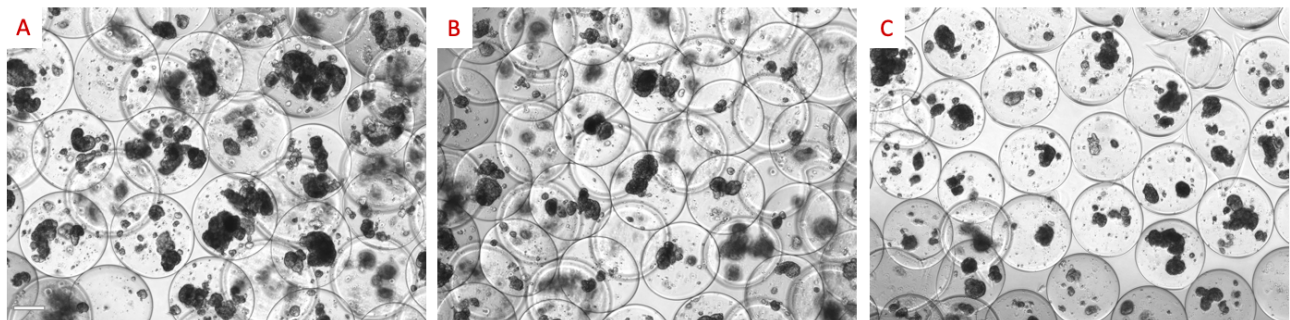
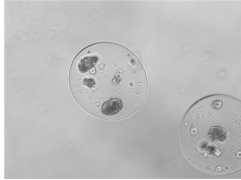
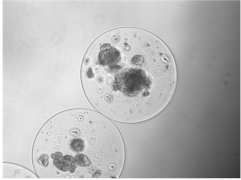
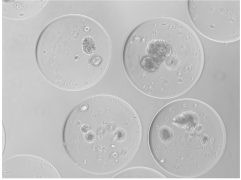


Figure 4.12: HLCs generated by forward programming encapsulated in three alginate mixes. Unmodified UPLVG (A), sulfated alginate mixed with unmodified UPLVG in a 20:80 ratio (B) and sulfated alginate mixed with unmodified UPLVG in a 40:60 ratio (C). Scale = 200 μ m.

Table 4.2 Characterisation of alginate beads from encapsulations of FoP-derived HLCs. Characterisation was performed on the day of encapsulation of three different batches of three types of alginate mixes. SA 20/80 and SA 40/60 = Sulfated alginate mixed with unmodified UPLVG in a 20:80 and a 40:60 ratio. Size is diameter mean \pm SD.

	UPLVG	SA 20/80	SA 40/60
Alginate capsule			
Batch 1			
Number of cells ($\times 10^6$)	4.1	3.8	3.8
Flow rate (mL/h)	10.0	7.0	6.5
Applied voltage (kV)	7.0	7.0	7.0
Size (μm)	479 \pm 22	581 \pm 13	452 \pm 18
Irregularities			
Total	5.0%	6.7%	20%
Ellipse formed	3.3%	-	-
Tails	1.7%	3.3%	20%
Batch 2			
Number of cells ($\times 10^6$)	4.3	4.1	4.3
Flow rate (mL/h)	9.5	7.5	6.0
Applied voltage (kV)	7.0	7.0	7.0
Size (μm)	446 \pm 24	539 \pm 17	510 \pm 26
Irregularities			
Total	5.0%	16.7%	36.7%
Ellipse formed	3.3%	6.7%	6.7%
Tails	1.7%	10%	30%
Batch 3			
Number of cells ($\times 10^6$)	4.5	4.5	4.5
Flow rate (mL/h)	9.5	7.5	6.5
Applied voltage (kV)	7.0	7.0	6.8
Size (μm)	582 \pm 35	535 \pm 35	582 \pm 35
Irregularities			
Total	10%	23.3%	43.3%
Ellipse formed	10%	6.67%	-
Tails	-	0.1%	43.3%

The stability of the functionalized alginate capsules in the culture media was determined by measuring the diameter of 30 beads at the day of encapsulation and day 5 post encapsulation ($n=2$), see Table 4.3. Fresh media was added to the wells containing capsules on the second day after the last media change, and it was completely changed on the third day. Using a two-tailed paired t.test, the differences in diameter in all tested experiments were judged as not significant ($p>0.05$). It was therefore determined that the culture media of the FoP-derived HLCs provide a good environment for cell survival and functionalized capsule stability.

Table 4.3 Changes in sulfated alginate capsule diameter over time. The size of functionalized alginate capsules was measured on the day of encapsulation (day 0) and after 5 days of exposure to the cell culture media. SA 20/80 and 40/60 = sulfated alginate mixed with unmodified UPLVG in a 20:80 and 40:60 ratio.

	exp. no.	Size day 0 ($\mu\text{m}\pm\text{SD}$)	Size day 5 ($\mu\text{m}\pm\text{SD}$)
SA 20/80	1	581 \pm 13	574 \pm 14
	2	452 \pm 18	451 \pm 16
SA 40/60	1	510 \pm 26	515 \pm 29
	2	539 \pm 17	538 \pm 15

4.4.1 Gene expression analysis of FoP-derived HLCs

To study the effect of encapsulation in different types of alginate on the gene expression of important hepatocyte markers in HLCs generated by forward programming, the beads were dissolved and RNA was extracted for qPCR analysis. The number of experiments used to analyze gene expression varies from 1-4 as several RNA samples were degraded. The results show that while the expression of albumin was already low in the 2D cultures of FoP-derived HLCs, the expression was not retained in encapsulated HLCs, see Figure 4.13. However, the expression of the fetal hepatocyte-marker AFP decreased in encapsulated cells from the day of encapsulation, which is a sign of increasing maturity. The expression of the mature hepatocyte markers A1AT and HNF4 α was high and competitive with the expression in the 2D cultures in all alginate conditions, and especially in HLCs encapsulated in SA 20/80.

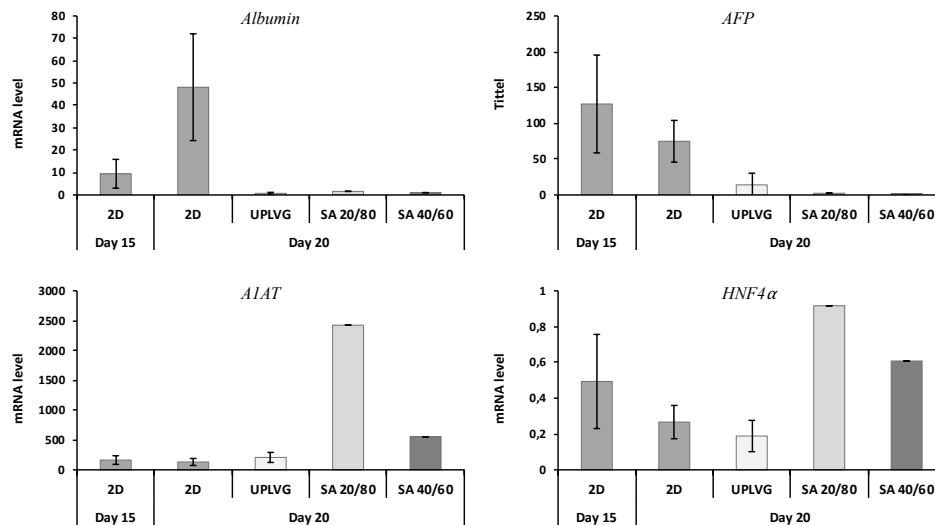


Figure 4.13: Changes in gene expression in encapsulated FoP-derived HLCs. Variation in mRNA levels of four hepatocyte marker genes were studied and compared to the 2D expression after encapsulation in three different alginates (mean \pm SD, n = 1-4). mRNA levels were normalized to the average of two housekeeping genes (PBGD, RPLP0).

Immunohistochemistry of encapsulated HLCs

IHC of encapsulated FoP-derived HLCs in three different alginate mixes was performed, and it was stained for the protease inhibitor A1AT due to its high expression in all encapsulated HLCs. As with the encapsulated HLCs generated by direct differentiation, the antibodies used for the staining of A1AT appeared not to have penetrated the center of the clusters, see Figure 4.14. Interestingly, the capsules consisting of different concentrations of sulfated alginate were observed to emit a considerable amount of green fluorescence (B and C). This was especially true for the SA 40/60 capsules, which suggests that the higher the concentration of sulfate groups, the more antibodies are retained in the matrix instead of being sufficiently washed out as with the unmodified alginate.

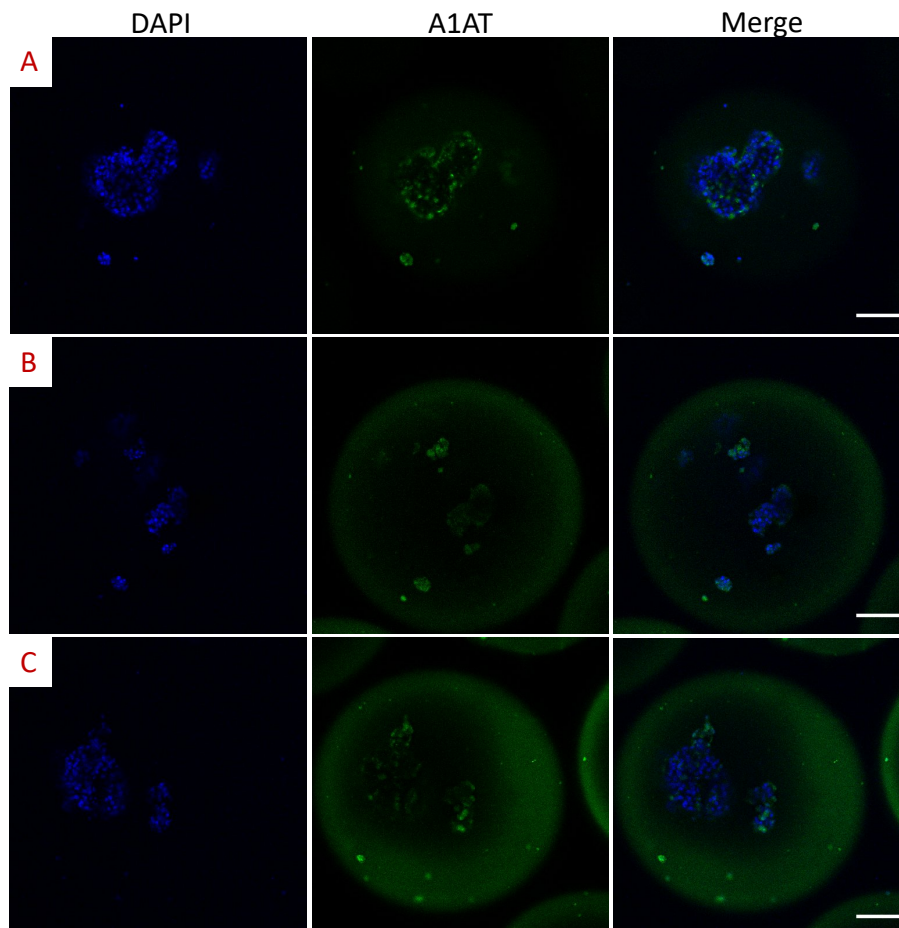


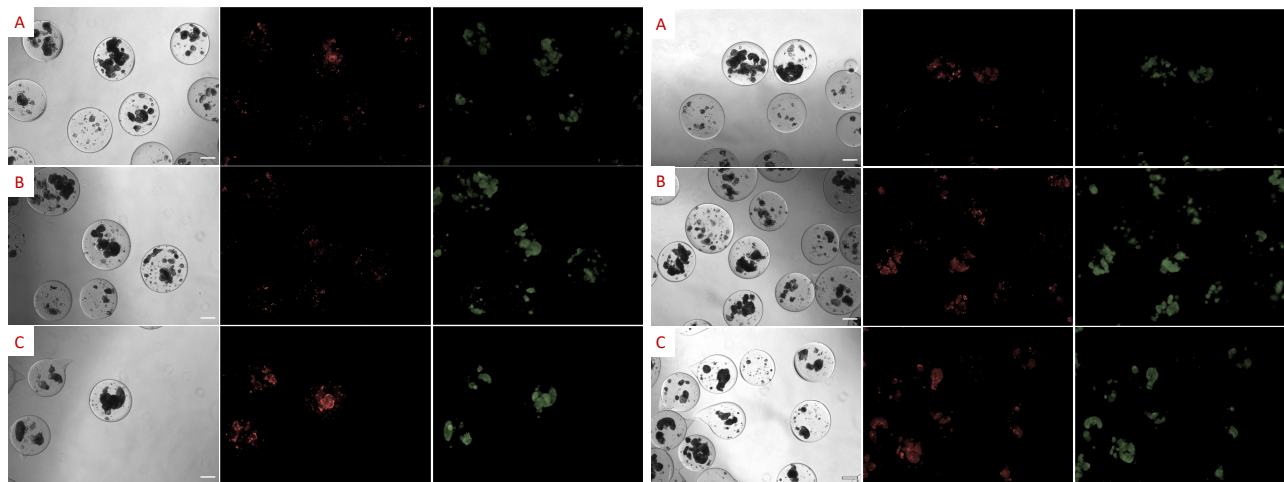
Figure 4.14: IHC of encapsulated HLCs generated by forward programming. The staining was performed on HLCs encapsulated in three different alginates. The cytoplasmic protein A1AT was detected with a green fluorescing secondary antibody with emission max at 525 nm, while nuclei were stained with the nuclear dye DAPI. CLSM images were obtained with a 20x objective. Unmodified UPLVG (A), SA 20/80 (B), SA 40/60 (C). Scale: 100 μ m.

4.4.2 Functional analyses of encapsulated FoP-derived HLCs

To study how the different alginate mixes affects the encapsulated HLCs, functional analyses were performed. Conducting the same analyses as for the encapsulated HLCs described in Section 4.2.2 also provided a means for comparison of the therapeutic potential between HLCs generated by direct differentiation and forward programming.

Live/dead staining of encapsulated FoP-derived HLCs

Live/dead staining was performed on FoP-derived HLCs encapsulated in the three alginate mixes both 24h and 5 days post encapsulation, or at day 15 and 20 of differentiation. Figure 4.15 (I) shows live/dead staining of encapsulated cells in the three alginate mixes 24h after encapsulation. The staining indicates that a large share of the cells survived the encapsulation in both unmodified UPLVG (A) and in SA 20/80 (B). Very few dead cells were observed in the latter condition. Cells encapsulated in SA 40/60, however, showed a much higher TRITC signal (C). This was also true 5 days post encapsulation (Figure 4.15 (II)). The observed amount of red fluorescing cells in the two other alginate conditions had also increased at this time point, and the change was especially visible in cells encapsulated in SA 20/80.



I Live/dead staining 24h post encapsulation

II Live/dead staining 5 days post encapsulation

Figure 4.15: Live/dead staining of FoP-derived HLCs encapsulated in three different alginate mixes. The staining was performed at 24h post encapsulation (I) and at day 20 of differentiation (II). Unmodified UPLVG (A), Sulfated alginate mixed with unmodified alginate 20/80 (B), Sulfated alginate mixed with unmodified alginate 40/60 (C). Scale: 200 μ m.

Cell function and viability of encapsulated FoP-derived HLCs

To further study the observed decrease in viability of cells encapsulated in SA 20/80 and SA 40/60, viability measurements were performed on the 3D cultures and the 2D cultures at day 20 and day 27 of differentiation, or day 5 and 12 post encapsulation. The measurements substantiates the observations, as the measured viability decreased between the two time points in SA 20/80, and especially SA 40/60-encapsulated cells, see Figure 4.16 (A). The measured RFU-values decreased by 41% in cultures with SA 40/60-encapsulated cells and 26% in SA 20/80-encapsulated cells (data not shown). There was no measured decrease in the viability of cells encapsulated in unmodified UPLVG, while an expected 19% decrease of viable cells from day 20 to 27 was measured in the 2D cultures. As noted in Section 4.2.2, the discrepancy in measured viability between the 2D and 3D cultures is not necessarily due to a difference in viability, but rather to a difference in number of cells as the measured RFU is not normalized to cell number.

Cell function of the HLCs in the form of enzymatic activity was significantly ($p < 0.05$) lower in the encapsulated cells compared with the 2D cultures, see Figure 4.16 (B). Measured CYP3A4 activity increased slightly between the two time points when normalized to the viability of the cells, across all conditions. The normalized enzymatic activity measurements (RLU/mL/RFU) revealed that the largest increase in CYP3A4 activity was calculated for HLCs encapsulated in SA 40/60 with a 2.85 fold increase between the two time points (data not shown). The activity increased 1.58 fold in HLCs encapsulated in SA 20/80 and 1.42 fold in 2D cultures. There was no marked increase in enzymatic activity in HLCs encapsulated in unmodified UPLVG, and all in all the data shows that CYP3A4 activity is not retained to any great degree in the HLCs after encapsulation.

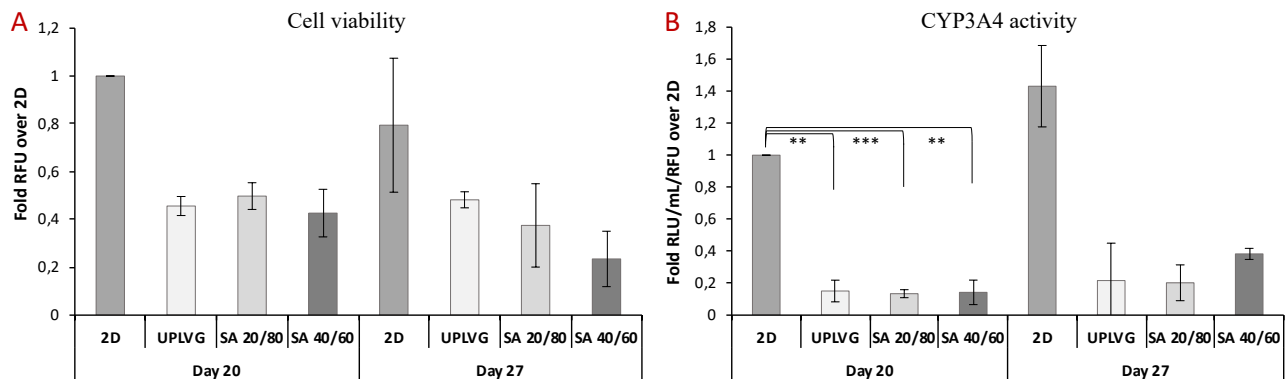


Figure 4.16: Cell viability and enzymatic activity of FoP-derived HLCs encapsulated in three different alginates. Cell viability was assessed using PrestoBlue Cell Viability Reagent (Invitrogen™) at two time points, and normalized to the 2D value at day 20. The assays revealed a decrease of viability in both 2D and encapsulated cultures (mean \pm SD, $n = 4$ (2D), $n = 2-3$ (3D)). RFU = relative fluorescence unit (A). The activity of enzyme CYP3A4 at two time points was measured using a CYP3A4 assay (Promega®), and first normalized to the viability at both time points, and subsequently normalized to the 2D value of day 20. Enzyme activity was significantly lower in all alginate conditions compared with the corresponding 2D cultures (mean \pm SD, $n = 4$ (2D), $n = 2-3$ (3D), ** $P < 0.01$, *** $P < 0.001$ by two-tailed t.test). RLU = relative fluorescence unit (B).

4.5 Performance of encapsulated HLCs generated by forward programming and direct differentiation

To investigate the relative maturity of the HLCs generated by direct differentiation (DD) and forward programming, the gene expression of the HLCs was measured at day 30 and day 20, respectively, and compared to the gene expression of primary human hepatocytes (PHHs). As seen in Figure 4.17, neither strategy for differentiation achieved the high level of albumin expression measured for PHHs. The expression of the fetal protein AFP was also much higher in the HLCs than in the PHHs, and this was especially true for the 2D cultures of the FoP-derived HLCs. The expression of AFP was, however, much lower in the cells encapsulated in sulfated alginates, and the expression was at a level which was approximately the same as that of the mature hepatocytes. Interestingly, HLCs in the same two alginate conditions, as well as the encapsulated cells from DD I (UPLVG I) also exhibited a considerably higher expression of A1AT than both the PHHs and their respective 2D cultures.

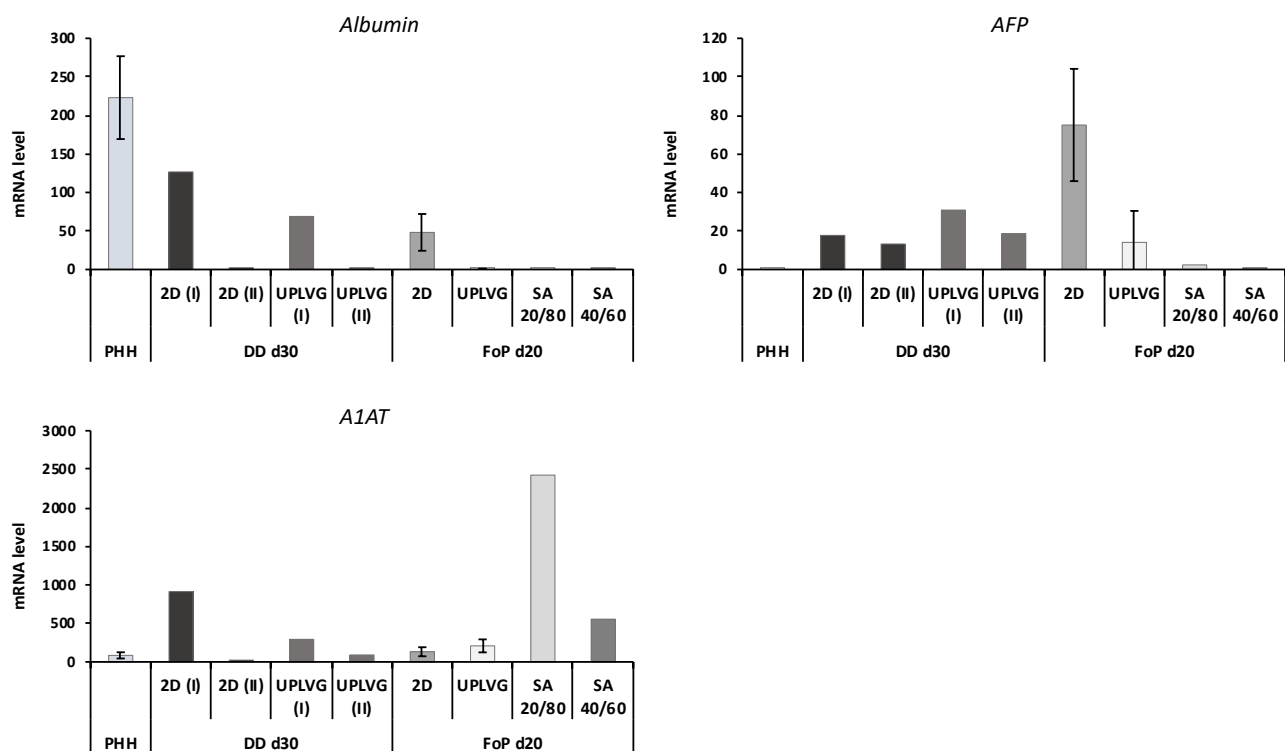


Figure 4.17: Gene expression at day 30 of direct differentiation (DD) and day 20 of forward programming of hPSCs to HLCs. The mRNA levels of four hepatocyte markers in PHHs (Tomaz et al, unpublished) was compared with the expression results of both strategies for HLCs differentiation. None of the 2D cultures or encapsulated HLCs achieved the expression level of PHHs for albumin, but the expression of A1AT was higher in the differentiations than in the PHHs. All conditions except the sulfated alginate resulted in a higher AFP expression than in PHHs (mean \pm SD, n = 4 (PHHs), n = 1-3 (FoP), n = 1 (DD)). mRNA levels were normalized to the average of two housekeeping genes (PBGD, RPLP0).

To further study the difference in maturity of the HLCs generated by the two different methods of differentiation, the day of the highest measured enzymatic activity in both types of HLCs was compared. The CYP3A4 activity for the two types of HLCs at the two time points, and the cell viability which the enzymatic activity is normalized to, is displayed in Figure 4.18. The data shows that the enzymatic activity in the 2D cultures of the FoP-derived HLCs was markedly higher than in both the direct differentiated HLCs and all encapsulated HLCs. It also shows that the enzymatic activity of the HLCs encapsulated in the sulfated alginate was comparable to the activity in the HLCs from direct differentiation I encapsulated in unmodified UPLVG. However, the latter is only comprised of one data point.

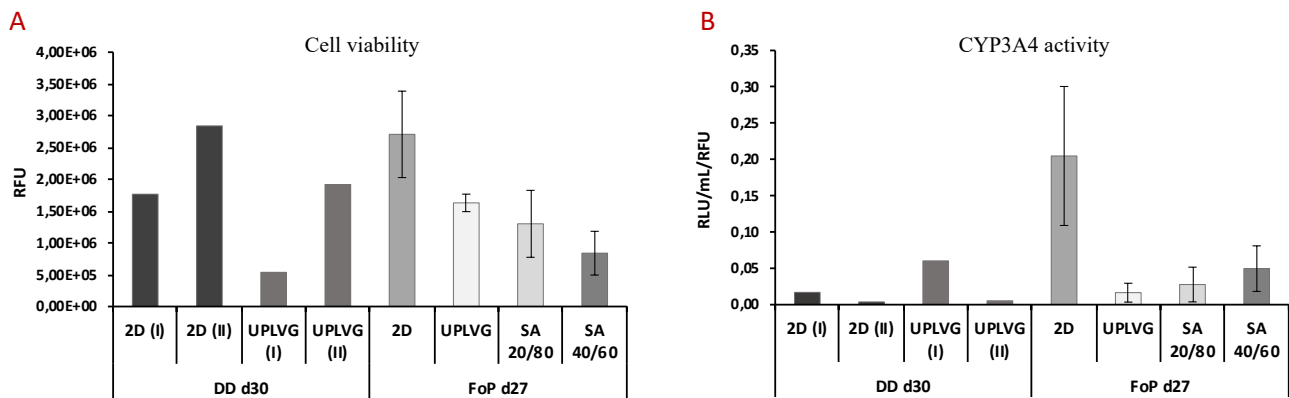


Figure 4.18: Cell viability and enzymatic activity at day 30 of direct differentiation (DD) and at day 27 of forward programming of hPSCs to HLCs. Cell viability was assessed using PrestoBlue Cell Viability Reagent (Invitrogen™). The viability measurements were used to normalize the measured activity of the enzyme CYP3A4 (mean ± SD, n = 1 (DD), 2-4 (FoP)) (A). The CYP3A4 assay (Promega®) showed that the enzymatic activity in the 2D cultures of FoP-derived HLCs was markedly higher than in the HLCs generated by direct differentiation. Enzymatic activity in encapsulated HLCs from differentiation I (UPLVG I) matched that of HLCs encapsulated in SA 40/60 (mean ± SD, n = 1 (DD), 2-4 (FoP)) (B).

5 Discussion and Future work

Two strategies for the generation of hepatocyte-like cells were studied through functional and genetic analyses of mature hepatocyte markers. Direct differentiation of human pluripotent stem cells to HLCs *in vitro* mimics the events of embryonic development leading to the differentiation of mature hepatocytes *in vivo* [38]. Conversely, forward programming of hPSCs to HLCs aims to minimize the time of differentiation, the use of resources, and to display increased functions through bypassing the normal stages of differentiation by overexpression of master regulators [42]. The potential of FoP-derived HLCs to be used for cell therapy was studied through encapsulation of both HLC types in alginate capsules. Encapsulation in alginate hydrogels protects the potentially therapeutic cells from the immune responses of the host, while providing a hydrated environment through which nutrients can access the cells [6, 58]. While both types of HLCs survived the encapsulation, they differed in which hepatocyte functions or markers that was maintained or improved.

To reduce the foreign body response of the host to the alginate capsules after a potential transplantation, and to improve function and attachment of encapsulated cells, functionalized alginates were tested for encapsulation of FoP-derived HLCs. The functionalized alginates included sulfated alginate as a heparin analog to reduce inflammation, galactosylated alginate to provide sites for cell attachment and an alginate without substituents but with the same mechanical properties as Gal-alg. Cell function and survival in bioinert unmodified alginate was compared to the cells encapsulated in the functionalized alginates.

5.1 Generation of Hepatocyte-like cells

hiPS cell line A1ATD^{R/R} derived from somatic cells of patients with A1AT deficiency, with subsequent correction of the point mutation causing the disease [77], was first cultured and differentiated to HLCs by direct differentiation. This was done to set up protocols for alginate encapsulation of HLCs and suitable functional analyses of encapsulated HLCs using a thoroughly tested protocol for differentiation [38]. However, as has been noted earlier [11], HLCs generated through the known methods of direct differentiation exhibits some features of immature hepatocytes and limited features of mature adult hepatocytes. This is supported by the findings of this work, as demonstrated with the high expression of the fetal hepatocyte marker α -fetoprotein (AFP) (Figure 4.3). Additionally, this study has found that the efficiency of the differentiation can be highly variable. However, this might have been caused by differences in the quality and state of the starting material, and/or batch-to-batch variations in the many media components required in the protocol. Still, several more direct differentiations were conducted throughout this project, but most failed to differentiate into functioning HLCs or detached from the culture plate and died during the differentiation (data not shown).

To increase the reproducibility of the experiments in this work, a novel forward programming line, genetically engineered hES cell line H9rtTa-AAVS1-136R, was tested. The overexpression of the transcription factors HNF1 α , FOXA3, HNF6 and RORc are induced to generate more mature and functional hepatocytes (Tomaz et al. unpublished). The protocol leads to functional HLCs with a clear hepatocyte morphology already after 20 days of differentiation, while the corresponding time point in direct differentiation is approximately 30 days. However, the expression of four hepatocyte markers tested using qPCR did not indicate that forward programming generated more mature HLCs than direct differentiation. The expression of albumin did not increase meaningfully until day 27 of differentiation, and the measurements were variable (Figure 4.11). The expression of the hepatocyte marker was greater in a high quality direct differentiation such as direct differentiation I, but much lower in direct differentiation II. Unexpectedly, the level of AFP increased in direct differentiation I from day 30. AFP is a protein that is highly expressed during hepatocyte development, and should not be expressed at a high level in mature hepatocytes [11]. However, the AFP expression was still lower compared with that seen in the FoP-derived HLCs. The expression of AFP in these cells decreased at every time point, but at a high level. The expression of the protease inhibitor A1AT and the hepatocyte transcription factor HNF4 α decreased in both the FoP-derived HLCs and HLCs from direct differentiation I, but the expression in the latter was several fold higher for A1AT. Altogether, the expression data shows that FoP-derived HLCs do not outperform a high quality direct differentiation such as direct differentiation I, but the measured expression is more reliable and does not decrease to the levels of direct differentiation II.

In the functional assay studying the activity of the drug-metabolizing enzyme CYP3A4, on the other hand, the FoP-derived HLCs displayed a much higher enzymatic activity than both the direct differentiation experiments (Figure 4.18 (B)). This was true even as the viability measurements which the enzyme activity is normalized to was approximately the same. The measurements indicate that even as direct differentiation I displays a more mature expression profile, the FoP-derived HLCs can still show more mature functional characteristics. Importantly, as the Cytochrome P450s (CYPs) are central contributors in the metabolism of xenobiotics [30], the high CYP3A4 activity points to a greater capacity of FoP-derived HLCs to metabolize such drugs. This could be particularly relevant as the cells are intended as a short term treatment of acute liver disease.

Partly because of the more reproducible gene expression results and the functional assay, the FoP-derived HLCs were deemed a suitable alternative for cell therapy compared with direct differentiated HLCs. This strategy for differentiation is also much less time-consuming, and it has an easier protocol that requires fewer media shifts and less cytokines giving a reduced chance of batch to batch variability. The cells were also more resilient and less demanding, as the forward programming strategy invariably generated morphologically and functionally similar cells that survived until end of experiment.

5.2 Alginate encapsulation of HLCs

The protocol for alginate encapsulation of HLCs for use in cell therapy was initially optimized in this project using HLCs generated by direct differentiation, and encapsulation was carried out using native alginate. As summarized in Table 3.1, the alginate had a high molecular weight and average G-block length ($N_{G>1}$), resulting in a viscous alginate solution with good gelling properties. Two flow rates were tested based on the protocol used for encapsulation [83, 84], where the lower flow rate was tested to see the effect of this adjustment on a viscous alginate solution containing cell clusters. While the percentage of irregular beads increased, both encapsulation parameters gave capsules that supported cell viability and that were stable in the cell culture media. This stability was an intended effect of the addition of 1mM Ba^{2+} in the gelling solution. Previous studies have shown that the addition of this divalent cation at low concentrations is sufficient in drastically reducing capsule instability. It reduces sensitivity to chelating agents like phosphate, which can be present in the cell culture media or washing solutions [52]. Supplementing the culture media with calcium have also been demonstrated to counteract the displacement of calcium by other non-gelling cations like sodium which can lead to partial bead dissolution and swelling [12]. A potential presence of the gelling cation in the culture media will thus also have contributed to the measured stability. An additional important factor in HLCs encapsulation is the cell cluster size. 3D cell-cell interactions are important to maintain and improve hepatocyte functions [93]. However, when testing cluster sizes (Figure 4.4), the HLCs in the beads containing the largest clusters did not survive. This can be explained by oxygen and nutrient deprivation, as too large cell clusters will slow or prevent diffusion to the center of the clusters and thereby impede cell survival [94]. Testing different cluster sizes eventually generated clumps that supported cell function and were judged to be appropriate through visual inspection.

5.2.1 Encapsulation in functionalized alginates

Functionalizing bioinert alginates were performed with the intention of decreasing a potential foreign-body response in the host and/or increase encapsulated cell attachment and function. While the modifications should lead to increased communication with encapsulated cells and the environment, it is also important that the alginate is stabilized to avoid degradation. This was accomplished by reducing the galactosylated alginate and its control to remove the highly degradable aldehyde groups [72]. However, another result of the modifications was that all functionalized alginates had a much lower viscosity than the native alginate, resulting from the decreased molecular weights (Table 3.2) [55]. While depolymerization following chlorosulfonic acid exposure or oxidation will have resulted in the lower molecular weight, breaking of the ring structure of the alginate subunits due to oxidation, and the steric hindrance caused by bulky substituents will have had deteriorating effects on the gelling properties of the alginate [45, 71]. These changes cause disruption of the G-blocks and MG-blocks

needed to form stable cross-links with the Ca^{2+} - and Ba^{2+} -ions [12, 95]. To ensure that the modified alginates were still capable of gelling, they were mixed with native alginate in a ratio of 20/80 and 40/60, as incorporation of unmodified alginate has previously been demonstrated to improve gelling capacity in functionalized alginates with a high DS [12]. Previous studies have still found a high degree of substitution to be an important factor in the properties of mixed alginate hydrogels, and this is especially true for gels tested with a high fraction of functionalized alginates [95].

The lower viscosity posed a problem in both concentrations of functionalized alginate solutions, as it made the resulting hydrogels unpredictable. It has been established that the viscosity of an alginate solution heavily influences the shape of the resultant beads [96]. The number of irregular capsule shapes increased drastically when encapsulating with the modified alginates (Table 4.2 and Table C.2) compared with the higher viscosity native alginate (Table 4.1). This was especially true for the alginate solutions with the higher concentration of functionalized alginate. While a spherical capsule shape is mostly important to reduce FBR after transplantation [97], irregular shapes might also influence diffusion through the beads and thus affect *in vitro* studies. The alginates were also observed to respond differently with and without cell clusters to encapsulation parameters such as the flow rate and applied voltage, which made it difficult to optimize a protocol for encapsulation using functionalized alginates that produced uniform spherical capsules. This is why the parameters for the encapsulation was changed several times during the project, in an attempt to lower the percentage of observed irregularities. However, even with the high occurrence of irregular shapes, both concentrations of all functionalized alginates were found to be stable in the culture media, without any significant changes in capsule size after generation of the capsules (Table 4.3 and Table C.1). While other groups have found that a high degree of sulfation increases swelling due to increased hydrophilicity from the negative charges [65] and the weak gel-forming ability which can cause alginate leakage, it has also been reported that inclusion of native alginate in the modified alginate improves the osmotic stability of the gel [12]. This, along with the previously discussed reasons for increased capsule stability, will have contributed to the stability measured in the functionalized gels.

5.3 Functional analysis of encapsulated HLCs

5.3.1 Embedding of HLCs generated by direct differentiation and forward programming in native alginate

To study the difference in effect of alginate encapsulation on HLCs derived from the two methods of differentiation, several functional and genetic analyses were performed. Additionally, a primary concern was the survival of the HLCs after encapsulation in alginate. A live/dead staining conducted on direct differentiation II six days post encapsulation revealed that the bead suspension contained both live and dead cells (Figure 4.7). The dead cells were primarily found in the smaller cell clumps,

as expected due to the lack of cell-cell interaction discussed previously. However, dead cells were also observed in the larger clumps which could be explained by poor diffusion of nutrients into the center of the cell clusters. Both of these findings indicate that even as the approximate clump size had been optimized, the variability of the approach still lead to clusters of varying sizes which could affect cell viability. Nevertheless, the single time point for the live/dead staining could not reveal if the cells primarily died as a result of the encapsulation procedure, poor diffusion or cell-cell interaction, or from being immobilized in alginate over time. For staining of the FoP-derived HLCs encapsulated in native alginate, an additional time point was therefore included (Figure 4.15). These capsules also contained both live and dead cells at 24h after encapsulation, however, the observed share of dead cells had not increased at the next time point. This indicates that these cells might have died during the encapsulation procedure or from the dissociation of the 2D layer.

Cell viability assays utilizing the reducing environment of live cells performed at two time points substantiates the observations in that unmodified alginate provides a suitable environment for the viability of FoP-derived HLCs. While the viability was not measured to have decreased between time points in these cells, it went down across all other conditions, also in 2D. This was expected towards the end of the differentiation as a 2D layer is not compatible with long-term culture for cells which are normally highly organized in their native 3D tissues [68]. The same trend was also seen in the encapsulated direct differentiated HLCs (Figure 4.8). However, even as the viability of FoP-derived HLCs encapsulated in unmodified alginate was favorable, gene expression analysis of the HLCs indicates that the cells were less mature than the encapsulated cells from direct differentiation I (Figure 4.17). The exception to this analysis was that the expression of A1AT appeared approximately the same in PHHs as in both types of encapsulated HLCs. To confirm the expression of this hepatocyte marker on the protein level, an anti-A1AT primary antibody was used for IHC staining of both types of HLCs embedded in unmodified alginate capsules. The results showed that the expression was translated into a functional protein, but it also appeared as if the antibodies had not penetrated to the center of the cell clusters. This could also be due to cell death in the center from lack of access to nutrients, as discussed previously.

This study found that the embedded cells from differentiation I were also more functionally mature than the FoP-derived HLCs encapsulated in unmodified alginate (Figure 4.18). Although signifying only one data point, these cells had a higher normalized enzymatic activity at day 30 than its corresponding 2D culture (Figure 4.8). This, together with increasing gene expression, demonstrates that immobilization can facilitate some level of maturation. The same was observed in the encapsulated FoP-derived HLCs, but the measurement were variable. However, these cells had a significantly lower measured enzymatic activity after encapsulation compared with the 2D cultures (Figure 4.16). This indicates that the loss of cell adhesion to the growth plate and the lack of adhesion sites in the inert alginate might affect the FoP-derived HLCs more than those generated by direct differentiation. To this

end, it would be highly interesting to have some data on the enzymatic activity of PHHs to determine the degree of functional maturity of the encapsulated and 2D-cultured HLCs. However, unknown elements that could influence the validity of the viability and the enzymatic activity measurements is the diffusion rates of the active molecules of the two assays, resazurin and pro-luciferin. Diffusion rates were not measured in this project, though it has previously been noted that cells can give a delayed response to molecules added in the media as the molecules have to pass the alginate matrix [6]. These rates could therefore have influenced the readings as the assays were performed with the same incubation time for both the 2D and 3D cultures. Additionally, if the two molecules diffuse through the gel at different rates, the measurements will have been skewed as the enzyme activity is normalized to the viability measurements, and these measurements would no longer be comparable to those of the 2D cultures.

Together, the expression data and functional analysis indicates that the encapsulated HLCs from differentiation I were slightly more mature than the FoP-derived HLCs. However, embedded cells from differentiation II had a more fetal-like expression of all tested genes, and a lower enzymatic activity. This reveals that the variability of the differentiations is translated into the encapsulated cells. Alginate encapsulation of FoP-derived HLCs was therefore considered more reproducible, and the cells were encapsulated in functionalized alginates in an attempt to increase cell function and maturity.

5.3.2 Embedding of FoP-derived HLCs in functionalized alginates

To investigate which of the functional alginates that provide the most suitable environment for cell function, and thus the alginate that is most promising for future cell therapy, the same functional and genetic analyses were performed on encapsulated HLCs. However, due to time constraints both concentrations of the galactosylated alginate and its control were only tested once. The decision was based on poor gene expression results (Figure C.3).

The viability of the HLCs differed between the cells encapsulated in the two concentrations of sulfated alginate. At 24h after encapsulation, a live/dead staining revealed that SA 20/80 contained the highest share of live cells, while the opposite was true for SA 40/60 (Figure 4.14). These cells were encapsulated on the same day with the same technique, and originated from the same culture plate. This could indicate that the cells are not extensively harmed by the encapsulation procedure, but rather that the alginate influences the survival. However, this is somewhat contradicted by the fact that the share of live cells in SA 40/60 was not observed to have diminished as drastically at the next time point. Five days post encapsulation, the share of dead cells had increased in SA 20/80 to a level similar to that of HLCs encapsulated in native alginate. The observations contradict the findings from the HLCs encapsulated in native alginate as these stainings indicate that the cells do survive the encapsulation procedure. Cell viability assays support the findings of the live/dead staining in that SA

40/60 provides the least favorable environment for the viability of encapsulated HLCs (Figure 4.16). The reason why the higher concentration of sulfated alginate resulted in a lower viability of HLCs is unknown, but some functions of the heparin analogs might not yet have been discovered. The HLCs encapsulated in the SA 20/80, Gal-alg and POAred 20/80 conditions followed the trend observed for the 2D cultures with a more gradual decrease (Figure C.2).

It was found through genetic analysis that the encapsulation in functionalized alginates did not induce a higher expression of albumin in the HLCs (Figure 4.13). However, the expression of the three other hepatocyte markers changed considerably in the HLCs encapsulated in both concentrations of sulfated alginates. The expression of AFP decreased to the level of PHHs, and the expression of the two mature hepatocyte markers had markedly increased (Figure 4.17). This was especially notable in HLCs encapsulated in SA 20/80 which outperformed the other HLCs and PHHs in their expression of A1AT several-fold. The changes in gene expression could mean that the environment provided by the sulfated alginate assists in reducing some of the immature characteristics of the cells. Conversely, the gene expression of HLCs encapsulated in Gal-alg and POAred was lower for all markers except for the expression of AFP (Figure C.3), which indicates that the intended progression in differentiation due to increased adhesion of the cells to the matrix did not occur. This is somewhat supported by the functional analysis, which while at a high level, was lower in Gal-alg 20/80 than its control (Figure C.2). However, not enough replicates were tested during this project to determine if any of these changes were significant.

While the enzymatic activity in the HLCs encapsulated in both sulfated alginates decreased significantly compared with the 2D cultures, the activity increased between time points also in these conditions to a level higher than that measured in the HLCs encapsulated in unmodified alginate (Figure 4.16). This supports the findings of the genetic analysis in that encapsulation in the sulfated alginate increases maturity compared with native alginate, though the enzymatic activity was higher in cells encapsulated in SA 40/60 than SA 20/80. Except for the expression of albumin, the FoP-derived HLCs encapsulated in both concentrations of sulfated alginate thus performed exceedingly well with both the functional analysis and all tested hepatocyte markers. This might be because sulfated alginate has previously been shown to increase cell proliferation and differentiation through mediating a heparan sulfate/heparin-interaction between growth factors like HGF and their cell-surface receptors. This is achieved through binding of the growth factors, which also protects them from degradation [65, 66]. Additionally, as the hepatocyte ECM is rich in fibronectins which bind heparin [28], the sulfated alginate could have introduced characteristics similar to the native ECM of the cells.

However, the expression data for the sulfated alginates are comprised of only one experiment for each concentration, and can therefore not be used for any definitive conclusions. The reason for this could be that the protocol formulated in this work for the dissociation of alginate capsules is too harsh for the sulfated alginates as the protocol was optimized with native alginate. This could have

resulted in the RNA being degraded before cDNA synthesis for qPCR. The theory is supported by the fact that the beads were observed to be completely dissolved, and the HLCs originating from sulfated alginate beads that did not have any amplification of the hepatocyte markers, also did not have any amplification of the housekeeping genes. Optimization of the protocol for the dissociation of sulfated alginates could therefore be important to further study the effect of this functionalized alginate on the gene expression of encapsulated HLCs and to generate more reproducible results. Furthermore, in addition to the challenges previously described regarding the validity of the viability and CYP3A4 measurements, differences in how freely the active molecules of the assays diffuse through the functionalized gels compared with the unmodified gel remains undiscovered.

The expression of A1AT was confirmed on the protein level by IHC staining of the HLCs encapsulated in sulfated alginates. The results were interesting as these alginates appeared to retain a substantial amount of antibodies, causing fluorescing capsules. This was not observed to the same extent in capsules comprised of native alginate. The observation implies either that free antibodies had not been sufficiently washed out of the gels, or that they had somehow bound to the sulfated matrix. In the future, this should be investigated by implementing more and longer washing steps between the addition of antibodies. Moreover, a method for fixing the capsules to avoid movement during imaging could achieve a higher resolution. Another method for confirming the translation of the gene expression to functional proteins is to analyze the secretion of the proteins into the cell culture media using ELISA [98]. Media samples were collected from all experiments during the project, but shutdowns due to the Covid-19 pandemic resulted in these not yet having been analyzed. The presence of larger molecules like albumin in the media surrounding the encapsulated cells would also have revealed information about the pore size of the different alginate hydrogels which was not otherwise investigated in this work.

Altogether, the expression data and functional analyses indicates that the sulfated alginate mixed with native alginate in a 20:80 ratio was the alginate condition that provided the best environment for the performance of encapsulated HLCs. The expression of mature hepatocyte markers was highest in HLCs encapsulated in this alginate, and while the enzymatic activity was greater in the higher concentration of sulfated alginate, so was the mortality. SA 20/80 is therefore a promising alginate for the encapsulation of FoP-derived HLCs for future cell therapy. Nevertheless, it is important to reiterate that few of the assays performed with encapsulated HLCs were tested with enough biological replicates to determine whether the results are significant and the results are therefore not conclusive. A minimum of three trials with reproducible results would have been favorable. However, the data from this work can be used to inspire further research into the encapsulation of FoP-derived HLCs for short-term treatment of liver disease.

5.4 *In vivo* studies

To study cell survival and function after transplantation in the alginate that was deemed the most suitable for cell function, FoP-derived HLCs encapsulated in SA 20/80 was injected into immunodeficient mice (n = 4). FoP-derived HLCs encapsulated in native alginate was also injected into mice in a parallel experiment as a point of comparison (n = 4). The experiment was planned to last for two weeks, with extraction of capsules after seven and 14 days. Because of shut-downs due to the Covid-19 pandemic, the alginate capsules were extracted only eight days after transplantation, a time period in which the mice had shown no signs of discomfort. Visual inspection revealed no deterioration of the capsules before they were dissolved and RNA was extracted from the explanted HLCs. The isolated RNA was stored for future qPCR analysis to reveal any genetic changes induced by *in vivo* culturing. Serum samples from blood harvested at two time points, 24h and eight days post transplantation, were also stored for future ELISA analysis of the content of circulating human albumin and A1AT produced by the human HLCs. This would reveal if the encapsulated HLCs transplanted into the peritoneal cavity of mice were functional through the duration of the experiment, and if function increased or decreased with time.

It has already been established that sulfated alginate in a 20:80 ratio suppresses the immune responses when transplanted into immunocompetent mice (Strand et al., unpublished). Future *in vivo* studies should therefore focus on examining cell function over a longer period of time than what was conducted in this project to study the duration of the therapeutic potential of encapsulated HLCs. If further investigations into the effect of galactosylated alginates on encapsulated HLCs reveal increased functions, studies of the immune reactions of immunocompetent hosts to transplantation of the modified alginate capsules would also be highly interesting.

6 Conclusion

Alginate encapsulation of hPSCs-derived hepatocyte-like cells was investigated to study their potential for use in cell therapy medicine. Different alginates modified for improved cell function and immune suppression after transplantation were tested for the encapsulation of HLCs generated by two strategies for differentiation. While direct differentiation of hiPSCs seeks to mimic the natural embryonic pathway of hepatocyte differentiation, the novel differentiation of hESCs through forward programming (FoP) is achieved by the over-expression of a few specific master regulators. Both strategies were found to produce HLCs that varied in maturity of different functional and genetic markers, yet the FoP-derived HLCs generated more reproducible results. The forward programming protocol was also less time- and resource-consuming, making the resulting HLCs suitable alternatives to direct differentiated HLCs for cell therapy purposes.

The FoP-derived HLCs were encapsulated in the different functionalized alginates made for this work. While the alginate solutions containing functionalized alginates had a much lower observed viscosity which resulted in the generation of alginate beads with highly irregular shapes, the beads were found to be stable in the cell culture media. Assays examining the viability and enzymatic activity of the encapsulated HLCs, as well as qPCR for analysis of changes in gene expression, were performed and compared to results from the 2D cultures. These tests found that sulfated alginate with an 80% degree of substitution mixed with native alginate in a 20:80 ratio provided the most suitable environment for encapsulated HLCs. The hydrogel mix contained HLCs with a high degree of viability and a higher expression of the hepatocyte protease inhibitor A1AT than what was measured in primary human hepatocytes. However, several assays did not obtain results from enough replicates to determine the significance of the findings. While the *in vivo* experiment with FoP-derived HLCs encapsulated in sulfated alginate was cut short, the results of his work invites additional research.

References

- [1] Mokdad, A. A., Lopez, A. D., Shahraz, S., Lozano, R., Mokdad, A. H., Stanaway, J., et al. Liver cirrhosis mortality in 187 countries between 1980 and 2010: a systematic analysis. *BMC Med.*, 12(145), dec 2014. doi: 10.1186/s12916-014-0145-y.
- [2] Ibars, E. P., Cortes, M., Tolosa, L., Gómez-Lechón, M. J., López, S., Castell, J. V., et al. Hepatocyte transplantation program: Lessons learned and future strategies. *World J. Gastroenterol.*, 22(2):874–886, 2016. doi: 10.3748/wjg.v22.i2.874.
- [3] Schwartz, R. E., Fleming, H. E., Khetani, S. R., and Bhatia, S. N. Pluripotent stem cell-derived hepatocyte-like cells. *Biotechnol. Adv.*, 32(2):504–513, 2014. doi: 10.1016/j.biotechadv.2014.01.003.
- [4] Blackford, S. J., Ng, S. S., Segal, J. M., King, A. J., Austin, A. L., Kent, D., et al. Validation of Current Good Manufacturing Practice Compliant Human Pluripotent Stem Cell-Derived Hepatocytes for Cell-Based Therapy. *Stem Cells Transl. Med.*, 8(2):124–137, 2019. doi: 10.1002/sctm.18-0084.
- [5] Shiota, G. and Itaba, N. Progress in stem cell-based therapy for liver disease. *Hepatol. Res.*, 47(2):127–141, 2017. doi: 10.1111/hepr.12747.
- [6] Lim, F. and Sun, A. M. Microencapsulated islets as bioartificial endocrine pancreas. *Science*, 210(4472):908–910, 1980. doi: 10.1126/science.6776628.
- [7] Bochenek, M. A., Veisoh, O., Vegas, A. J., McGarrigle, J. J., Qi, M., Marchese, E., et al. Alginate encapsulation as long-term immune protection of allogeneic pancreatic islet cells transplanted into the omental bursa of macaques. *Nat. Biomed. Eng.*, 2(11):810–821, 2018. doi: 10.1038/s41551-018-0275-1.
- [8] Dufrane, D., Goebbels, R. M., Saliez, A., Guiot, Y., and Gianello, P. Six-month survival of microencapsulated pig islets and alginate biocompatibility in primates: Proof of concept. *Transplantation*, 81(9):1345–1353, 2006. doi: 10.1097/01.tp.0000208610.75997.20.
- [9] Gombotz, W. R. and Wee, S. F. Protein release from alginate matrices. *Adv. Drug Deliv. Rev.*, 31(3):267–285, 1998. doi: 10.1016/S0169-409X(97)00124-5.
- [10] Thanos, C. G., Gaglia, J. L., and Pagliuca, F. W. Considerations for successful encapsulated β -cell therapy. In Emerich, D. F. and Orive, G., editors, *Cell Therapy*, pages 19–52. Humana Press, Cham, 2017. ISBN 9783319571539. doi: 10.1007/978-3-319-57153-9_2.
- [11] Baxter, M., Withey, S., Harrison, S., Segeritz, C.-p., Zhang, F., Atkinson-Dell, R., et al. Phenotypic and functional analyses show stem cell-derived hepatocyte-like cells better mimic fetal rather than adult hepatocytes. *J. Hepatol.*, 62(3):581–589, mar 2015. doi: 10.1016/j.jhep.2014.10.016.

- [12] Arlov, Ø., Öztürk, E., Steinwachs, M., Skjåk-Bræk, G., and Zenobi-Wong, M. Biomimetic sulphated alginate hydrogels suppress IL-1B-induced inflammatory responses in human chondrocytes. *Eur. Cells Mater.*, 33:76–89, 2017. doi: 10.22203/eCM.v033a06.
- [13] Yang, J., Goto, M., Ise, H., Cho, C. S., and Akaike, T. Galactosylated alginate as a scaffold for hepatocytes entrapment. *Biomaterials*, 23(2):471–479, 2002. doi: 10.1016/S0142-9612(01)00129-6.
- [14] Si-Tayeb, K., Lemaigre, F. P., and Duncan, S. A. Organogenesis and Development of the Liver. *Dev. Cell*, 18(2):175–189, 2010. doi: 10.1016/j.devcel.2010.01.011.
- [15] Gordillo, M., Evans, T., and Gouon-Evans, V. Orchestrating liver development. *Development*, 142(12):2094–2108, jun 2015. doi: 10.1242/dev.114215.
- [16] Malarkey, D. E., Johnson, K., Ryan, L., Boorman, G., and Maronpot, R. R. New Insights into Functional Aspects of Liver Morphology. *Toxicol. Pathol.*, 33(1):27–34, 2005. doi: 10.1080/01926230590881826.
- [17] Roberts, R. A., Ganey, P. E., Ju, C., Kamendulis, L. M., Rusyn, I., and Klaunig, J. E. Role of the Kupffer Cell in Mediating Hepatic Toxicity and Carcinogenesis. *Toxicological Sciences*, 96(1):2–15, 11 2007. doi: 10.1093/toxsci/kfl173.
- [18] Kordes, C., Sawitza, I., Müller-Marbach, A., Ale-Agha, N., Keitel, V., Klonowski-Stumpe, H., et al. CD133+ hepatic stellate cells are progenitor cells. *Biochem. Biophys. Res. Commun.*, 352(2):410–417, jan 2007. doi: 10.1016/j.bbrc.2006.11.029.
- [19] Pober, J. S. and Sessa, W. C. Evolving functions of endothelial cells in inflammation. *Nat. Rev. Immunol.*, 7(10):803–815, oct 2007. doi: 10.1038/nri2171.
- [20] Tabibian, J. H., Masyuk, A. I., Masyuk, T. V., O’Hara, S. P., and LaRusso, N. F. Physiology of Cholangiocytes. *Compr. Physiol.*, 3(1):541–565, jan 2013. doi: 10.1002/cphy.c120019.
- [21] Hofmann, A. F. Current concepts of biliary secretion. *Dig. Dis. Sci.*, 34(12):16–20, 1989. doi: 10.1007/BF01536657.
- [22] Bataller, R. and Brenner, D. a. Science in medicine Liver fibrosis. *J. Clin. Invest.*, 115(2): 209–218, 2005. doi: 10.1172/JCI200524282.The.
- [23] Martinez-Hernandez, A. and Amenta, P. S. The extracellular matrix in hepatic regeneration. *FASEB J.*, 9(14):1401–1410, nov 1995. doi: 10.1096/fasebj.9.14.7589981.
- [24] Hynes, R. O. Integrins: Bidirectional, Allosteric Signaling Machines. *Cell*, 110(6):673–687, sep 2002. doi: 10.1016/S0092-8674(02)00971-6.
- [25] Geiger, B., Spatz, J. P., and Bershadsky, A. D. Environmental sensing through focal adhesions. *Nat. Rev. Mol. Cell Biol.*, 10(1):21–33, 2009. doi: 10.1038/nrm2593.
- [26] Hynes, R. O. The extracellular matrix: Not just pretty fibrils. *Science (80-.)*, 326(5957): 1216–1219, 2009. doi: 10.1126/science.1176009.

- [27] Martinez-Hernandez, A. and Amenta, P. S. The hepatic extracellular matrix. *Virchows Arch. A Pathol. Anat. Histopathol.*, 423(1):1–11, jan 1993. doi: 10.1007/BF01606425.
- [28] Mosher, D. Physiology of Fibronectin. *Annu. Rev. Med.*, 35(1):561–575, 1984. doi: 10.1146/annurev.med.35.1.561.
- [29] Godoy, P., Hewitt, N. J., Albrecht, U., Andersen, M. E., Ansari, N., Bhattacharya, S., et al. Recent advances in 2D and 3D in vitro systems using primary hepatocytes, alternative hepatocyte sources and non-parenchymal liver cells and their use in investigating mechanisms of hepatotoxicity, cell signaling and ADME. *Arch. Toxicol.*, 87(8):1315–1530, 2013. doi: 10.1007/s00204-013-1078-5.
- [30] Omiecinski, C. J., Vanden Heuvel, J. P., Perdew, G. H., and Peters, J. M. Xenobiotic metabolism, disposition, and regulation by receptors: From biochemical phenomenon to predictors of major toxicities. *Toxicol. Sci.*, 120(SUPPL.1), 2011. doi: 10.1093/toxsci/kfq338.
- [31] Wang, L. and Boyer, J. L. The Maintenance and Generation of Membrane Polarity in Hepatocytes. *Hepatology*, 39(4):892–899, 2004. doi: 10.1002/hep.20039.
- [32] Vinken, M. and Hengstler, J. G. Characterization of hepatocyte-based in vitro systems for reliable toxicity testing. *Arch. Toxicol.*, 92(10):2981–2986, 2018. doi: 10.1007/s00204-018-2297-6.
- [33] Gluchowski, N. L., Becuwe, M., Walther, T. C., and Farese, R. V. Lipid droplets and liver disease: From basic biology to clinical implications. *Nat. Rev. Gastroenterol. Hepatol.*, 14(6): 343–355, 2017. doi: 10.1038/nrgastro.2017.32.
- [34] Grandy, R., Tomaz, R. A., and Vallier, L. Modeling Disease with Human Inducible Pluripotent Stem Cells. *Annu. Rev. Pathol. Mech. Dis.*, 14(1):449–468, jan 2019. doi: 10.1146/annurev-pathol-020117-043634.
- [35] Hannoun, Z., Steichen, C., Dianat, N., Weber, A., and Dubart-Kupperschmitt, A. The potential of induced pluripotent stem cell derived hepatocytes. *J. Hepatol.*, 65(1):182–199, 2016. doi: 10.1016/j.jhep.2016.02.025.
- [36] Rashid, S. T. and Vallier, L. Induced pluripotent stem cells - alchemist’s tale or clinical reality? *Expert Reviews in Molecular Medicine*, 12:14–25, 08 2010. doi: 10.1017/S1462399410001596.
- [37] Gieseck III, R. L., Vallier, L., and Hannan, N. R. F. Generation of Hepatocytes from pluripotent Stem Cells for Drug Screening and Developmental Modeling. In Vinken, M. and Rogiers, V., editors, *Protoc. Vitro. Hepatocyte Res.*, volume 1250 of *Methods in Molecular Biology*, pages 123–159. Springer, New York, NY, 2015. ISBN 978-1-4939-2073-0. doi: 10.1007/978-1-4939-2074-7.
- [38] Hannan, N. R. F., Segeritz, C.-p., Touboul, T., and Vallier, L. Production of hepatocyte-like cells from human pluripotent stem cells. *Nat. Protoc.*, 8(2):430–437, feb 2013. doi: 10.1038/nprot.2012.153.
- [39] Si-Tayeb, K., Noto, F. K., Nagaoka, M., Li, J., Battle, M. A., Duris, C., et al. Highly efficient generation of human hepatocyte-like cells from induced pluripotent stem cells. *Hepatology*, 51(1):297–305, 2010. doi: 10.1002/hep.23354.

- [40] Sullivan, G. J., Hay, D. C., Park, I.-h., Fletcher, J., Hannoun, Z., Payne, C. M., et al. Generation of functional human hepatic endoderm from human induced pluripotent stem cells. *Hepatology*, 51(1):329–335, jan 2010. doi: 10.1002/hep.23335.
- [41] Zhang, Y., Pak, C., Han, Y., Ahlenius, H., Zhang, Z., Chanda, S., et al. Rapid Single-Step Induction of Functional Neurons from Human Pluripotent Stem Cells. *Neuron*, 78(5):785–798, jun 2013. doi: 10.1016/j.neuron.2013.05.029.
- [42] Moreau, T., Evans, A. L., Vasquez, L., Tijssen, M. R., Yan, Y., Trotter, M. W., et al. Large-scale production of megakaryocytes from human pluripotent stem cells by chemically defined forward programming. *Nat. Commun.*, 7, 2016. doi: 10.1038/ncomms11208.
- [43] Pawlowski, M., Ortmann, D., Bertero, A., Tavares, J. M., Pedersen, R. A., Vallier, L., et al. Inducible and Deterministic Forward Programming of Human Pluripotent Stem Cells into Neurons, Skeletal Myocytes, and Oligodendrocytes. *Stem Cell Reports*, 8(4):803–812, apr 2017. doi: 10.1016/j.stemcr.2017.02.016.
- [44] Draget, K. I., Moe, S. T., Skjåk-Bræk, G., and Smidsrød, O. Alginates. In Stephen, A. M., Phillips, G. O., and Williams, P. A., editors, *Food Polysaccharides and Their Applications*, pages 290–325. CRC press, Boca Raton, 2nd edition, 2006. ISBN 9781420015164.
- [45] Arlov, Ø. and Skjåk-Bræk, G. Sulfated alginates as heparin analogues: A review of chemical and functional properties. *Molecules*, 22(5):1–16, 2017. doi: 10.3390/molecules22050778.
- [46] Lee, K. Y. and Mooney, D. J. Alginate: Properties and biomedical applications. *Prog. Polym. Sci.*, 37(1):106–126, jan 2012. doi: 10.1016/j.progpolymsci.2011.06.003.
- [47] Haug, A., Larsen, B., Smidsrød, O., Møller, J., Brunvoll, J., Bunnenberg, E., et al. A Study of the Constitution of Alginic Acid by Partial Acid Hydrolysis. *Acta Chem. Scand.*, 20(1):183–190, 1966. doi: 10.3891/acta.chem.scand.20-0183.
- [48] Draget, K. I. and Taylor, C. Chemical, physical and biological properties of alginates and their biomedical implications. *Food Hydrocoll.*, 25(2):251–256, 2011. doi: 10.1016/j.foodhyd.2009.10.007.
- [49] Braccini, I. and Pérez, S. Molecular basis of Ca²⁺-induced gelation in alginates and pectins: The egg-box model revisited. *Biomacromolecules*, 2(4):1089–1096, 2001. doi: 10.1021/bm010008g.
- [50] Grant, G. T., Morris, E. R., Rees, D. A., Smith, P. J., and Thom, D. Biological interactions between polysaccharides. *FEBS Lett.*, 32(1):195–198, 1973. doi: 10.1002/rmv.519.
- [51] Grant, G. T., Morris, E. R., Rees, D. A., Smith, P. J., and Thom, D. Biological interactions between polysaccharides and divalent cations: The egg-box model. *FEBS Lett.*, 32(1):195–198, may 1973. doi: 10.1016/0014-5793(73)80770-7.
- [52] Mørch, Ý. A., Donati, I., Strand, B. L., and Skjåk-Bræk, G. Effect of Ca²⁺, Ba²⁺, and Sr²⁺ on alginate microbeads. *Biomacromolecules*, 7(5):1471–1480, 2006. doi: 10.1021/bm060010d.
- [53] Martinsen, A., Skjåk-Bræk, G., and Smidsrød, O. Alginate as immobilization material: I. Correlation between chemical and physical properties of alginate gel beads. *Biotechnol. Bioeng.*, 33(1):79–89, 1989. doi: 10.1002/bit.260330111.

- [54] Stokke, B. T., Smidsrød, O., Zanetti, F., Strand, W., and Skjåk-Bræk, G. Distribution of uronate residues in alginate chains in relation to alginate gelling properties - 2: Enrichment of β -d-mannuronic acid and depletion of α -l-guluronic acid in sol fraction. *Carbohydr. Polym.*, 21(1): 39–46, 1993. doi: 10.1016/0144-8617(93)90115-K.
- [55] Martinsen, A., Skjåk-Bræk, G., Smidsrød, O., Zanetti, F., and Paoletti, S. Comparison of different methods for determination of molecular weight and molecular weight distribution of alginates. *Carbohydr. Polym.*, 15(2):171–193, 1991. doi: 10.1016/0144-8617(91)90031-7.
- [56] Smidsrød, O. and Skjåk-Bræk, G. Alginate as immobilization matrix for cells. *Trends Biotechnol.*, 8(1):71–78, mar 1990. doi: 10.1016/0167-7799(90)90139-O.
- [57] Krishnan, R., Alexander, M., Robles, L., Foster, C. E., and Lakey, J. R. Islet and stem cell encapsulation for clinical transplantation. *Rev. Diabet. Stud.*, 11(1):84–101, 2014. doi: 10.1900/RDS.2014.11.84.
- [58] Dalheim, M., Vanacker, J., Najmi, M. A., Aachmann, F. L., Strand, B. L., and Christensen, B. E. Efficient functionalization of alginate biomaterials. *Biomaterials*, 80:146–156, 2016. doi: 10.1016/j.biomaterials.2015.11.043.
- [59] King, A., Sandler, S., and Andersson, A. The effect of host factors and capsule composition on the cellular overgrowth on implanted alginate capsules. *J. Biomed. Mater. Res.*, 57(3):374–383, 2001. doi: 10.1002/1097-4636(20011205)57:3<374::AID-JBM1180>3.0.CO;2-L.
- [60] Aljohani, W., Wenchao, L., Ullah, M. W., Zhang, X., and Yang, G. Application of Sodium Alginate Hydrogel. *IOSR J. Biotechnol. Biochem.*, 03(3):19–31, 2017. doi: 10.9790/264x-03031931.
- [61] Vegas, A. J., Veiseh, O., Doloff, J. C., Ma, M., Tam, H. H., Bratlie, K., et al. Combinatorial hydrogel library enables identification of materials that mitigate the foreign body response in primates. *Nat. Biotechnol.*, 34(3):345–352, 2016. doi: 10.1038/nbt.3462.
- [62] Anderson, J. M., Rodriguez, A., and Chang, D. T. Foreign body reaction to biomaterials. *Semin. Immunol.*, 20(2):86–100, 2008. doi: 10.1016/j.smim.2007.11.004.
- [63] Young, E. The anti-inflammatory effects of heparin and related compounds. *Thromb. Res.*, 122(6):743–752, 2008. doi: 10.1016/j.thromres.2006.10.026.
- [64] Casu, B. Structure of Heparin and Heparin Fragments. *Ann. N. Y. Acad. Sci.*, 556(1):1–17, jun 1989. doi: 10.1111/j.1749-6632.1989.tb22485.x.
- [65] Öztürk, E., Arlov, Ø., Aksel, S., Ling, L., Ornitz, D. M., Skjåk-Bræk, G., et al. Sulfated Hydrogel Matrices Direct Mitogenicity and Maintenance of Chondrocyte Phenotype through Activation of FGF Signaling. *Adv. Funct. Mater.*, 26(21):3649–3662, 2016. doi: 10.1002/adfm.201600092.
- [66] Arlov, Ø., Aachmann, F. L., Sundan, A., Espevik, T., and Skjåk-Bræk, G. Heparin-like properties of sulfated alginates with defined sequences and sulfation degrees. *Biomacromolecules*, 15(7):2744–2750, 2014. doi: 10.1021/bm500602w.
- [67] Arlov, Ø., Skjåk-Bræk, G., and Rokstad, A. M. Sulfated alginate microspheres associate with factor H and dampen the inflammatory cytokine response. *Acta Biomater.*, 42:180–188, 2016. doi: 10.1016/j.actbio.2016.06.015.

- [68] Moghe, P. V., Berthiaume, F., Ezzell, R. M., Toner, M., Tompkins, R. G., and Yarmush, M. L. Culture matrix configuration and composition in the maintenance of hepatocyte polarity and function. *Biomaterials*, 17(3):373–385, 1996. doi: 10.1016/0142-9612(96)85576-1.
- [69] Wall, D. A. and Hubbard, A. L. Galactose-specific recognition system of mammalian liver: Receptor distribution on the hepatocyte cell surface. *J. Cell Biol.*, 90(3):687–696, 1981. doi: 10.1083/jcb.90.3.687.
- [70] Lopina, S. T., Wu, G., Merrill, E. W., and Griffith-Cima, L. Hepatocyte culture on carbohydrate-modified star polyethylene oxide hydrogels. *Biomaterials*, 17(6):559–569, 1996. doi: 10.1016/0142-9612(96)88706-0.
- [71] Kristiansen, K. A., Potthast, A., and Christensen, B. E. Periodate oxidation of polysaccharides for modification of chemical and physical properties. *Carbohydr. Res.*, 345(10):1264–1271, 2010. doi: 10.1016/j.carres.2010.02.011.
- [72] Kristiansen, K. A., Tomren, H. B., and Christensen, B. E. Periodate oxidized alginates: Depolymerization kinetics. *Carbohydr. Polym.*, 86(4):1595–1601, 2011. doi: 10.1016/j.carbpol.2011.06.069.
- [73] Donati, I., Draget, K. I., Borgogna, M., Paoletti, S., and Skjåk-Bræk, G. Tailor-made alginate bearing galactose moieties on mannuronic residues: Selective modification achieved by a chemoenzymatic strategy. *Biomacromolecules*, 6(1):88–98, 2005. doi: 10.1021/bm040053z.
- [74] Painter, T., Larsen, B., Sjövall, J., Kääriäinen, L., Rasmussen, S. E., Sunde, E., et al. Formation of Hemiacetals between Neighbouring Hexuronic Acid Residues during the Periodate Oxidation of Alginate. *Acta Chem. Scand.*, 24:813–833, 1970. doi: 10.3891/acta.chem.scand.24-0813.
- [75] Drury, J. L. and Mooney, D. J. Hydrogels for tissue engineering: Scaffold design variables and applications. *Biomaterials*, 24(24):4337–4351, 2003. doi: 10.1016/S0142-9612(03)00340-5.
- [76] Ertesvåg, H. and Skjåk-Bræk, G. Modification of Alginate Using Mannuronan C-5-Epimerases. In Bucke, C., editor, *Carbohydrate Biotechnology Protocols*, volume 10, pages 71–88. Humana Press, 1999. ISBN 978-1-59259-261-6.
- [77] Rashid, S. T., Corbineau, S., Hannan, N., Marciniak, S. J., Miranda, E., Alexander, G., et al. Modeling inherited metabolic disorders of the liver using human induced pluripotent stem cells. *J. Clin. Invest.*, 120(9):3127–3136, sep 2010. doi: 10.1172/JCI43122.
- [78] Yusa, K., Rashid, S. T., Strick-Marchand, H., Varela, I., Liu, P. Q., Paschon, D. E., et al. Targeted gene correction of α 1-antitrypsin deficiency in induced pluripotent stem cells. *Nature*, 478(7369):391–394, 2011. doi: 10.1038/nature10424.
- [79] Chen, G., Gulbranson, D. R., Hou, Z., Bolin, J. M., Ruotti, V., Probasco, M. D., et al. Chemically defined conditions for human iPSC derivation and culture. *Nat. Methods*, 8(5):424–429, may 2011. doi: 10.1038/nmeth.1593.
- [80] Takeichi, M. The cadherins: cell-cell adhesion molecules controlling animal morphogenesis. *Development*, 102(4):639–655, 1988. ISSN 0950-1991.

- [81] Bajpai, R., Lesperance, J., Kim, M., and Terskikh, A. V. Efficient propagation of single cells accutase-dissociated human embryonic stem cells. *Mol. Reprod. Dev.*, 75(5):818–827, 2008. doi: 10.1002/mrd.20809.
- [82] Strand, B. L., Gåserød, O., Kulseng, B., Espevik, T., and Skjåk-Bræk, G. Alginate-polylysine-alginate microcapsules: effect of size reduction on capsule properties. *J. Microencapsul.*, 19(5): 615–630, jan 2002. doi: 10.1080/02652040210144243.
- [83] Rokstad, A. M., Donati, I., Borgogna, M., Oberholzer, J., Strand, B. L., Espevik, T., et al. Cell-compatible covalently reinforced beads obtained from a chemoenzymatically engineered alginate. *Biomaterials*, 27(27):4726–4737, 2006. doi: 10.1016/j.biomaterials.2006.05.011.
- [84] Qi, M., Mørch, Y., Laci, I., Formo, K., Marchese, E., Wang, Y., et al. Survival of human islets in microbeads containing high guluronic acid alginate crosslinked with Ca²⁺ and Ba²⁺. *Xenotransplantation*, 19(6):355–364, 2012. doi: 10.1111/xen.12009.
- [85] Abcam. Live and Dead Cell Assay (ab115347), 2019. URL <https://www.abcam.com/live-and-dead-cell-assay-ab115347.html>. [accessed: 2020–02–25].
- [86] Invitrogen™ P50200. Invitrogen™ PrestoBlue™ HS Cell Viability Reagent, 2020. URL <https://www.fishersci.no/shop/products/prestoblue-hs-cell-viability-reagent/16294822>. [accessed: 2020–04–17].
- [87] Wilkinson, G. R. Drug therapy: Drug metabolism and variability among patients in drug response. *N. Engl. J. Med.*, 352(21):2211–2221, 2005. doi: 10.1056/NEJMra032424.
- [88] Promega. P450-Glo™ Assays, 2016. URL <https://www.promega.com/-/media/files/resources/protocols/technical-bulletins/101/p450-glo-assays-protocol.pdf>. [accessed: 2020–03–15].
- [89] Bustin, S. A. Absolute quantification of mRNA using real-time reverse transcription polymerase chain reaction assays. *J. Mol. Endocrinol.*, 25(2):169–193, 2000. doi: 10.1677/jme.0.0250169.
- [90] Griko, Y. V. Energetics of Ca²⁺-EDTA interactions: Calorimetric study. *Biophys. Chem.*, 79(2):117–127, 1999. doi: 10.1016/S0301-4622(99)00047-2.
- [91] Sigma-Aldrich. GenElute™ Mammalian Total RNA Kit User Guide, 2017. URL <file:///E:/Year3/MDSC408/Winterlabs/lab7,8readings/SIGMA-RNAisolation1.pdf>. [accessed: 2020–04–18].
- [92] KAPA BioSystems. KAPA SYBR FAST qPCR Master Mix (2X) Kit, 2017. URL <https://www.sigmaaldrich.com/content/dam/sigma-aldrich/docs/Roche/Datasheet/1/sfukbdat.pdf>. [accessed: 2020–05–02].
- [93] Chang, T. T. and Hughes-Fulford, M. Molecular mechanisms underlying the enhanced functions of three-dimensional hepatocyte aggregates. *Biomaterials*, 35(7):2162–2171, 2014. doi: 10.1016/j.biomaterials.2013.11.063.
- [94] Lavrentovich, M. O., Koschwanez, J. H., and Nelson, D. R. Nutrient shielding in clusters of cells. *Phys. Rev. E - Stat. Nonlinear, Soft Matter Phys.*, 87(6):1–17, 2013. doi: 10.1103/PhysRevE.87.062703.

- [95] Dalheim, M., Omtvedt, L. A., Bjørge, I. M., Akbarzadeh, A., Mano, J. F., Aachmann, F. L., et al. Mechanical properties of Ca-saturated hydrogels with functionalized alginate. *Gels*, 5(2), 2019. doi: 10.3390/gels5020023.
- [96] Bhujbal, S. V., Paredes-Juarez, G. A., Niclou, S. P., and de Vos, P. Factors influencing the mechanical stability of alginate beads applicable for immunoisolation of mammalian cells. *J. Mech. Behav. Biomed. Mater.*, 37:196–208, 2014. doi: 10.1016/j.jmbbm.2014.05.020.
- [97] King, A. *Evaluation of Alginate Microcapsules for Use in Transplantation of Islets of Langerhans*. PhD thesis, Uppsala University, 2001.
- [98] Engvall, E. and Perlmann, P. Enzyme-Linked Immunosorbent Assay, Elisa. *J. Immunol.*, 109 (1):129–135, 1972. ISSN 0022-1767.

A $^1\text{H-NMR}$ spectra

$^1\text{H-NMR}$ analyses were performed by Wenche Iren Strand at NTNU as described previously [76]. Figure A.1 shows the $^1\text{H-NMR}$ spectra of the periodate oxidized alginate and a control, revealing that oxidation had taken place. The $^1\text{H-NMR}$ spectra of a sample of the phenyl-containing control for Gal-Alg (phenyl-Gal-Alg) is displayed in Figure A.2. Wench I. Strand calculated the DS based on the chemical shifts of the aromatic protons of the substituent in relation to the G-1 and M-1 peaks.

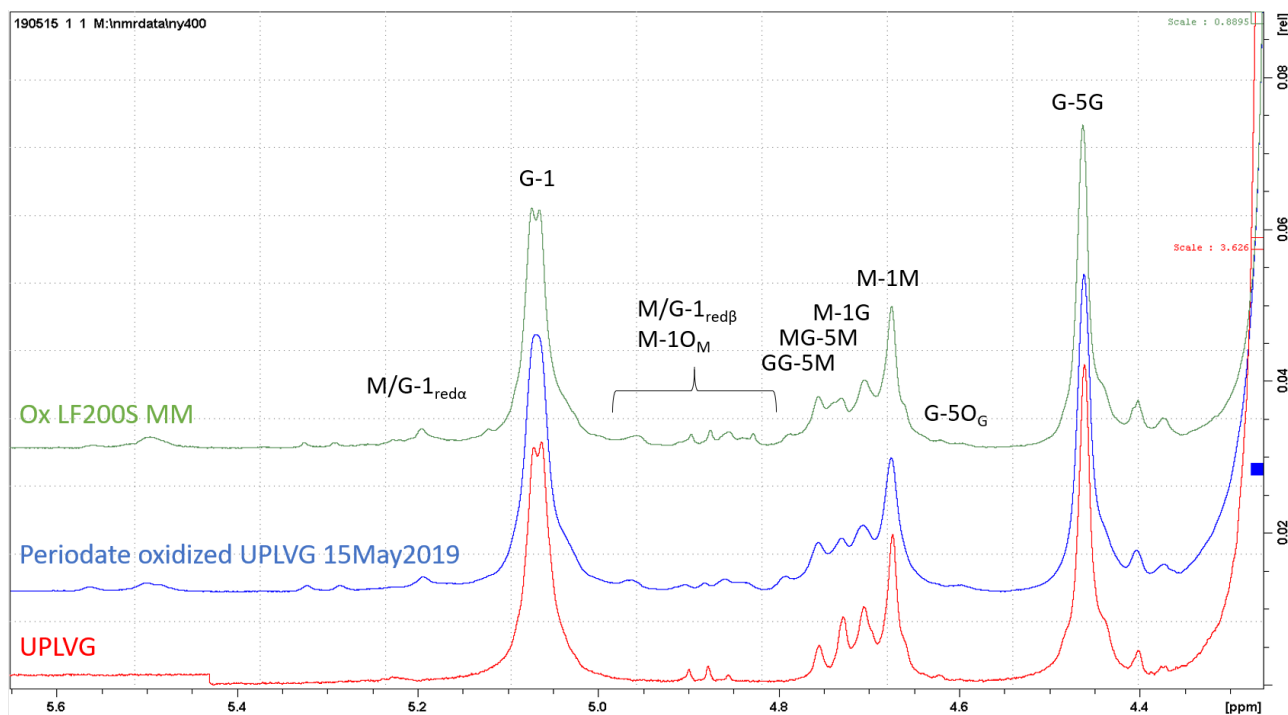


Figure A.1: $^1\text{H-NMR}$ spectra of POA. $^1\text{H-NMR}$ analysis was performed at 400 MHz and 82°C on POA made from UP-LVG (Pronova[®]) and a control periodate oxidized LF200S sample. Peaks denoted with an “O” refer only to the oxidized material. Peaks are assigned according to Kristiansen et al. 2009

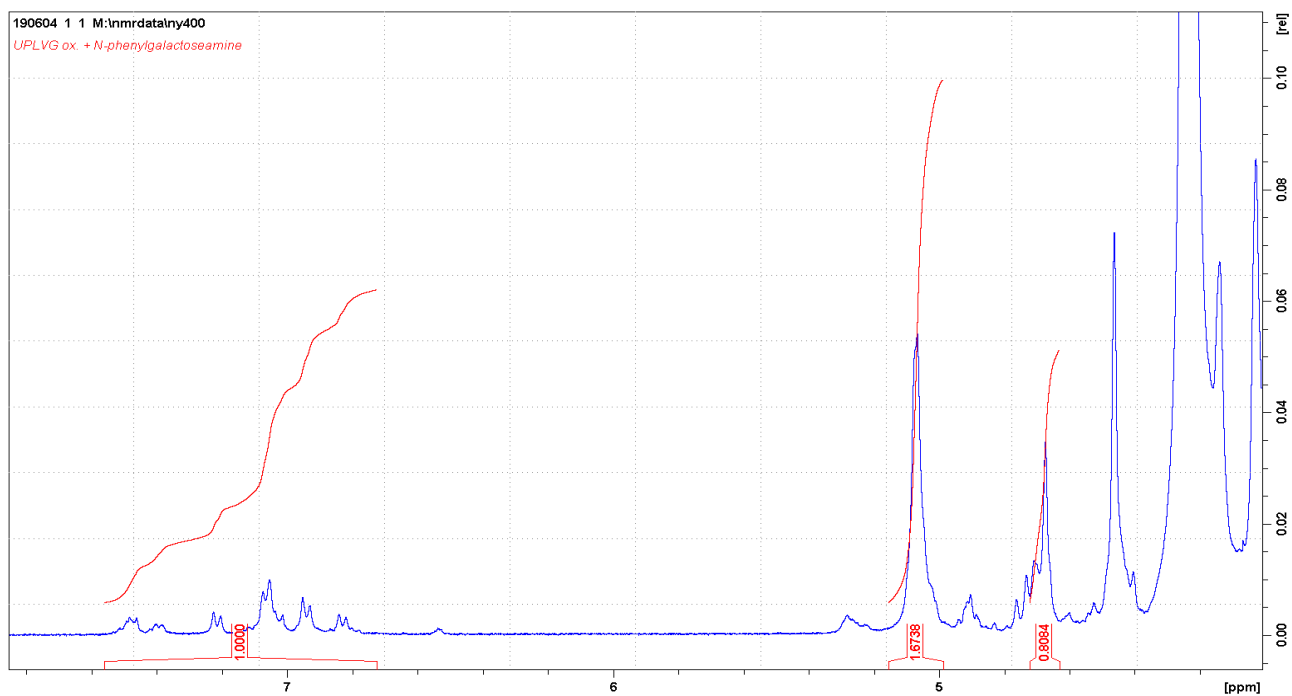


Figure A.2: $^1\text{H-NMR}$ spectra of phenyl-Gal-Alg. $^1\text{H-NMR}$ analysis was performed at 400 MHz and 82°C on POA from UP-LVG (Pronova[®]) functionalized with a galactose substituent connected through a phenyl ring and an amine bond to the C3 carbon of alginate monomers. Four aromatic protons of the substituent has chemical shifts between 6.75 and 7.55 ppm (left), while G-1 and M-1 peaks of the alginate monomers have chemical shifts in the region 5.1 and 4.7 ppm, respectively (Grasdalen et al., 1979).

B Primer sequences for qPCR

qPCR was performed on cDNA synthesized from RNA extracted from hepatocyte-like cells generated by direct differentiation and forward programming. For specific amplification, primers for four target genes were chosen, see Table B.1.

Table B.1 Primers used for qPCR of four target genes and two housekeeping genes (*). Orientation indicates the direction of amplification; forward (F) and reverse (R).

Description	Orientation	Primer sequence (5'-3')
RPLP0*	F	GGCGTCCTCGTGGAAGTGAC
	R	GCCTTGCGCATCATGGTGTT
RBGD*	F	GGAGCCATGTCTGGTAACGG
	R	CCACGCGAATCACTCTCATCT
Albumin	F	CCTTTGGCACAATGAAGTGGGTAACC
	R	CAGCAGTCAGCCATTTACCATAG
AFP	F	AGAACCTGTCACAAGCTGTG
	R	GACAGCAAGCTGAGGATGTC
A1AT	F	CCACCGCCATCTTCTTCCTGCCTGA
	R	GAGCTTCAGGGGTGCCTCCTCTG
HNF4 α	F	CATGGCCAAGATTGACAACCT
	R	TTCCCATATGTTCTGCATCAG

C Functional assays of HLCs encapsulated in POAred and Gal-Alg

Hepatocyte-like cells generated by forward programming were encapsulated in two concentrations of Gal-alg. The modified alginate was mixed with unmodified UPLVG in a 20:80 ratio (Gal-Alg 20/80) and a 40:60 ratio (Gal-Alg 40/60). In addition to being galactosylated, several other changes occurred during the synthesis of the alginate. As described in Section 2.3.1, this results in changes in the mechanical properties of the alginate. To test if any changes in cell function resulted from the galactose substituent or the changed mechanical properties of the alginate, a control for the mechanical changes was also tested. Reduced periodate oxidized alginate (POAred) was used to encapsulate cells from the same 2D culture as Gal-Alg, and tested in corresponding concentrations.

Due to time constraints, only one experiment (n=1) was conducted for each alginate concentration, and the experiment with Gal-Alg and POAred 40/60 had to be stopped after day 20 of differentiation, or day 5 post encapsulation. To check if the capsules made in a 40:60 ratio with the unmodified alginates were stable in the cell culture media, the diameter (size) was measured on the day of encapsulation and after 5 days of exposure to the media. Results are summarized in Table C.1. Using a two-tailed paired t.test, the differences in diameter between day 0 and day 5 of encapsulation were deemed insignificant ($p > 0.05$). However, the difference in capsule size within the batch of POAred 40/60 was too large ($> 10\%$ of average diameter).

Table C.1 Changes in Gal-alg and POAred capsule diameter over time. The size (diameter) of functionalized alginate capsules was measured on the day of encapsulation (day 0) and after 5 days of exposure to the cell culture media. POAred and Gal-Alg 40/60 = Reduced periodate oxidized alginate (POAred) and galactosylated POAred mixed with unmodified UPLVG in a 40:60 ratio.

Alginate	Size day 0 ($\mu\text{m} \pm \text{SD}$)	Size day 5 ($\mu\text{m} \pm \text{SD}$)
POAred 40/60	481 \pm 53	480 \pm 58
Gal-Alg 40/60	569 \pm 31	556 \pm 21

The observed percentage of irregular capsule shapes are summarized in Table C.2 along with the applied voltage and flow rate during encapsulation. However, the greatest irregularity observed was the difference in capsule size within each batch of POAred and Gal-Alg 40/60, see Figure C.1. There were also fewer cells encapsulated than expected (4.5 million cells), as there was observed many empty capsules.

Table C.2 Characterisation of Alginate capsules made with Gal-alg and POAred. Flow rate and applied voltage during encapsulation, and resulting irregularities observed in 30 beads on the day of encapsulation. POAred and Gal-Alg 20/80 and 40/60 = Reduced periodate oxidized alginate (POAred) and galactosylated POAred mixed with unmodified UPLVG in a 20:80 and a 40:60 ratio.

	Alginate	Flow rate (mL/h)	Applied voltage (kV)	Ellipse formed	Tailed	Total
20/80	POAred	8.0	7.0	20%	6.7%	33.3%
	Gal-Alg	8.0	7.0	10%	1%	20%
40/60	POAred	6.5	6.5	3.3%	10%	16.7%
	Gal-Alg	6.5	6.5	3.3%	10%	16.7%

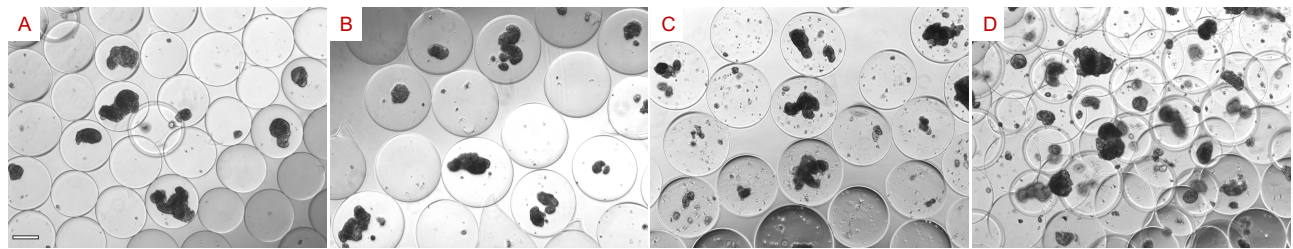
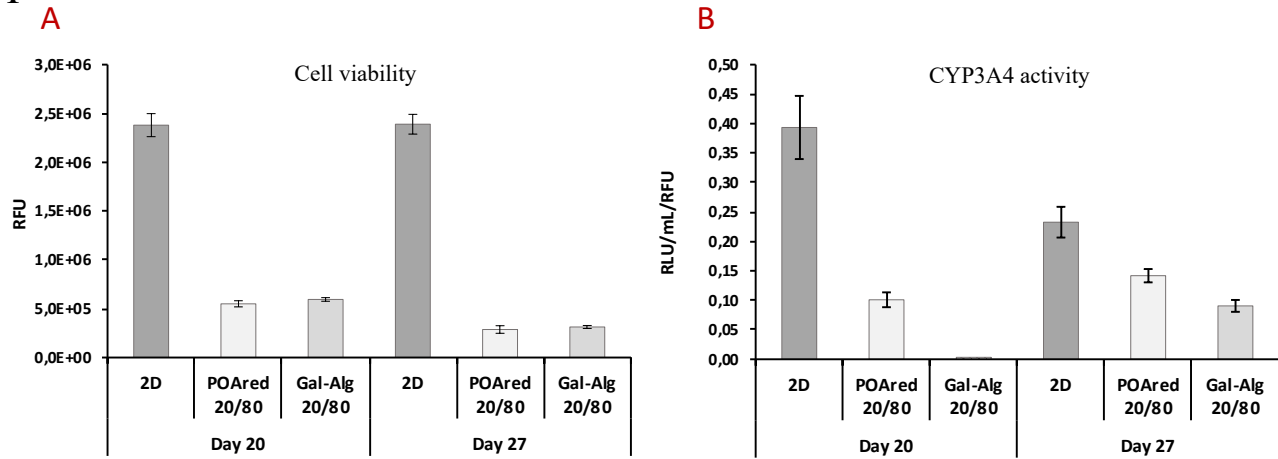


Figure C.1: FoP-derived HLCs encapsulated in two concentrations of Gal-alg and POAred. Gal-Alg (A) and POAred (B) mixed with UPLVG in a 20:80 ratio, and Gal-alg (C) and POAred (D) mixed with UPLVG in a 40:60 ratio.

Figure C.2 shows viability and cell function measurements of the two experiments (I and II). Experiment I (B) indicates that the non-galactosylated control for Gal-Alg has a greater cell function, while the improvement of Gal-alg 20/80 from day 20 to day 27 is greater. Conversely, results from experiment II (B) indicates that Gal-Alg 40/60 has a greater cell function than the control. However, the difference is marginal.

qPCR results of the two experiments (Figure C.3) support the findings of the cell function and viability measurements. While there is very little difference between the alginates of the 20/80 concentration for all the hepatocyte markers, with slightly favorable measurements for the control (Figure C.3 A and C), the stronger concentration of Gal-alg performs better than its control as seen in experiment II. However, except for the still-low albumin measurements (I:A), all other markers were lower than seen in Figure 4.13.

I



II

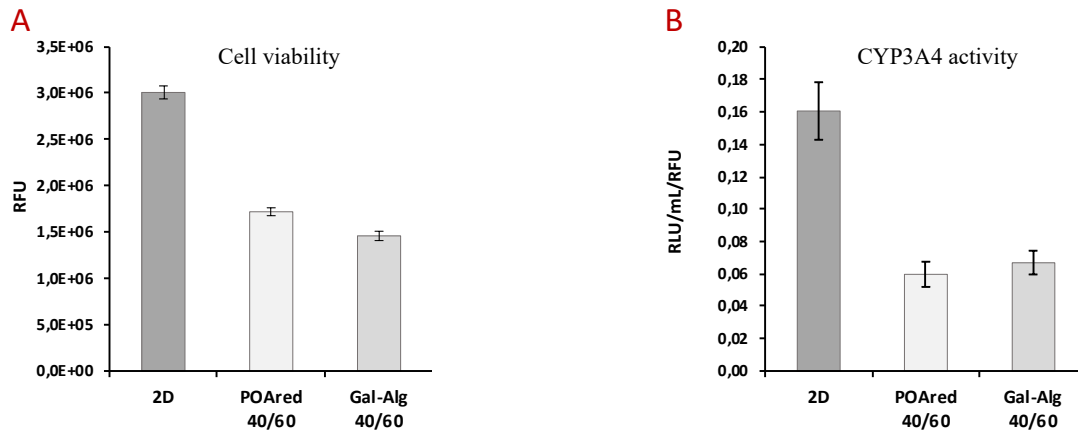


Figure C.2: Cell viability and function of FoP-derived HLCs encapsulated in Gal-alg and POAred. Cell viability (A) and cell function (B) measured on day 20 and day 27 of differentiation of HLCs encapsulated in POAred and Gal-Alg 20/80 (I), and measured on day 20 of differentiation of HLCs encapsulated in POAred and Gal-alg 40/60 (II). Viability was measured using PrestoBlue Cell Viability Reagent (Invitrogen™). Cell function was measured as the activity of enzyme CYP3A4 using P450-Glo™ CYP3A4 assay (Promega®). The measurements were normalized to the viability at each time point. RFU = relative fluorescence unit. RLU = relative luminescence unit. (mean ± SD of three technical replicates, n = 1)

